DESIGN AND CHARACTERIZATION OF CONVECTIVE THERMAL CYCLERS FOR HIGH-SPEED DNA ANALYSIS

A Dissertation

by

NITIN AGRAWAL

Submitted to the Office of Graduate Studies of
Texas A&M University
in partial fulfillment of the requirements for the degree of

DOCTOR OF PHILOSOPHY

December 2006

Major Subject: Chemical Engineering

DESIGN AND CHARACTERIZATION OF CONVECTIVE THERMAL CYCLERS FOR HIGH-SPEED DNA ANALYSIS

A Dissertation

by

NITIN AGRAWAL

Submitted to the Office of Graduate Studies of
Texas A&M University
in partial fulfillment of the requirements for the degree of

DOCTOR OF PHILOSOPHY

Approved by:

Chair of Committee,	Victor M. Ugaz
Committe Members,	Arul Jayaraman
	Michael A. Bevan
	Yassin A Hassan
Head of Department,	Kenneth R. Hall

December 2006

Major Subject: Chemical Engineering

ABSTRACT

Design and Characterization of Convective

Thermal Cyclers for High-Speed DNA Analysis. (December 2006)

Nitin Agrawal, B.S., Regional Engineering College-Durgapur, India

Chair of Advisory Committee: Dr. Victor M. Ugaz

An ideal polymerase chain reaction (PCR) system should be capable of rapidly amplifying a wide range of targets in both single and multiplex formats. Unfortunately, the timescales and complexities involved in many existing technologies impose significant limitations on achievable throughput. Buoyancy driven PCR is emerging as a simplified version of thermally driven bio-analysis systems. Here, we demonstrate a simplified convectively driven thermocycler capable of performing single and multiplex PCR for amplicons ranging from 191 bp to 1.3 kb within 10 to 50 minutes using 10 to 25 μL reaction volumes. By positioning two independent thermoelectric heating elements along the perimeter of a flow loop reactor constructed using ordinary plastic tubing, a buoyancy-driven flow is established that continuously circulates reagents through temperature zones associated with the PCR process. Unlike conventional benchtop thermocyclers, this arrangement allows reactions to be performed without the need for dynamic temperature control of inactive hardware components while maintaining comparable product yields and requiring no modifications to standard PCR protocols. We also provide a general correlation that can be applied to design reactor geometries satisfying virtually any combination of reagent volume and cycling time. In addition to

offering an attractive combination of cost and performance, this system is readily adaptable for portable battery powered operation, making it feasible to perform PCR-based assays in a broader array of settings.

DEDICATION

To

My parents and brother
whose love and support nurtured me throughout my life

ACKNOWLEDGEMENTS

Acknowledgement is a small word for the amount of help, support, and encouragement that I received from many people around. First and foremost is Dr. Victor M. Ugaz who is not only my research advisor, but also a role model for my academic and professional growth. His patience and tolerance is unbeatable. I owe him more than just a *thank you*.

I would like to thank Dr. Arul Jayaraman for providing his guidance and lab facilities. I am also thankful to my other committee members Dr. Michael A. Beven and Dr. Yassin A. Hassan who provided continuous motivation throughout my doctoral program. Stimulating discussions with Dr. Mihir Sen were useful and contributed greatly to my research. I thank Ling Zhen for her help with computational modeling and Roger Lo who, as a team member provided, great help with DNA sequencing procedure. I would also like to thank all of my lab members and fellow graduate students for their help and advice in making my stay at Texas A&M enjoyable. I especially cherish the great company provided by Abhay Singh, Shahebaz Mulla and Bhavana Singh who were always there to listen to my ideas and to offer me their sincere comments and a great deal of motivation.

Last but not least, I owe a great deal to my family which includes my father Mr. Rama Shanker Agarwal, my mother Mrs. Meena Agarwal and my elder brother Sachin Agrawal whose moral strength and support on an every day basis cannot be forgotten. I feel a deep sense of gratitude for my brother who is also my intellectual decision making partner since the beginning of my academic career.

TABLE OF CONTENTS

CHAPTER Page

LIST OF FIGURES

FIGURE Page

FIGURE Page

FIGURE Page

FIGURE Page

FIGURE Page

NOMENCLATURE

Abbreviations

A, T, C, G	Adenine, thymine, cytosine, guanine
bp	Base pairs
CLTC	Closed loop thermocycler
dATP	2’-deoxyadenosine 5’-triphosphate
dCTP	2’-deoxycytidine 5’-triphosphate
ddNTP	2',3'-dideoxynucleotide triphospate
dGTP	2’-deoxyguanosine 5’-triphosphate
DNA	Deoxyribonucleic acid
dNTP	Deoxyribonucleotide triphosphate
dNTP	Deoxyribonucleotide triphosphate
dsDNA	Double-stranded DNA
EDTA	Ethylenediaminetetraacetic acid
FEP	Fluorinated Ethylene Propylene tubing
IR	Infrared
kb	Kilo base pairs
PCR	Polymerase chain reaction
PVC	Polyvinyl chloride
RNA	Ribonucleic acid
ssDNA	Single-stranded DNA

TAE	Tris-acetate-EDTA
TBE	Tris-Borate-EDTA
UV	Ultraviolet

Symbols

$\tilde{g}$	Local component of gravity
ΔT	Temperature gradient
µL	Microliter
µM	Micromole
µm	Micrometer
A	Cross-sectional area
cm	Centimeter
Cp	Specific heat at constant pressure
D	Diameter
g	Acceleration due to gravity
h	Characteristic length scale, Heat transfer coefficient
k	Thermal conductivity
L	Length
mL	Milliliter
mM	Millimole
mm	Millimeter
n	Number of cycles
ng	Nanogram

p	Pressure
P	Perimeter
Q	Heat flow rate
q	Heat flow rate per unit length
r	Radius
Ra	Rayleigh number
Ra_{crit}	Critical Rayleigh number
s	Directional coordinate
T	Temperature
t	Time
T_m	Primer melting temperature
u	velocity
x	Mean efficiency per cycle
Y	Copy yield

Greek letters

β	Thermal expansion coefficient
ν	Kinematic viscosity
κ	Thermal diffusivity
ρ	Density
μ	Viscosity
τ_w	Wall shear stress

CHAPTER I

INTRODUCTION

DNA sequence information generated from the Human Genome Project continues to stimulate new research in a variety of areas including medical diagnostics, genomic analysis, and drug discovery (1). Consequently, DNA fingerprinting assays are becoming an increasingly common component of diagnostic procedures from pathogen and infectious disease detection (2) to forensics (3) to population-scale polymorphism and mutation analysis (4,5). Most modern genomic analysis strategies rely on the polymerase chain reaction (PCR) to amplify a specific region of interest from a longer DNA template before subsequent separation, purification and detection steps can be performed. The ability to reliably replicate long amplicons (> 1 kb) is also an area of intense interest due to its key role in many whole-genome analysis procedures. However, PCR continues to be one of the key rate determining steps in the overall analysis process. An ideal PCR system should be capable of rapidly amplifying a wide range of targets in both single and multiplex formats. Unfortunately, the timescales and complexities involved in existing technologies impose significant limitations on achievable throughput stipulating the emergence of more advanced and efficient techniques to address the current limitations.

The underlying biochemistry of the PCR is fundamentally simple requiring reagents (template DNA, primers, dNTPs, thermostable *Taq* polymerase enzyme, etc.) to

---

This dissertation follows the style of *Nucleic Acids Research.*

be repeatedly cycled approximately 30-35 times through three distinct temperatures associated with denaturation, annealing and extension processes. This thermal cycling is carried out in instruments typically known as thermocyclers. Several instruments designs have been proposed so far in which thermocycling can be accomplished in a variety of ways including (i) placing tubes containing the PCR reagent mixture in a stationary metal block whose temperature is electronically varied, (ii) loading PCR reagents into high surface-to-volume capillary tubes that are heated and cooled by an external air stream (e.g., Light Cycler, Roche), or (iii) by mechanically transporting the PCR reagents between individual blocks or baths maintained at constant temperatures (e.g., Robocycler, Stratagene). A simple schematic of the general PCR cycling process is presented in Figure 1.1 below.

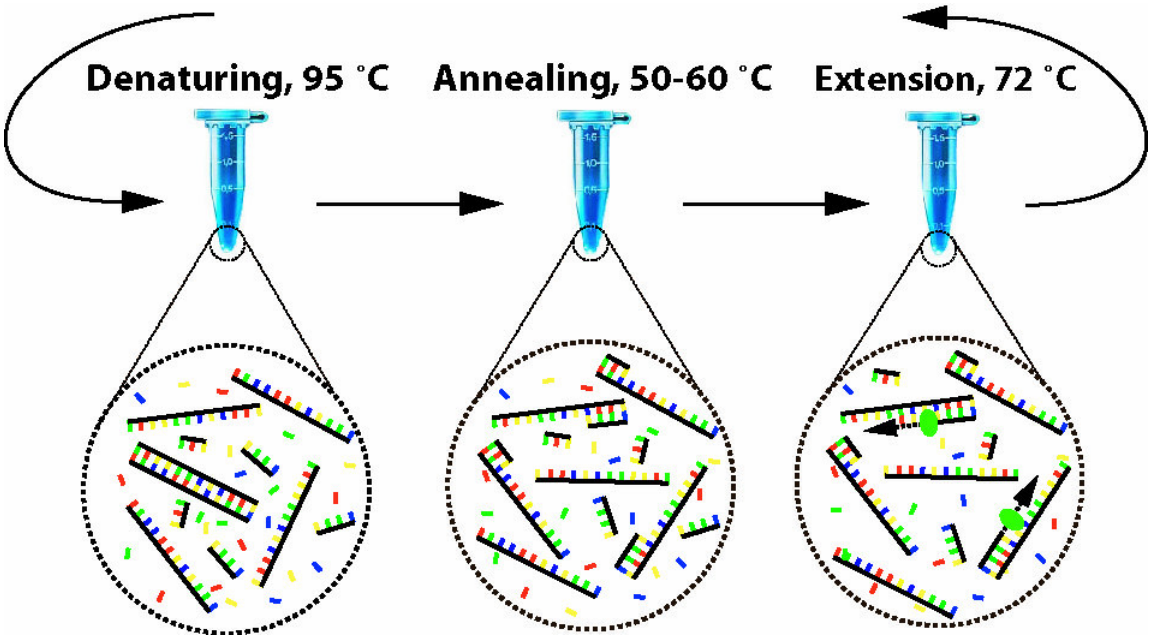

Figure 1.1 A 3-Step schematic of general PCR mechanism occurring in benchtop thermocyclers

Despite the advances in PCR biochemistry, the timescales required to perform a typical amplification reaction are still relatively slow, generally on the order of an hour or more - a rate much slower than would be expected based on kinetics alone. Under ideal conditions, this scheme yields a doubling of dsDNA (double-stranded DNA) copies of the target region upon completion of each cycle ($Y = (1 + x)^n$ where Y is the copy yield, n is the number of cycles, and x is the mean efficiency per cycle). The total time required to complete one cycle of amplification includes the time over which the temperature of the reaction mixture must be held constant at each temperature step ('hold time'), as well as the time required to heat and cool the reaction mixture between successive steps ('ramping time'). In conventional benchtop thermocyclers, cycling times are primarily limited by the rate at which inactive hardware elements (e.g. metal blocks) can be heated and cooled, rather than the kinetics of the reaction itself. Consequently, it is not uncommon for a 30 – 40 cycle amplification reaction to require 2 to 3 hours of total time to complete, thereby limiting achievable throughput. The high heat capacity of the metal block, combined with the relatively low thermal conductivity of the plastic tubes or multi-well plates used to contain the reagents, primarily limits the achievable amplification speed. The majority of time and electrical power consumed in the thermocycling process is wasted regulating the temperature of structural elements associated with the instrument hardware that have nothing to do with the reaction. While these designs are conceptually straightforward, the desire to provide faster cycling while maintaining adequate temperature control often introduces a considerable degree of electronic and mechanical complexity.

An innovative approach to tackle these complexities involves harnessing natural convective forces to perform thermal cycling (6-10). Convective thermocyclers use the same heat required to maintain PCR temperatures to simultaneously circulate reagents through each temperature zone thereby eliminating the unnecessary ramping time and energy requirements. Natural convection has been extensively studied and characterized in literature (11-13). Convective flows occur as a result of buoyant instabilities that develop due to differences in density at different locations within a fluid. At very large scales, for example, convectively generated ocean currents can give rise to devastating hurricanes. When the underlying physics are considered, a dimensionless parameter called the Rayleigh number emerges that expresses the ratio of buoyant forces to the restoring thermal and viscous diffusive forces.

$$Ra = \frac{\tilde{g}\beta\Delta T l^3}{\nu\kappa}$$

Here, $\tilde{g}$ is the local component of the acceleration due to gravity, β is the thermal expansion coefficient of the fluid, ΔT is the temperature gradient across the fluid body, l a characteristic length scale, ν is kinematic viscosity and κ is the thermal diffusivity. When Ra is below a critical value heat transfer occurs primarily by conduction, and when it exceeds the critical value heat transfer is dominated by convection. The critical Rayleigh number provides a characteristic value that determines the onset of flow due to natural convection. In the case of fluid confined between two infinitely wide horizontal surfaces separated by a vertical distance l, for example, the value of Ra_{crit} is approximately 1700.

Convective flows can occur in a variety of formats, including cavities and closed loops (11-13). In the closed loop case, often referred to as a thermosyphon, convection can be generated either by applying horizontal or vertical temperature gradients across the loop. The closed loop design with horizontal temperature gradient is particularly attractive for thermocycling applications because unidirectional flow through the loop can be generated allowing residence times within specific temperature zones to be precisely controlled. Rapid cycling times are achievable because the convected fluid elements are able to quickly attain thermal equilibrium with their surroundings as they are transported through successive temperatures without any time lag associated with heating and cooling inactive hardware components. These unique characteristics are ideally suited to meet the requirements of thermally actuated biochemical reactions like PCR.

In order for any advanced thermocycling instrumentation to seriously compete with current-generation systems, it must offer significant improvements in reaction speed at a greatly reduced cost in a format that requires little or no modification to existing laboratory protocols. In the current work, we present the development of a simplified closed loop convective flow thermocycling system that addresses these needs. This system is ideally suited for integration with upstream and downstream analysis and detection processes for automated operation with the capability of performing rapid DNA amplification. Using this system, PCR amplification has been performed in as little as 10 minutes with reactors constructed from ordinary plastic tubing mounted in an apparatus incorporating inexpensive thermoelectric heaters that do not require dynamic

temperature control. Robustness is demonstrated by amplifying a wide variety of target sizes in both single and multiplex formats incorporating 10–25 μL reaction volumes. Product yields are comparable to those achievable in a conventional benchtop thermocycler, and no modifications to conventional PCR protocols are necessary. We further show that reactor geometries satisfying virtually any combination of reagent volume and cycling time can be straightforwardly designed.

We also perform mathematical modeling of the proposed system and compare it with empirical results to provide a general correlation that can be applied to design reactor geometries satisfying virtually any combination of reagent volume and cycling time. The closed loop thermocyclers (CLTC) ultimately require no modifications to the existing PCR protocols and are capable of performing high speed DNA amplification in single as well as multiples formats with similar or better throughputs as compared to benchtop thermocyclers. The complete CLTC setup can be arranged in a small handheld assembly and is especially suited for onsite pathogen detection in emergency conditions where power availability is critical and an immediate response is required.

In the following background section, various PCR assays have been outlined with emphasis on the convection based thermocyclers that may become an integral part of the next generation thermocycling hardware. While closed loop thermocyclers are the focus of this work with demonstrated capabilities of performing high-speed PCR in a miniaturized and portable battery operated formats, electrophoresis results obtained under varying experimental conditions for different DNA templates are also highlighted in this work.

CHAPTER II

BACKGROUND AND SIGNIFICANCE OF PCR

All living organisms are composed of deoxyribonucleic acid (DNA) molecules that contain vital information defining the functionality and morphology of cells as well as the organism. Similar to human fingerprints, every individual's DNA has a unique pattern that differentiates it from others'. DNA molecules are composed of a unique sequence of repeating bases called adenine, guanine, cytosine and thymine. The sequence in which these bases are arranged within a DNA molecule is the key that determines the cell's characteristics. Analogous to the computer memory banks where all the information is stored as bits and bytes (zeros and ones); it is this specific sequence of the DNA base pairs that stores vital genetic information of every individual. Due to this feature of DNA molecules, genetic research has received overwhelming response in the past few years.

Since the advent of polymerase chain reaction in 1985 by Kary B. Mullis and co-workers (14,15), it has become a reliable and powerful diagnostic tool in forensic and genetic research. PCR is especially important in forensic science where minute amounts of valuable genetic samples are extracted from crime scenes that need to be amplified to detectable quantities for further investigation (16,17). In medical science, PCR is used to diagnose infected samples by amplifying specific regions of DNA (using appropriate oligonucleotides as primers) corresponding to bacteria, viruses or other pathogens based

on patient's symptoms. In genetic research, PCR plays a key role in identifying and investigating new genes, viruses and diseases (18).

The fundamental principle of PCR is well known wherein a mixture of reagents is repeatedly subjected to the three temperature cycles corresponding to denaturing (95°C), annealing (50-60°C) and extension (72°C) processes. The procedure enables precise multiplication of the targeted regions of DNA using amounts as little as one target molecule by five to six logs, making them easy to be handled and examined by routine molecular biological methods. The PCR is useful where the amount of starting material is limited, poorly preserved or many samples have to be processed in parallel.

DNA is a double stranded molecule that remains stabilized by weak hydrogen bonds established between its two complimentary single strands. All the A-T pairs form double hydrogen bonds while all G-C pairs form triple hydrogen bonds between them (Figure 2.1). When the DNA molecule is subjected to elevated temperatures of about 94°C or more, the vibrational energy of the molecule (due to gain in thermal energy) is enough to overcome these hydrogen bonds and the two strands separate, a process called denaturation. Usually, DNA molecules with lower G-C content require less energy for denaturation as compared to those with higher G-C content because more hydrogen bonds must be broken down in order to separate the two strands of DNA.

Subsequently, if the temperature is reduced to 50-60°C in the presence of specifically synthesized fragments of single stranded DNA (known as primers), then these primers bind to the 3' end of the denatured template DNA, a process called annealing. The temperature is then raised to 72°C and the polymerase enzyme from the reaction mixture binds to the annealed primer thereby facilitating the extension of the incomplete strand. Typically, about 30 cycles are sufficient to yield a billion copies of the original DNA target. Amplification output after each cycle depends on the number of initial template molecules used to initiate the PCR process. A general guideline of the number of copies generated after each cycle under ideal conditions is given in APPENDIX A. Denaturing and annealing occurs almost instantaneously while the extension timescale depends on the length of target sequence to be amplified. The amplicon extension rate ranges from 2kb-4kb per minute.

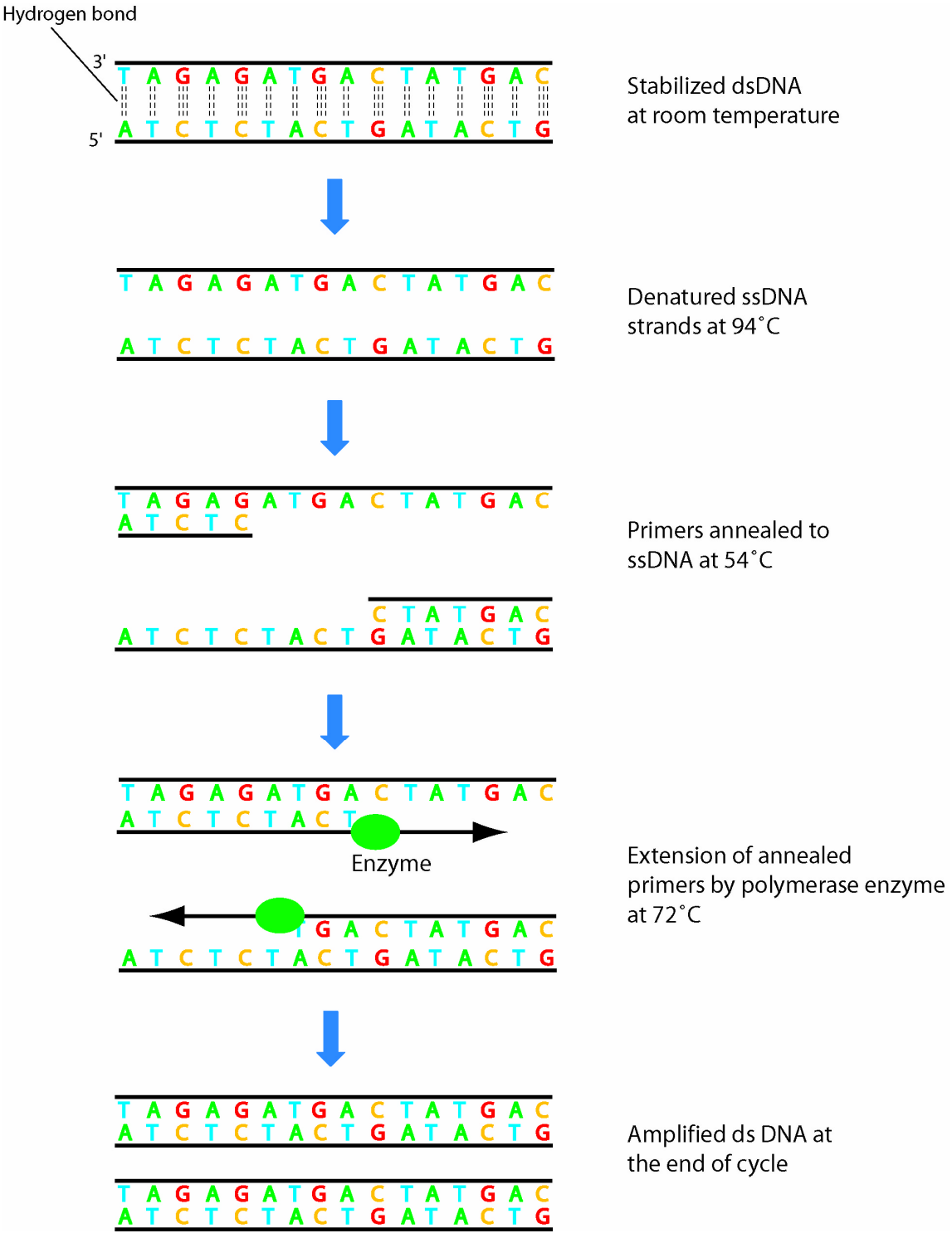

Figure 2.1 Schematic of the 3-step PCR cycle showing denaturing, annealing and extension processes

2.1 Factors affecting the fidelity of DNA synthesis during PCR amplification

DNA template: Usually the concentration of initial DNA template ranges from 0.01-1ng for plasmid or phage DNA and 0.1-1µg for genomic DNA, for a total reaction mixture of 50µL. Higher amounts of template DNA usually increase the yield of nonspecific PCR products, but if the fidelity of synthesis is crucial, maximal allowable template DNA quantities together with a limited number of PCR cycles should be used to increase the percentage of "correct" PCR products. Nearly all routine methods are suitable for template DNA purification. Although even trace amounts of agents used in DNA purification procedures (phenol, EDTA, Proteinase K, etc.) strongly inhibit *Taq* DNA polymerase, ethanol precipitation of DNA and repetitive treatments of DNA pellets with 70% ethanol is usually effective in removing traces of contaminants from the DNA sample. PCR is very sensitive to contamination from outside DNA.

Concentration of dNTPs: The concentration of each dNTP in the reaction mixture is usually 200µM. It is important to have equal concentrations of each dNTP (dATP, dCTP, dGTP, dTTP), as inaccuracy in the concentration of even a single dNTP dramatically increases the misincorporation level. When maximum fidelity of the PCR process is crucial, the final dNTP concentration should be 10-50µM, since the fidelity of DNA synthesis is maximal in this concentration range.

DNA polymerase: The availability of thermostable polymerases and the design of thermal cycler machines have made PCR widely accessible. DNA polymerase reads the

template and incorporates a complimentary nucleotide yielding a newly assembled complimentary strand. Usually 0.25 µL of 5 units/µL DNA polymerase is used in 50µl of reaction mixture. Higher polymerase concentrations may cause synthesis of nonspecific products. However, if inhibitors are present in the reaction mixture (e.g., if the template DNA used is not highly purified), higher amounts of DNA polymerase may be necessary to obtain a better yield of amplification products. All nucleic acid polymerases catalyze the addition of a deoxynucleotide or nucleotide monophosphate (NMP) to the 3' oxygen of an existing polynucleotide chain. High-fidelity DNA amplification will be best achieved by using a polymerase with an active 3'→5' proofreading exonuclease activity. For those enzymes that are proofreading-deficient, the in vitro reaction conditions can significantly influence the polymerase error rates. To maximize fidelity at the dNTP insertion step, any type of deoxynucleotide triphosphate pool imbalance should be avoided. Similarly, stabilization of errors by polymerase extension from mispaired or misaligned primer-termini can be minimized by reactions using short synthesis times, low dNTP concentrations, and low enzyme concentrations. Additional improvements in fidelity can be made by further manipulating the reaction conditions.

PCR buffer: PCR buffer (1X) provides optimal pH and salt conditions.

Concentration of $MgCl_2$: While performing new PCRs, it is usually recommended to do magnesium optimization and the optimal magnesium chloride concentration should be

determined empirically by testing concentrations up to 4 mM $MgCl_2$ for each set of primers. Since Mg^{2+} ions form complexes with dNTPs, primers and DNA templates, the optimal concentration of $MgCl_2$ has to be selected for each experiment. Too few Mg^{2+} ions result in a low yield of PCR product, and too many increase the yield of non-specific products and promote misincorporation. Lower Mg^{2+} concentrations are desirable when fidelity of DNA synthesis is critical. The recommended range of $MgCl_2$ concentration is 1-4mM, under the standard reaction conditions. If the DNA samples contain EDTA or other chelators, the $MgCl_2$ concentration in the reaction mixture should be raised proportionally.

Primer design and specificity of primers: PCR Primers are short single-stranded, synthetically synthesized oligonucleotides usually shorter than 50 nucleotides (often 18-25 nucleotides). During the PCR annealing cycle, primers anneal to the complementary region of the DNA. PCR primers are important as they are complementary to the beginning and end of the DNA fragment of interest which one needs to amplify. Primers therefore select the boundaries of the region to be amplified by PCR. DNA polymerase binding and the 3' -OH of the oligonucleotide allows the synthesis of DNA to occur. Primers anneal to denatured DNA at homologous regions. A large number of criteria for the primer design can be set. Following parameters are considered for choosing a specific set of primers (19):

(i) *Melting temperature (Tm) of primer:* Calculated Tm (melting temperature) for both primers used in reaction should not differ >5°C. If the primer is shorter than 25 nucleotides, the approximate melting temperature (Tm) is calculated using the following formula:

$$Tm = 4 (G + C) + 2 (A + T)$$

G, C, A, T - number of respective nucleotides in the primer.

Annealing temperature should be approximately 5°C lower than the melting temperature. However it should be chosen empirically for individual conditions. Optimal Tm is ~ 50-60°C.

(ii) *Length:* Primers are usually chosen to be between 18-25 nucleotides in length. During PCR, a GC clamp at the 5' end of the primers is useful. Thus it is recommended to design primers with 1 or 2 nucleotides GC at the start and ends of the primers.

(iii) *GC content:* Oligonucleotide GC-content should be between 40-60%.

(iv) *Primer concentration:* In PCR reactions usually primer concentration is 50pmol of each primer per reaction. Two primers are required to amplify the target DNA sequence for most PCR reactions. Primers are diluted in the sterile water free from DNAse (that catalyzes the cleavage of DNA).

(v) *Self annealing:* Inner self-complementary hairpins of >4 and of dimers >8 should be avoided.

(vi) *Secondary structure:* Primers should not have any extensive secondary structure or self-complementarities (can result in Primer-dimers).

(vii) *3' end G/C restrictions:* 3' terminus is extremely case sensitive - it must not be complementary to any region of the other primer used in the reaction and must provide correct base matching to template. A low G/C content of the primer/probe 3' end increases the specificity of the reaction. A high G/C content facilitates a tight binding of the oligonucleotide to the template but also increases the possibility of mis-priming.

(viii) *5' end G/C restrictions:* Primers should end with 1-2 G or C residues which increases the specificity of reaction.

Cycling Conditions: Amplification parameters depend greatly on the template, primers and amplification apparatus used. It is relevant to ensure sufficient residence times for each cycling steps. An initial denaturing step facilitates in obtaining better yields. Similarly, care should be taken to provide sufficient residence time for the extension process depending on the length of the target amplicons.

2.2 Detection and analysis of the amplified products (gel electrophoresis)

In molecular biology, DNA gel electrophoresis has emerged as one of the most important tools in many aspects of genetic manipulation and identification of viral, plasmid or particular segments of chromosomal DNA. The term electrophoresis refers to the migration of charged particle under the influence of an electric field. The term *Electro* describes the energy of electricity and the word *Phoresis*, is derived from a Greek verb *phoros*, meaning "to carry across." DNA Gel electrophoresis is a procedure

that separates negatively charged DNA molecules on the basis of their size that affects their mobility through a gel under the influence of an electrical field. In gel electrophoresis DNA molecules normally migrate from negative to positive potential due to the net negative charge of the phosphate backbone of the DNA chain. The electrical charge at cathode (-) repels the negatively charged DNA molecules while the anode (+) simultaneously attracts the molecules forcing migration of DNA molecules across a span of gel. The frictional force of the porous gel matrix acts as a "molecular sieve" while the driving force is provided by the activated electrodes at either end of the gel. Other physical properties of the DNA molecule such as size of DNA molecules determine how fast an electric field can move it through the gel. Longer DNA molecules migrate more slowly because they are more easily 'trapped' in the gel matrix. The separated DNA molecules in each lane can be seen in as series of bands spread from one end of the gel to the other. After the separation is completed, the fractions of DNA fragments of different length are often visualized using a fluorescent dye specific for DNA, such as ethidium bromide or SYBR Green I. The gel shows bands corresponding to different DNA molecules with different molecular weight or conformation. Depending upon whether single- or double-stranded DNA has been separated, fragment size is measured in "base pairs" (bp), "nucleotides" (nt) or "kb" (for kilo base pairs). Fragment size determination is done by comparison to commercially available DNA ladders containing linear DNA fragments of known length.

2.2.1 *The equipment and chemicals required for agarose gel electrophoresis*

An electrophoresis chamber and power supply: Gel electrophoresis equipment consists of electrophoresis chamber and a power supply. An electrophoresis chamber allows maintenance of a uniform electric field across a gel. It also provides for a cooling effect that prevents thermal artifacts and allows access to the gel for convenient loading and monitoring. An electrophoresis chamber consists of a positive and a negative charged pole generated by electrical currents to separate molecules. These chambers can be in horizontal or vertical forms. Horizontal gel electrophoresis chambers are boxes divided into two compartments by a middle platform. Gel electrophoresis equipment uses an electrophoresis power supply attached to electrophoresis chamber to provide a regulated electric current to separate the charged molecules.

Gel casting trays: These are composed of UV-transparent plastic. The open ends of the trays are closed with tape while the gel is being cast, then removed prior to electrophoresis.

Sample well combs: These are used to make sample wells in the agarose gel. These wells provide a different migration path to each of the DNA samples. Different DNA samples are inserted into each migration path and moved under the influence of electrophoresis.

Loading buffer: It contains highly dense and viscous glycerol to allow the sample to stay inside the sample wells, and one or two tracking dyes such as bromophenol blue and

Xylene cyanol, which migrate in the gel and allow visual monitoring of how far the electrophoresis has proceeded. Bromophenol blue and Xylene cyanol dyes migrate through agarose gels at roughly the same rate as double-stranded DNA fragments of 300 and 4000 bp, respectively. DNA bands are stained only by the amount of Ethidium in the dye, thus allowing the buffer and agarose to be free of Ethidium contamination.

The agarose gel is a cross-linked matrix that is somewhat like a three-dimensional mesh or screen. The types of gel most commonly used for DNA electrophoresis are agarose (for relatively long DNA molecules) and polyacrylamide (for high resolution of short DNA molecules, for example in DNA sequencing). Agarose is a linear polysaccharide (average molecular mass of about 12,000) made up of the basic repeat unit agarobiose, which comprises alternating units of galactose and 3,6-anhydrogalactose. Agarose is usually used at concentrations between 1% and 3%.Gels have conventionally been run in "slab" formats, but capillary electrophoresis has become important for applications such as high-throughput DNA sequencing. Electrophoresis techniques used in the assessment of DNA damage include alkaline gel electrophoresis and pulse field gel electrophoresis.

Ethidium bromide and SYBR Green I are common dyes used for detection of DNA on the agarose gels. Ethidium bromide is an intercalating fluorescent dye. They insert themselves between the bases that are stacked in the center of the DNA helix. One dye molecule binds to one base. As each dye molecule binds to the bases the helix is unwound to accommodate the strain from the dye. The quantum yield of the SYBR Green I-DNA complex is greater than that of equivalent ethidium bromide-DNA

complex and the fluorescent enhancement is >1000 times greater. As a result, less than 20 pg of double stranded DNA can be detected in an agarose gel which is up to 25 times less than amount visible after ethidium bromide staining (20).

Unknown DNA samples are usually run on the same gel with a ladder or a marker. A ladder is a sample of DNA where the sizes of the bands are known. Unknown fragments of DNA are compared to the ladder fragments and the approximate size of the unknown DNA bands is determined on the basis of how they match up to the known bands of the ladder.

The fast and reliable documentation of gel electrophoresis experiments is one of the most frequently applied bioimaging techniques in molecular biology labs today. Transilluminator is an ultraviolet light box is used to visualize ethidium bromide-stained DNA bands in gels. Protective eyewear should be worn while observing DNA on a transilluminator to prevent damage to the eyes from UV light.

2.2.2 Procedure for gel electrophoresis

Electrophoresis buffer (1x TAE or 0.5x TBE) is prepared to make a solution of agarose and for filling the electrophoresis tank. To make a gel solution, agarose powder is mixed with electrophoresis buffer to the desired concentration and is heated on a hot plate until completely melted. Gel is poured into a casting tray containing a sample comb and allowed to solidify at room temperature. After the gel gets polymerized, the comb is removed carefully and DNA samples are pipetted into the sample wells after filling the electrophoresis tank with buffer. Suitable DNA marker is also loaded into one of the

well (usually the first well). The lid is placed on the electrophoresis tank and tank is connected to the power supply and a current at appropriate voltage is applied. The flow of current can be confirmed by observing bubbles coming off the electrodes and migration of loading dye on to the gel. The distance DNA has migrated in the gel is judged by visually monitoring migration of the tracking dyes. DNA fragments are visualized by staining with ethidium bromide or SYBR Green I once adequate migration has occurred. Ethidium bromide is a fluorescent dye that intercalates between bases of DNA and can be seen in UV light. The presence of ethidium bromide helps visualize DNA at any stage during electrophoresis. The gel is usually stained after electrophoresis by soaking in a dilute solution of ethidium bromide but it can also be incorporated into the gel so that staining occurs during electrophoresis. SYBR Green I is used to stain a DNA by soaking the gel in diluted solution after separation of the DNA fragments. SYBR Green I should not be added to the molten agarose or the gel before electrophoresis because its presence in the gel may interfere with the electrophoretic properties of DNA causing deviations in the actual migration speeds. To visualize DNA bands the gel is placed on the ultraviolet transilluminator and the size of DNA fragments is determined by comparing it with bands of the ladder.

2.2.3 Factors affecting rate of migration of DNA molecules in electrophoresis

There are several factors that affect DNA migration through the polymerized agarose gel. The direction of movement of the DNA molecules is affected by the charge

of the molecules, and the rate of movement is affected by their size and shape, the density of the gel, and the strength of the electrical field.

Size and shape of DNA molecules: Fragments of linear DNA migrate through agarose gels with a mobility that is inversely proportional to the $\log_{10}$ of their molecular weight. Rate of migration also depends on the topological form of DNA (21). Circular forms of DNA migrate in agarose distinctly differently from linear DNAs of the same molecular weight. Circular forms of DNA such as uncut plasmids migrate more rapidly than the linearized plasmid. The supercoiled forms of plasmid DNA migrate faster than the nicked circular plasmid DNA.

The density of the gel medium: Higher concentrations of agarose facilitate separation of small DNA fragments while low agarose concentrations allow resolution of larger DNA molecules. Thus, by using gels with different concentrations of agarose different sizes of DNA fragments can be resolved. There is a linear relationship between the logarithm of electrophoresis mobility of the DNA (μ) and the gel concentration (T) that is described by the equation:

$$\log \mu = \log \mu_0 - K_r T$$

where μ_0 is the free electrophoretic mobility of the DNA and K_r is the retardation coefficient, a constant related to the properties of the gel and the size and shape of the migrating molecules (20).

Voltage: As the voltage applied to a gel is increased, larger fragments migrate proportionally faster than those small fragments. Therefore, the best resolution of fragments larger than about 2 kb is attained by applying no more than 5 volts per cm to the gel (the cm value is the distance between the two electrodes (20). The rate of migration of the linear DNA-dye complex through the gel is consequently retarded by a factor of 15.

The presence of labeling dye in the gel and electrophoresis buffer: Intercalation of the labeling dye causes a decrease in the negative charge of the double stranded DNA and an increase in both its stiffness and length. It binds to DNA with no sequence preference. At saturation in solutions of high ionic strength one ethidium bromide molecule intercalates per 2.5 bps of DNA (22).

CHAPTER III

LITERATURE REVIEW: TRADITIONAL PCR APPROACHES

Several PCR instruments have been proposed in the past few years that can be divided into two major categories: (i) stand-alone thermocyclers and (ii) continuous flow thermocyclers, depending on how the reactants navigate through the three cycles. Moreover, developments in microfluidics have gained great attention towards performing PCR in microfluidic platforms utilizing both stand-alone and continuous flow technologies. The continuous flow type thermocyclers are further categorized as (i) unidirectional, (ii) oscillatory and (iii) closed-loop thermocyclers.

In most stand-alone or benchtop PCR instruments, the temperature is repetitively alternated while maintaining the sample stationary, which makes it necessary to heat and cool the heating block along with the reagents placed within the block. This results in considerable thermal inertia, and makes the process relatively slow and energy-intensive. On the contrary, in continuous flow PCR reactors, the reagents are continuously propelled or circulated through the stationary thermal zones individually maintained at the corresponding PCR temperatures allowing reagents to rapidly attain thermal equilibrium as they pass through various temperature zones.

3.1 Stand-alone thermocycling approach

A considerable amount of research has been done since the invention of PCR to characterize the overall process and to maximize the ultimate throughput. The most

popular PCR instrument until recently has been the conventional benchtop thermocyclers implementing a stationary hot-plate arrangement consisting of a metal block designed to accept a multi-well array. This plate is actively heated and cooled 30-35 times to cycle the PCR reagents through appropriate temperatures. Individually loaded thin-walled plastic vials are placed in the wells as PCR reactors. The multi-well design offers a consistent, robust and high-throughput performance enabling several reactions to be performed simultaneously. Due to these features, benchtop thermocyclers are reliably used to carry out control reactions in the development of new technologies. While these thermocyclers have proved to be reliable, they suffer from limitations associated with cost and exorbitant time/energy consumption associated with active heating and cooling of the metal block. The heat capacity of the block imposes high thermal inertia thereby slowing down the temperature ramping time and causing unnecessary energy consumption. Also, these instruments are equipped with complex electronic circuitry for programmable controls making the equipment bulky and stand-alone.

Many approaches have been investigated to overcome these limitations, including replacing plastic reaction tubes with thin glass micro-capillaries to achieve more efficient heat transfer (e.g. Light Cycler, Roche) (23-25), and robotically transporting reagents between physically separated constant-temperature surfaces (e.g., RoboCycler, Stratagene). The capillary PCR approach successfully addresses the “ramping time” issues associated with the benchtop equipments enabling lower response times to achieve successive temperatures. Also, capillaries offer a platform to handle

extremely small amounts of reaction volumes. However, high surface to volume ratios associated with glass capillaries enhances binding interactions of the negatively charged DNA molecules with the glass surface. Wittwer and co-workers in 1989 proposed a capillary based thermocycler integrating relay operated valves to control the air flow into the reaction chamber (23). While a high power nichrome heating element (1000 W, 125 VAC) was used to maintain hot air supply making the whole device power intensive. A successful amplification of 560 bp fragment of *E. Coli* DNA was demonstrated using 100 μL of reaction volume. Capillary PCR was an improvement over the water bath based PCR designed proposed by Franco Rollo and his team in 1988 (26). They described an assembly containing several pumps and valves to drive hot water into the reaction chamber holding the PCR mixture. By operating a set of pumps and valves at a time, denaturing, annealing and extension could be achieved. In the race of automating the DNA amplification process, Foulkes group described a similar assembly using water baths; however, instead of pumping hot water into the reaction chamber, they suggested to utilize stationary water baths maintained at PCR temperatures and mechanically transporting the PCR tubes through subsequent baths for 30 cycles. Considering the immature level of the PCR technology during that time, these ideas have served a significant role in the development of current generation bio-analysis equipments.

Fundamentally, thermal cycling can be accomplished in two ways, either by contact heating or by non-contact heating. While non-contact heating involves remote heating source (e.g. an infrared/laser source) that is not in physical contact with the PCR reaction chamber, contact heating on the other hand includes heating elements fabricated

onto the microchip itself or an external heating source in thermal contact with the microchip. Both the methods have their advantages and disadvantages for example non-contact heating allows focused heating using commonly available infrared lamps with an ability to achieve fast heating/cooling rates. On the contrary, contact heating always contributes to some thermal inertia which severely inhibits the cycling times depending on the magnitude of the associated thermal mass. Detailed explanation of both heating techniques has been provided in the following sections with supporting literature review describing the pros and cons of each technique.

3.1.1 PCR through non-contact heating

To overcome the time lags associated with large thermal mass of the heating/cooling block, an approach was proposed to utilize focused infrared radiations to selectively heat only the reagents rather than heating the entire hardware block holding the reagents. This allows heating and cooling to be achieved at very high rates with significantly reduced ramp times. Moreover, infrared sources are inexpensive, easy to assemble and readily available in a variety of geometries and specifications. Considering these features associated with the infrared mediated non-contact heating approach, a second generation microfluidic PCR system utilizing a remote tungsten heat source was proposed by the Landers group in 1998 (27). A rectangular borosilicate glass chamber capable of holding about 28μL reagents was used to construct the reactor following the surface passivation steps to avoid binding interactions. Labview program was used to control the infrared lamp for heating and the solenoid valve for cooling (using

compressed air at room temperature). This technique demonstrated high rates of heating and cooling (10°C/sec and 20°C/sec respectively) with cycle times as short as 17 sec. Continuing their efforts of achieving faster cycles incorporating extremely low volumes, Landers group exploited the advantages associated with both capillary PCR and non-contact heating methods (28). They developed a thermal cycler comprising fused silica microcapillaries as PCR reactors and achieved rapid heating and cooling rates utilizing the previously used infrared lamp source. Successful amplification of a 150 nL sample of 500 bp fragment from λ-Phage DNA was demonstrated within 30 minutes of reaction time. Temperature measurements were carried out in an adjacent capillary incorporating miniature thermocouples and loaded with the same PCR reagents as the sample capillary. Infrared radiation was filtered and focused on the PCR chamber through converging lenses and filters. Thorough surface treatment was required prior to the PCR process for all the above techniques to avoid the deactivation of enzymes by adsorption to the reactor's surface.

Meanwhile, Braun and co-workers also reported their work based on non-contact heating technique where a laser beam was used to heat a specific location of the PCR sample while generating convective motion within the fluid (29). The generated convective forces are sufficient to drive the reagent molecules through different regimes developed within the fluid due to temperature gradient from the hot spot. Detailed explanation of this work will be discussed in the later section dedicated to convective PCR approaches.

3.1.2 PCR through contact heating

Despite the obvious advantages of lower thermal mass and faster cycling times associated with non-contact printing, this technique suffers from complexities involved with surface passivation steps and requires optical hardware to focus the infrared radiations at a confined region thereby limiting the overall throughput of the amplification process and making the entire assembly cumbersome. Moreover, loading and sealing microcapillaries can be complicated and may require specialized skills. Hence, most of the recent work in revolutionizing the PCR technology involves the contact heating approach. Although microfluidic devices also contribute towards a small amount of thermal mass, its magnitude is usually significantly lower as compared to the conventional block type assembly. Also, advancements in microfabrication technology allow integration of multiple functionalities on a single device minimizing analysis time and sample requirements. Therefore, majority of the work in microfluidic PCR technology has been directed towards investigating techniques using contact heating methods. Heaters can be fabricated on the chip itself allowing the entire hardware to be assembled in a miniaturized and portable format.

Some of the most common commercially available PCR instruments including the conventional benchtop thermocyclers (utilizing the metal block assembly) still utilize the contact heating approach. Since 1985, majority of the advanced PCR techniques proposed till date rely on contact heating method due to its ability to support miniaturized microfluidic devices with integrated heaters. The following section refers to

the microfluidic PCR approaches that have been proposed so far of which most of the techniques involve PCR chip utilizing contact heating strategy.

3.2 Microfluidic DNA amplification

Lately, significant efforts have been directed toward performing PCR in miniaturized microfluidic systems that, by virtue of their small size, can be rapidly heated and cooled with a high level of temperature homogeneity (30-33). Moreover, genomic analysis often involves multiple steps starting with the purification of complex biological fluids followed by DNA amplification and subsequent separation and detection steps of the amplified products.

The ability of microfluidics to integrate multiple functionalities on a single device combined with the advancements in microfabrication technology to reproducibly manufacture sub-micrometer structures on silicon and glass substrates has provided novel platforms for microscale DNA analysis studies in high speed formats. Microfluidic DNA amplification can be performed either in stand-alone or in the continuous format. Since 1985, several research groups have been trying to investigate different techniques to optimize the PCR efficiency and throughput. Despite the advancements in PCR technology, it still suffers from drawbacks such as high cost associated with each reaction due to expensive reagents and the sensitive nature of the reaction itself which is prone to contamination. Also the expanding applications of PCR has build up significant attraction within the scientific community to extend the current PCR technology to the

next level offering high throughput in miniaturized, portable and battery powered devices.

In 1993, Northrup and co-workers harnessed the significantly high thermal conductivity of silicon to construct the first prototype of microfluidic device for chip based PCR (34). Wilding et al. then constructed a similar silicon/glass hybrid PCRChip by etching 40-80 μm deep microchambers on a silicon wafer capable of holding 5-10 μL of PCR reagents (35). Wafer was capped with Pyrex glass by anodic bonding and holes were made at the ends to provide inlet and outlet ports. Heating was achieved placing the chip on a computer controlled peltier heater as shown in Figure 3.1.

Amplification of a 500 bp segment of bacteriophage λ-DNA was demonstrated with total cycling time of 1 hr. 45 mins. This was the first prototype of a PCR chip utilizing small amount of reaction volumes. However, similar to the capillary PCR, it was shown that silicon chips also demand for the surface treatment before a successful amplification can be demonstrated. It was later shown that silanization of the chip surface can provide best performance (36). Subsequently, similar devices were presented by several other research groups in different formats utilizing the continuous flow-through microchannels.

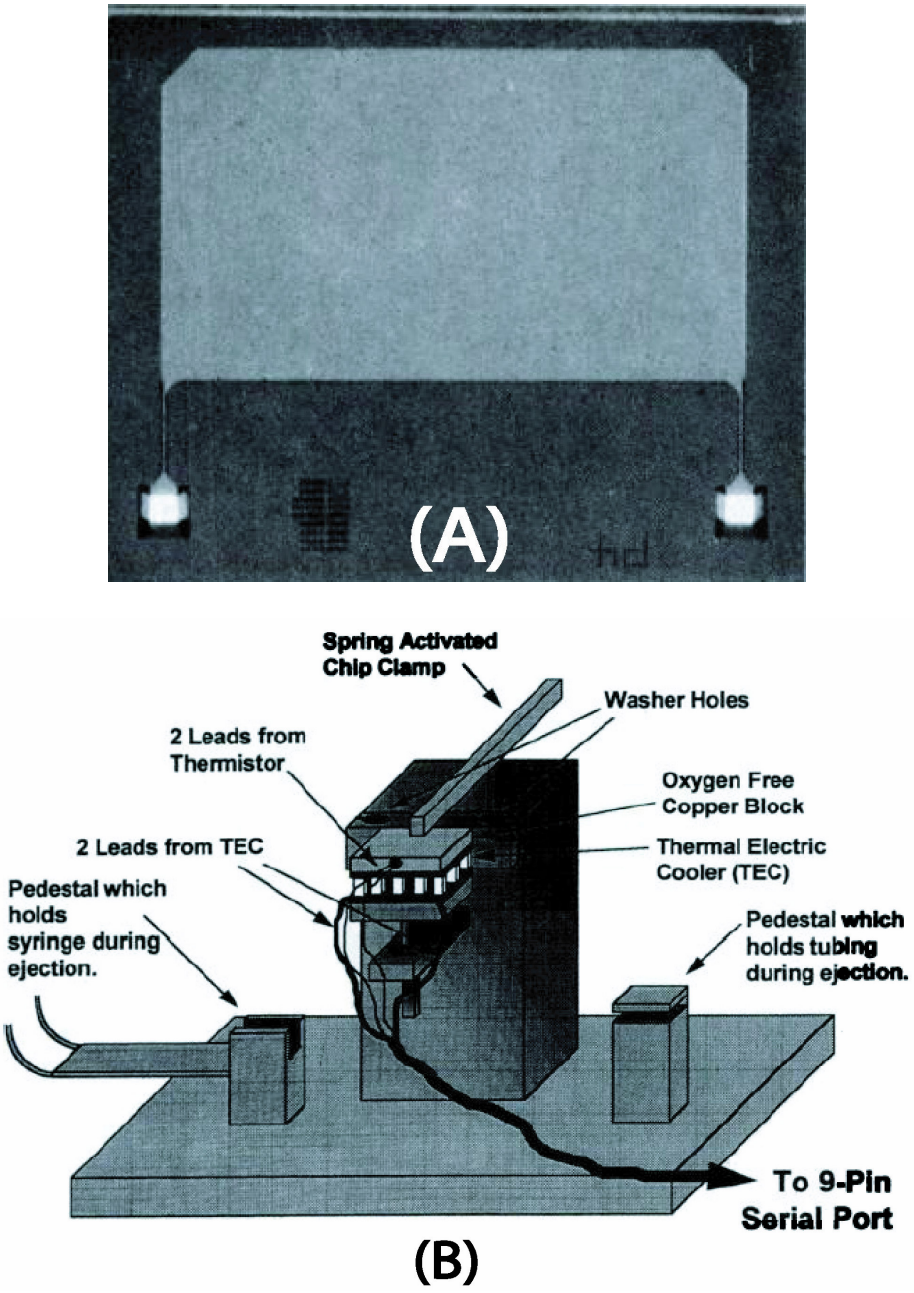

Figure 3.1 (A) The photograph of a single-chamber PCRChip etched on a silicon wafer. Silicon wafer is capped with Pyrex glass. Two white dots represent the inlet and outlet holes. Overall dimension of the chip is 17 x 15 mm and micro-well depth of 80 μm with total chamber volume of about 9 μL. (B) Schematic of the entire PCR apparatus assembly excluding the computer. Adapted from reference (35)

3.3 Continuous flow PCR

In continuous flow reactors, the reaction chamber (channel, well or any type of reactor) remains static while the reactants within the reactor move and travel through the various PCR temperature zones. This movement of reagents can be accomplished either by some sort of pumping mechanism or by utilizing buoyancy driven natural convective forces. The principle of continuous flow PCR was initially introduced by Nakano et al. (37) while others demonstrated the advantages of continuous PCR in microfluidic devices. The continuous PCR can be categorized as unidirectional (37-42), oscillatory (43) and closed loop (44-47) systems.

In unidirectional continuous flow PCR, usually the reaction mixture of PCR is driven by a pump at a constant flow rate. The sample travels across the three successive thermal stages as a function of the position in the channel. An example of the microfluidic unidirectional reaction system is shown in Figure 3.2 developed by Kopp et al. (38). The three bands of heaters are maintained at three PCR temperatures and the samples are pumped through the continuous channel while it travels back and forth through the specified temperature regimes. Flow rates ranging from 1.5 - 18.7 minutes were obtained and a successful amplification of 176 bp was demonstrated.

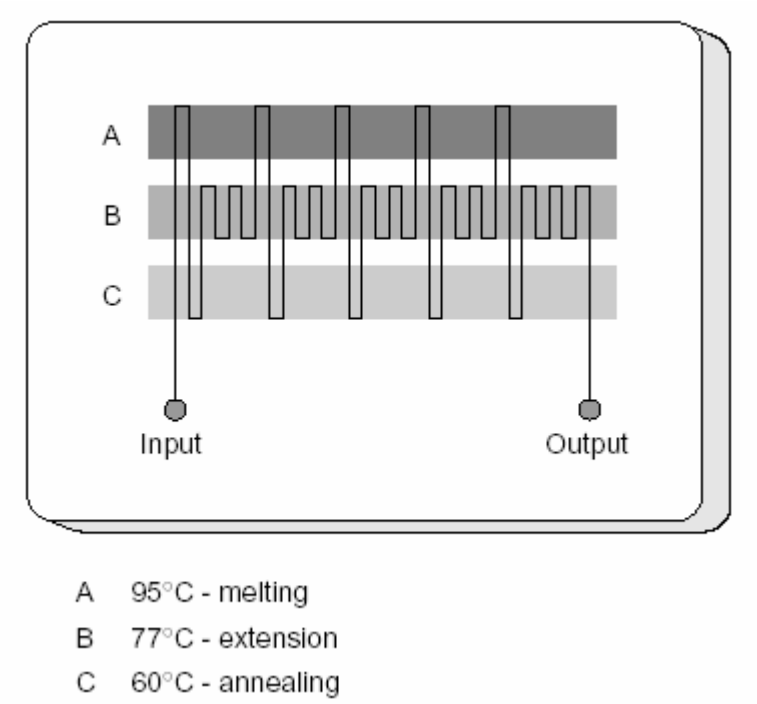

Figure 3.2 Schematic of a continuous flow PCR chip. Zones A, B and C are maintained at 95, 77 and 60°C by thermostated copper blocks. Samples are hydrostatically pumped through the inlet and collected at the outlet after 20 identical cycles. Picture adapted from (38)

In closed loop continuous flow, the samples are continuously propelled in the closed-loop format. Driving forces are generated either by using pneumatic valves or by utilizing convective forces. Liu et al. in 2002 developed a 3-layer closed loop network by fabricating heaters on one of the layers, sample channels on the other and the control channels on the third layer (44). The control channels were used to pneumatically drive and control the flow of reacting fluids in the closed loop within the sample channels. Figure 3.3 shows the three layer system consisting of heaters and the sample and control channels.

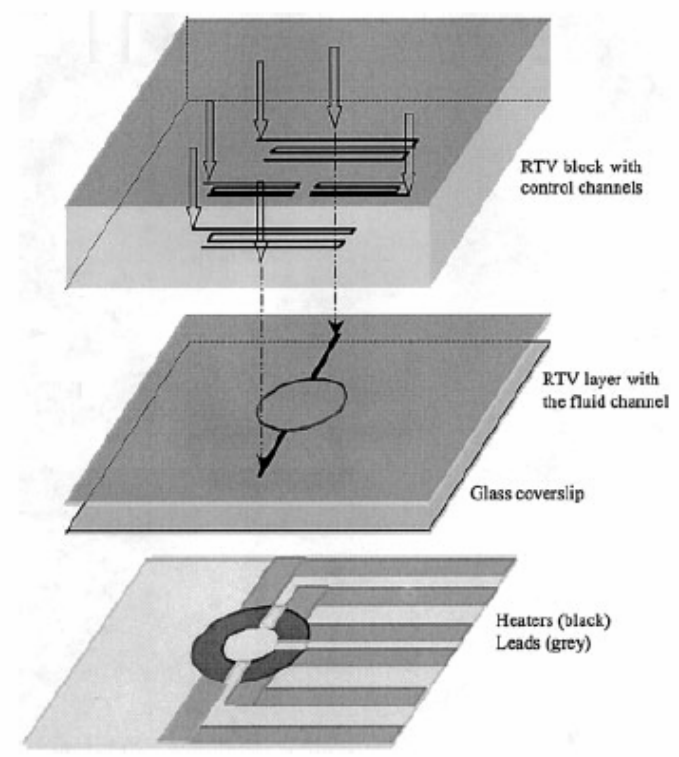

Figure 3.3 Schematic of the closed loop continuous flow cycling system. Top layer shows the control channels that are pneumatically actuated to control the samples in the middle channel which is the main reactor. The bottom layer shows the heaters and the connecting leads that are individually maintained at constant temperatures. Picture adapted from (44)

The in oscillatory continuous flow systems, the reagents are moved back and forth across the PCR temperature zones using a valve or a pumping mechanism. Bu et al. in 2003 presented an oscillatory type PCR system consisting of a bi-directional peristaltic pump actuated by three piezoelectric disks fabricated on the chip (43). A 1 μL drop of sample is injected into the reaction channel and is moved back and forth by the bi-directional pump across the temperature zones maintained at 90, 72 and 55℃. Flow rates of 3.14 μL/s were observed using this kind of pumping mechanism. Figure 3.4 shows schematic of the complicated oscillatory flow system.

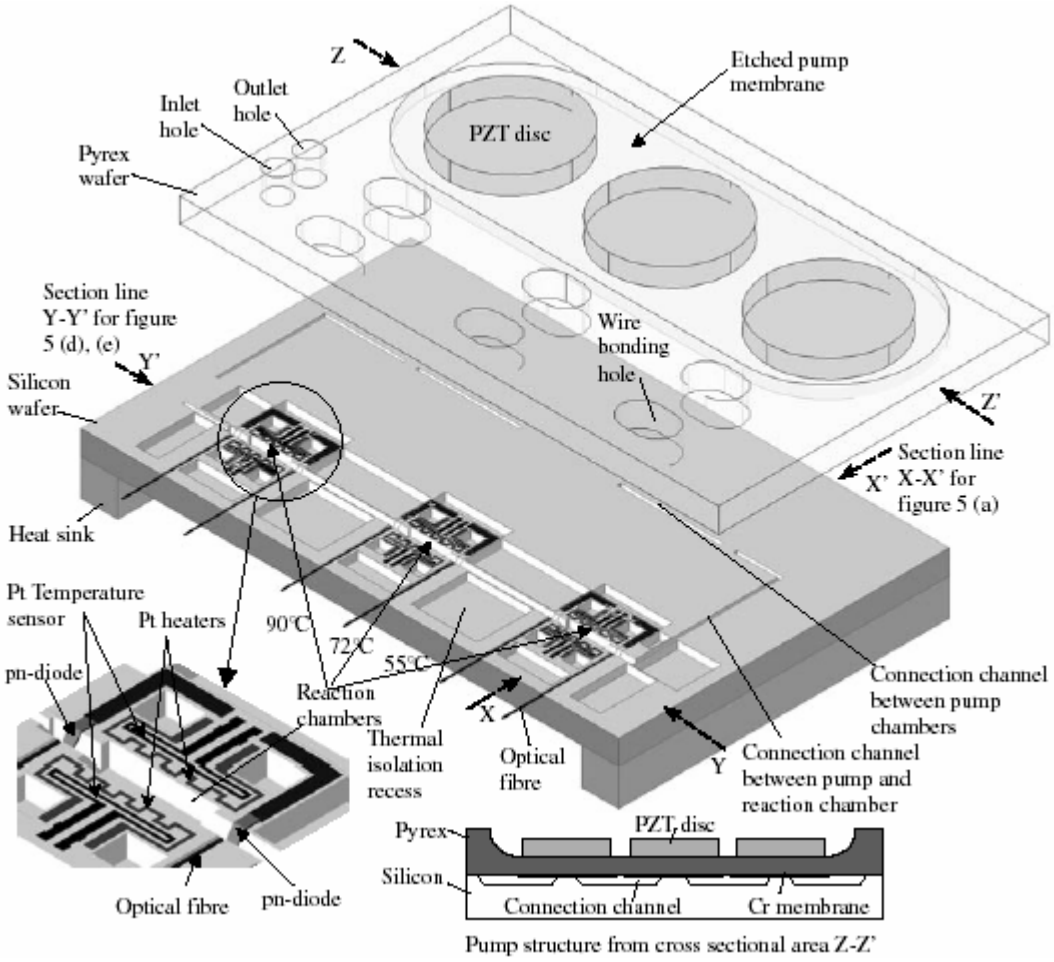

Figure 3.4 Schematic of the oscillatory flow network fabricated on a chip. The Piezoelectric disks are used to actuate a bi-directional peristaltic pump that drives the fluids back and forth through the PCR temperature zones. Picture adapted from (43)

Despite the advantages of dealing with significantly reduced thermal mass of the microchips, the continuous-flow PCR reactors mandates some sort of additional instrument for example, a syringe pump to propel the fluid. The micro- to nano-liter reaction volumes used in these systems are advantageous from the standpoint of achieving faster cycling times while simultaneously minimizing reagent consumption, however they are also accompanied by inherently high surface to volume conditions that can lead to non-specific binding interactions at the reactor walls that severely inhibit amplification. These issues, combined with complexities associated with integrating on-chip fluidic metering, pumping, mixing, reaction, and analysis operations in a format compatible with existing laboratory protocols, have thus far limited widespread adoption of these technologies and a variety of issues still remain to be addressed before performance and versatility comparable to conventional instruments can be achieved (30,35,48-51).

CHAPTER IV

ADVANCED PCR APPROACHES*

In order for any advanced thermocycling instrumentation to seriously compete with current-generation systems, it must offer significant improvements in reaction speed at a greatly reduced cost in a format that requires little or no modification to existing laboratory protocols. An emerging approach to address the limitations of conventional thermocycling hardware involves harnessing the combined advantages of both contact and non-contact heating methods. For example, the contact heating method allows miniaturization capabilities as the heating elements can be fabricated on chip itself without requiring any optical hardware to focus the IR radiation, while the non-contact heating approach offers the advantages of reducing thermal inertia allowing selective heating/cooling of the fluid and not the inactive structure. However, both of these characteristics can be combined by utilizing the effects of thermally driven convective flows to perform self-driven thermal cycling. These flows arise as a natural consequence of buoyancy driven instabilities that occur when a fluid is subjected to a temperature gradient. For example, if a confined liquid is heated from below a gradient in fluid density is established that is capable of generating a continuous circulatory flow between the upper and lower surfaces. This phenomenon can be applied to perform thermocycling by designing reactors in which a convective flow field is harnessed to

---

* Part of the data reported in this chapter is reprinted with permission from "A buoyancy-driven compact thermocycler for rapid PCR" by Agrawal, N. & Ugaz, V.M., (2006) *Journal of the Association for Laboratory Automation*, **11**, 167-284. Copyright 2006 by Elsevier, Inc.

continuously transport reagents through temperature zones corresponding to denaturing, annealing, and extension processes (Figure 4.1) (6).

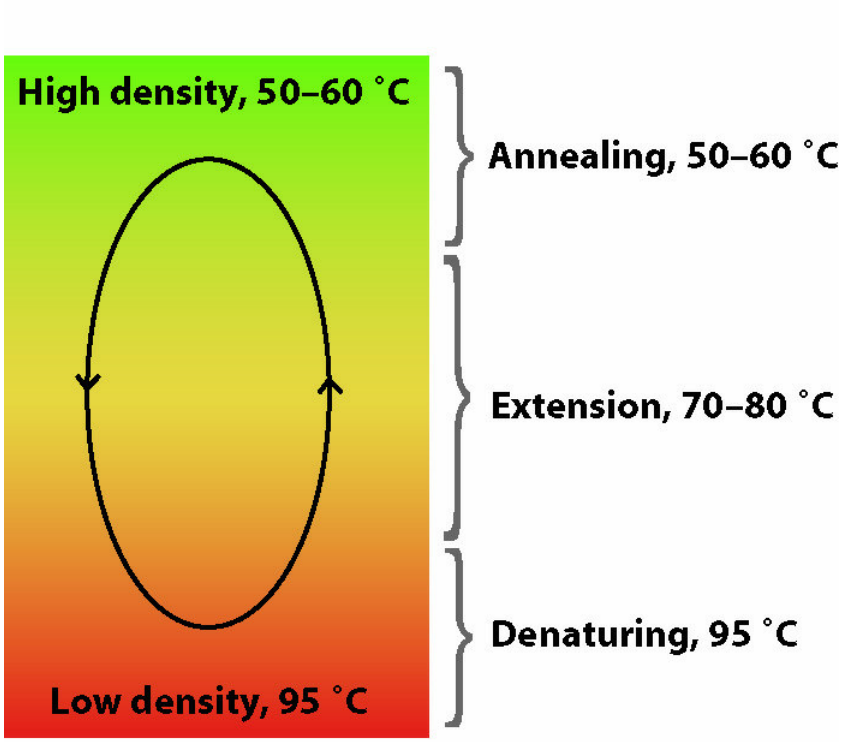

Figure 4.1 Schematic of the convective thermal cycling inside a cavity. When heated from below, a temperature gradient profile develops within the cavity providing sufficient buoyancy forces to start convection and to generate Rayleigh Benard cells

The relatively large variations in the magnitudes of temperatures required to perform PCR induce sufficient density difference within the fluid elements at different locations in order to generate convective motion (in the vertical plane). Under appropriate conditions, this convective motion can be precisely controlled and characterized to obtain desired cycle times. Since these systems merely require opposing surfaces of the reactor to be maintained at constant temperatures (i.e., the two reaction extremes: denaturing and annealing), dynamic thermal control is no longer needed and

the level of hardware complexity is greatly reduced. More importantly, rapid cycling times are achievable because the convected reagents are able to quickly attain thermal equilibrium with their surroundings as they are transported through successive temperature zones without the time lag associated with heating and cooling inactive hardware components.

Convective flow PCR in enclosed cavity reactors was first reported in 2002 by Krishnan et al. who used a 35 μL cylindrical reactor to successfully amplify a 295 bp β-Actin target from a human genomic DNA template (6). The preliminary prototype was constructed simply by drilling a hole in the Plexiglas block and sealing the ends after loading with PCR reagents. Maintaining denaturing temperature at the bottom while holding the top end of the cylindrical cavity at annealing temperature provided favorable conditions to successfully achieve DNA amplification. Temperatures were precisely maintained by sandwiching the Plexiglas block between two individually controlled aluminum plates. Flow visualization studies were performed by loading the cells with an aqueous suspension of fluorescent microspheres and closely monitoring their motion under the microscope. Characterization of convective flows in cylindrical cavities of different geometries/aspect ratios was also carried out by the same group under various temperature conditions. This simplified reactor design was subsequently extended to allow operation in a high-throughput format using a multiwell system consisting of interchangeable plastic reaction chamber ‘cartridges’ incorporating arrays of cylindrical reactors capable of amplifying a 191 bp target associated with influenza-A virus membrane channel proteins in 15 - 40 minutes (52).

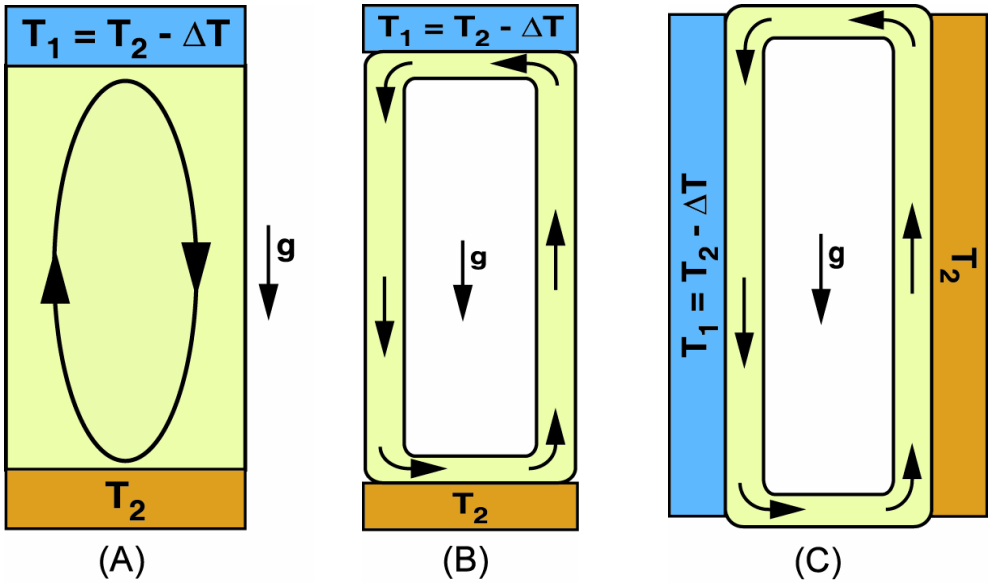

Figure 4.2 A variety of schemes for generating convective flows in cavity and closed loop systems. (A) Shows a cavity heated from below, (B) Shows a closed loop with vertical temperature gradient. The flow direction in this case can be either clockwise or anticlockwise depending on the initial perturbations developed inside the loop and (C) Shows a closed loop with lateral temperature gradient. Flow direction is always unidirectional with hot side fluid going up while the cold side fluid going down

Buoyancy driven flows can be generated in cavities or in closed loop geometries subjected to either vertically or horizontally imposed temperature gradients as shown in Figure 4.2.

This phenomenon can be applied to perform thermocycling by designing reactors in which a convective flow field is utilized to continuously transport reagents through temperature zones corresponding to denaturing, annealing, and extension processes (6,9,52). Although the innovative technique proposed by Krishnan et al. offers a novel approach to overcome the limitations of conventional thermocyclers, it still suffers from shortcomings associated with irregularities in flow trajectories followed by different fluid molecules. From the flow visualization studies, it was evident that all fluid

molecules do not follow identical flow paths within the cavity. While some molecules manage to reach the extreme ends, others bounce back earlier before reaching the ends. To minimize the effects of such variations in cycle times experienced by different fluid elements, cycling times must be described in an averaged sense integrated over the entire spectrum of flow trajectories while performing the quantitative analysis (6,9). This variation in cycle times traversed by the reactants may cause serious issues associated with non-specific amplification. Also, sealing the ends of the cavities could be tricky and may require specialized skills.

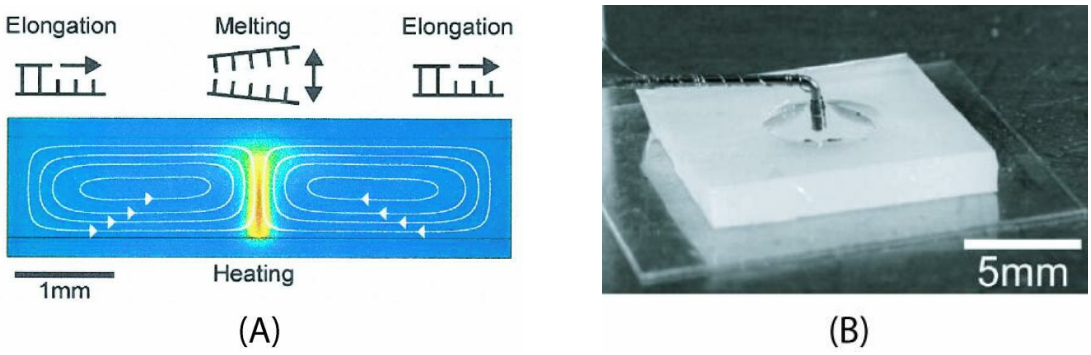

Figure 4.3 (A) Schematic of the convection cell showing a hot spot in the middle of the cylindrical chamber (1 X 5 mm, volume 25 µL) heated by focused IR radiations. (B) Photograph of the cylindrical chamber (1.75 X 4 mm, volume 20 µL) punched in a silicone rubber sheet and a heating element immersed from the top. Reagents are covered with a layer of 10 µL thickness silicone oil to avoid evaporation. Pictures adapted from (29,53)

4.1 Existing convective PCR approaches

To take advantage of the convective PCR approach, Braun et al. in 2003 utilized non-contact heating method to generate convection (7,29,53). They used a focused IR beam to generate a hot spot in the middle of the cylindrical cavity loaded with PCR solution (Figure 4.3 (A)).

They demonstrated amplification of 96 bp fragment of λ-DNA within 25 minutes. This model represents obvious advantages and disadvantages related to non-contact heating method as well as the convective PCR approach. In addition, a great advantage that is reflected in this case is that the developed convective flow is laminar in nature and is not accompanied by diffusion. This allows a more uniformly distributed temperature profile within the cavity. On the other hand, they also identified that all reagents along the horizontal plane of the cavity do not follow identical flow paths and the cycle times range from 6 to 14 sec depending on the vertical distance from the lower chamber wall at half the chamber radius. Moreover, natural variations in the surrounding conditions can interfere with the heat dissipation rates thereby affecting the cycle times which can be extremely difficult to control.

The same group later extended its work and replaced the IR source by a small heating element immersed in the middle of the cavity (Figure 4.3 (B)) (53). Heating the fluid in the middle gave rise to toroidal flow convection within the cylindrical chamber. An advantage of this technique over the previous model is that the IR laser source (costing around $1000) was replaced by a cheaper heating element. Otherwise, this design also had reactants at different planes following different cycle times, although the

return times in this case ranged from 4-6 seconds. Also, silicone oil was used to cover the open end of the chamber filled with PCR reagents to avoid evaporation and hence complete recovery of the amplified products could be difficult. These systems have only been studied at the conceptual level and lack information necessary to be applied for practical applications.

As mentioned earlier, convective flows can also be generated inside closed loops other than cavities. When generated in a loop, the phenomenon is referred to as thermosyphon. Both closed loop models heated vertically and sideways have been studied and reviewed in the literature (11,12).

Wheeler and co-workers in 2004 took advantage of the pumping and thermocycling capabilities of the closed-loop convection and developed a PCR thermal chamber by sandwiching a 12 μm thick polypropylene bag filled with PCR reagents between two epoxy circuit boards (etched with 200 μm deep elliptical channels and fabricated with resistive heaters defining the flow path) (Figure 4.4 (B)) (10). Multiple heaters (shown in red and blue in Figure 4.4 (A)) maintain the constant temperature zones of 94 and 55 °C within the thermal chamber guiding the fluid through the defined paths under the influence of buoyancy. This design may not be categorized as microfluidic PCR because the dimensions of the channels were of the order of millimeter scales. The elliptical flow channel developed within the polymer bag upon sandwiching has axes lengths of 2.5 mm and 400 μm and the total volume of the polymer bag was 75 μL. However, they clearly mentioned that the design was a prototype with significant

scope for further scaling down to develop miniaturized devices. Amplification of several amplicons ranging 58-160 bp was demonstrated using the above system.

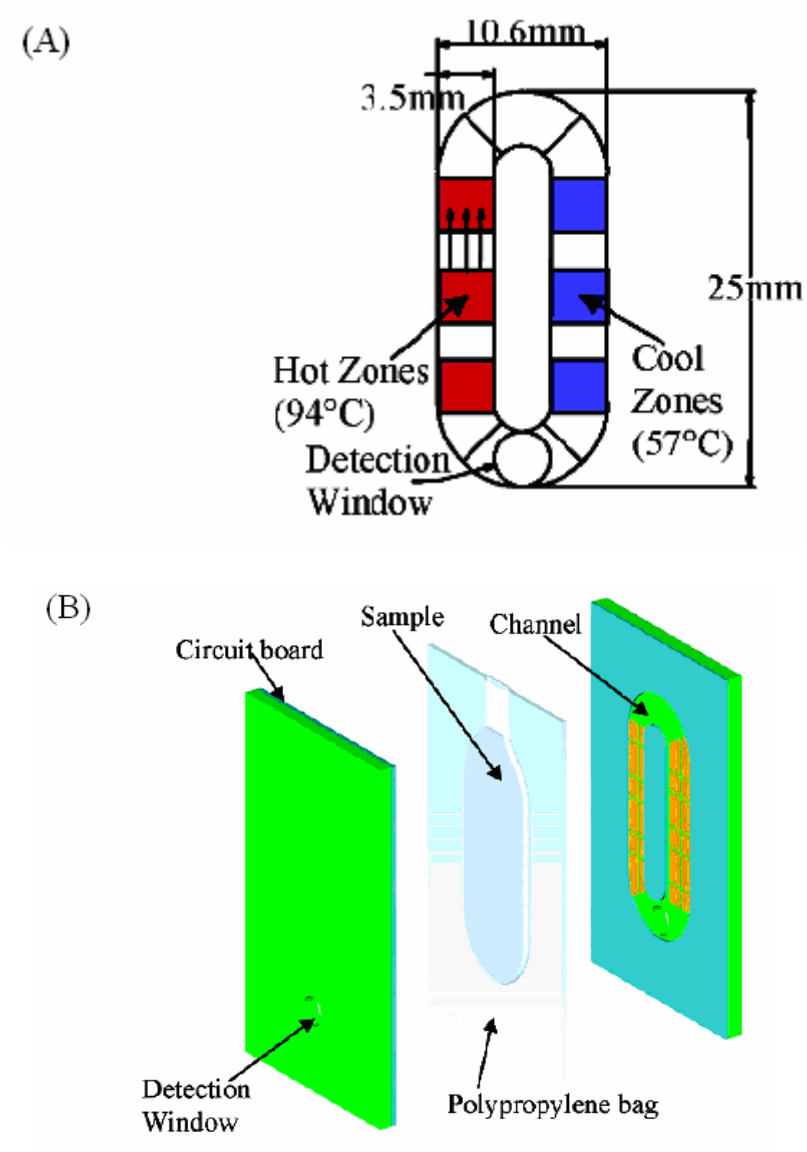

Figure 4.4 (A) Schematic of the convective flow path defined by fabricated heaters on the circuit board. Heaters are shown in red and blue depicting the hot and cold sides respectively, (B) Schematic of the entire assembly including a polypropylene bag loaded with PCR reagents and sandwiched between two circuit boards incorporating heaters, sensors and etched flow channels. Adapted from reference (10)

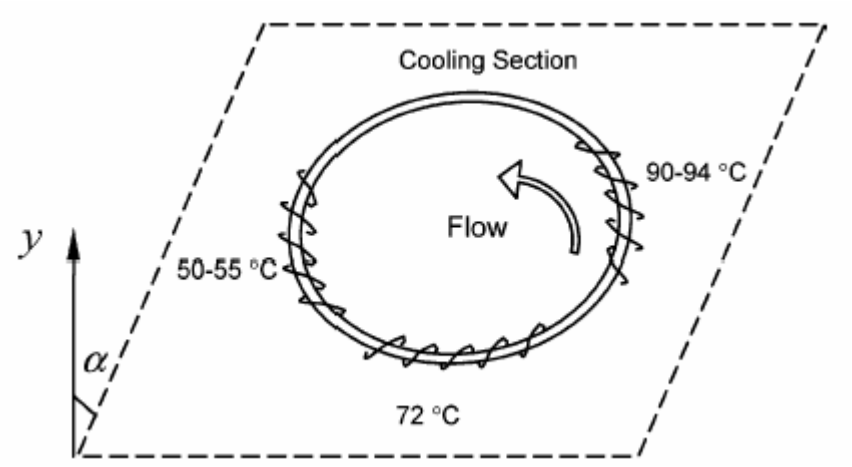

(A)

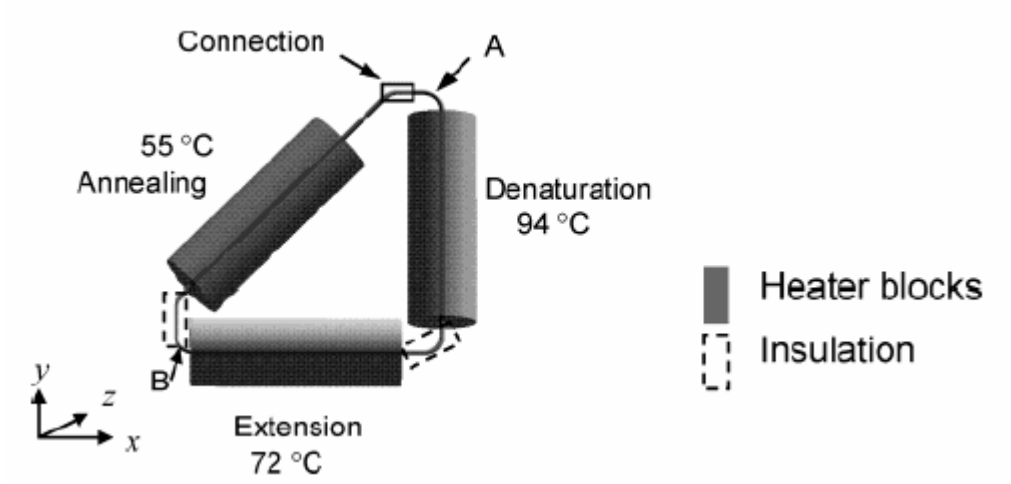

(B)

Figure 4.5 (A) Schematic of a toroidal closed loop maintained at three different temperatures at different locations. The angle (α) of the loop with vertical plane can be altered to control flow rate inside the loop. (B) Schematic of the triangular thermal cycler assemble showing Teflon tubing loop with each of its leg covered by a cylindrical heater. Picture adapted from (8)

Meanwhile in July 2004, Chen et al. developed a similar design in the form of an isosceles right triangular geometry with each side of the triangle replacing each step of the PCR cycle (8). They utilized similar concept as Wheeler et al. to generate convective

flow however with better control over the flow rates. A flow loop was constructed using a 764 μm inner diameter Teflon tubing and total loop length 26 cm capable of holding 119 μL samples (Figure 4.5).

Each leg of the triangular loop was surrounded by a 6 cm aluminum block incorporating resistive heaters and thermocouple probes. The two ends of the tube were joined using a sleeve of hermatic seal after loading with PCR reagents. Portions of the tube exposed between the heating blocks were insulated to avoid heat loss. By individually maintaining the heaters in each leg to sustain 94°C, 55°C and 72°C respectively, they managed to amplify a 305 bp and a 700 bp target within 73 minutes of run time. They utilized the effects of gravitational forces by manipulating the local component of gravity within the loop. This was accomplished by varying the angle of inclination of the entire loop with respect to the vertical plane (as explained by the mathematical formulation discussed in section 5 in this report). The maximum flow rate will persist when the angle of inclination is zero while the flow rate diminishes completely when the loop is orthogonal to gravity. This concept of controlling the fluid flow rates appear interesting however may not be feasible for practical implementation due to the requirement of an actuating mechanism in order to alter the flow rates when needed.

Most of these systems have been used to amplify targets ranging from 90–700 bp in timescales of 30–90 minutes using 15–119 μL reactor volumes (8-10). Despite these advancements, most work to date has been primarily directed at the *proof-of-concept* level and has not included multiplex capability. That is, reactions have been performed

using a limited range of template and target sizes, and often employ cumbersome designs that deliver long cycling times and/or large reactor volumes that are not practical for routine use.

4.2 Proposed approach - closed loop thermocycler

The inherent structure and ability of horizontally controlled closed loop geometry to circulate fluid between various temperature zones makes it ideally suited to perform temperature sensitive biochemical reactions like PCR. The self-actuated simplified mechanism of this system offers a complete passive thermocycling scheme. To optimize the reaction kinetics and the time spent by the fluid elements at various temperature zones, flow rates can be precisely tuned by controlling the independent variables such as channel radius (r), temperature gradient (ΔT) and spacing between the vertical arms (L). Another key advantage of such systems is that all fluid elements follow similar flow trajectories and are exposed to the various temperature zones for identical time frames thereby enhancing the amplification efficiency.

We harnessed the power of thermal forces and developed a simplified closed loop convective flow thermocycling system that addresses the limitations posed by the existing PCR technology. To reproduce the three-step PCR cycling scheme, we constructed a loop exhibiting triangular geometry such that each side of the triangle could be utilized for the individual PCR step (Figure 4.6).

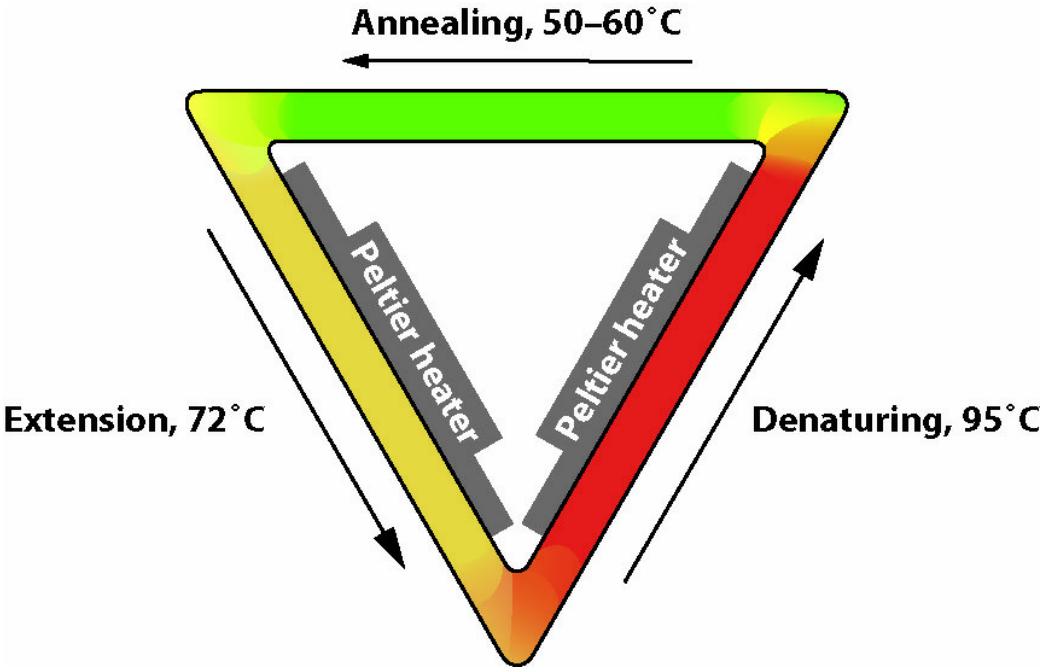

Figure 4.6 Schematic of the proposed triangular closed-loop thermocycler with peltier heaters attached to the two inclined legs. When the two inclined sides are maintained at 95℃ and 72℃, the horizontal side at the top passively attains around 50-60℃

The closed loop design with horizontal temperature gradient is particularly attractive for thermocycling applications because unidirectional flow through the loop can be generated allowing residence times within specific temperature zones to be precisely controlled (Figure 4.2 (C)). Rapid cycling times are achievable because the convected reagents are able to quickly attain thermal equilibrium with their surroundings as they are transported through successive temperature zones without the time lag associated with heating and cooling inactive hardware components. In addition, the value of Racrit is quite low in these systems (of order 1–10) meaning that convective flows can be readily generated under PCR temperature conditions (9). These unique

characteristics are ideally suited to meet the requirements of thermally actuated biochemical reactions like PCR.

Using this system, PCR amplification of 191 bp fragment from influenza-A virus has been demonstrated in as little as 10 minutes with reactors constructed from ordinary plastic tubing mounted in an apparatus incorporating inexpensive thermoelectric heaters those do not require dynamic temperature control. Robustness is demonstrated by amplifying a wide variety of target sizes in both single and multiplex formats incorporating 10–25 μL reaction volumes. Product yields are comparable to those achievable in a conventional benchtop thermocycler, and no modifications to conventional PCR protocols are necessary. We also show that reactor geometries satisfying virtually any combination of reagent volume and cycling time can be straightforwardly designed. We further extend the adaptability of CLTC to perform Sanger cycle sequencing reactions as well as a variety of PCR reactions in rapid real-time formats.

4.2.1 Potential for automation

Owing to its tubing-based design, the CLTC offers excellent potential for automation with both upstream sample preparation and downstream analysis operations (Figure 4.7). For example, a fluidic interface capable of metering discrete amounts of sample, mixing with PCR reagents, and pumping into the flow loop could be constructed using electronically controlled valves. Once the reaction is complete, the products can then be extracted for subsequent analysis followed by a rinsing operation so that the

same loop can be used to perform multiple reactions. Alternatively, because each loop is inexpensive, an ensemble of flow loops could be used in conjunction with a flow circuit capable of switching to a new loop for each reaction. Reagents could also be incorporated in replaceable dispenser cartridges containing a sufficient quantity to perform multiple reactions.

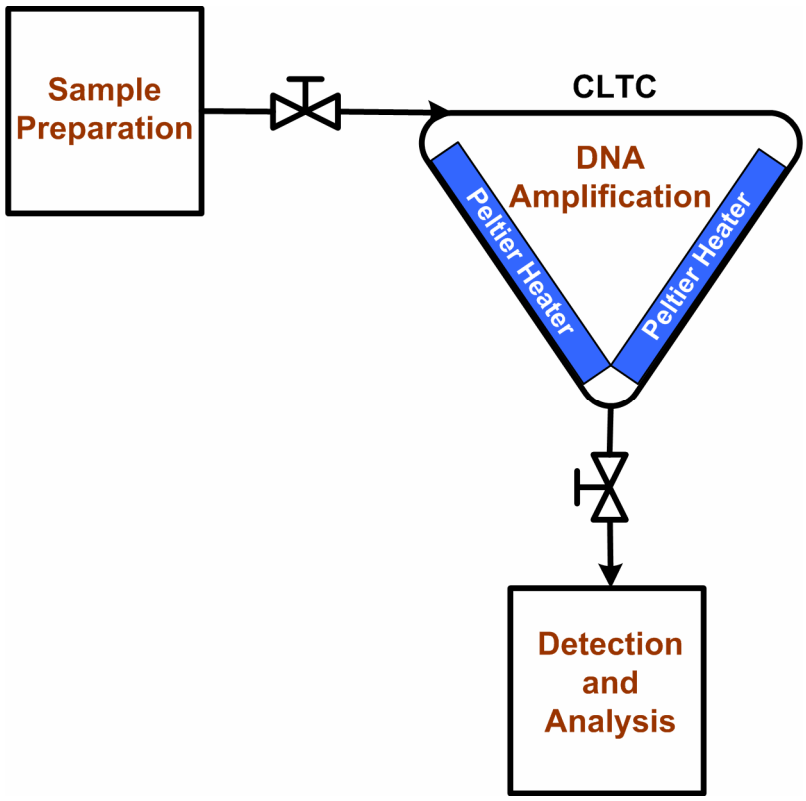

Figure 4.7 Schematic showing a block diagram of the overall analysis scheme. The CLTC can be easily integrated with upstream and downstream analysis assays for automated operation

CHAPTER V

FLOW CHARACTERIZATION AND REACTOR DESIGN

Natural convection has been extensively studied and characterized in literature (11-13). Convective flows occur as a result of buoyant instabilities that develop due to differences in density at different locations within a fluid. At very large scales, for example, convectively generated ocean currents can give rise to devastating hurricanes. For decades, the specific case of natural convection (closed loop convection-thermosyphon) has been studied as a clever approach for transferring heat from one place/phase to another (54,55). Some of the most common applications include solar energy utilization (56,57), nuclear reactor cooling systems (58) and heat dissipation of electrical components (59,60). Several heating and cooling systems have been developed incorporating a closed loop of pipe/tube filled with a working fluid (usually water or oil).

A technical report published by HP Labs in 2002 describes the great potential of thermosyphons have on cooling high heat dissipating electronics and presents the practical implementation of a compact thermosyphon for cooling of a Pentium 4 microprocessor in a Hewlett-Packard Vectra PC (Figure 5.1) (60). And now the utility of thermosyphons is expanding beyond heating/cooling systems to other areas of science of which a relevant application is to perform polymerase chain reaction.

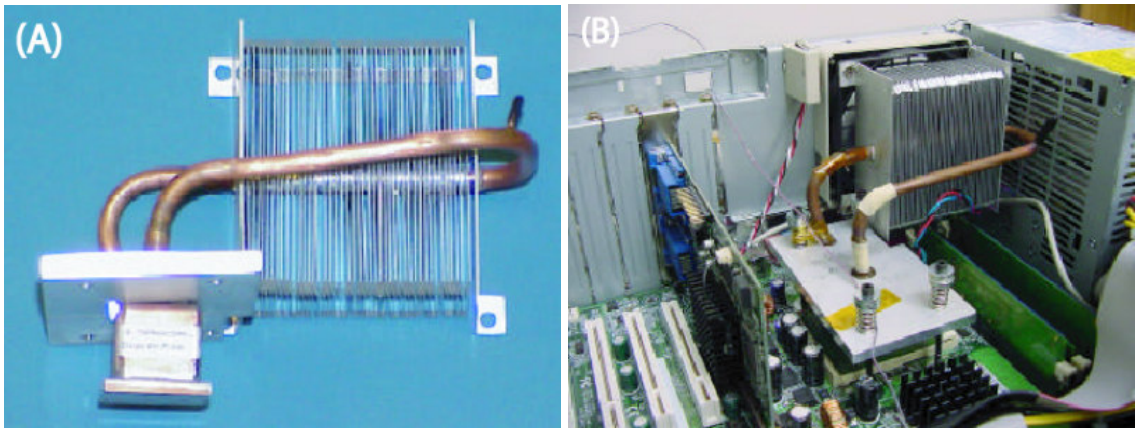

Figure 5.1 (A) Picture of two-phase thermosyphon hardware. (B) Hewlett-Packard HP Vectra VL800 PC fitted with the thermosyphon device as microprocessor cooler. Pictures adapted from (60)

In this section, a mathematical model of convection based thermal cycling systems has been presented showing the dependence of flow rates on fluid and geometric properties such as Rayleigh number, Prandtl number, loop length and the channel diameter. This model can be used to design thermocyclers for virtually any values of desired outputs without the need of performing experiments. Empirical values were used to generate master curves and to verify the data validity and computational modeling tools were utilized to confirm the above analysis.

5.1 Theory

When any lower region of a loop is exposed to a higher temperature environment with respect to the other part of the loop, the working fluid absorbs thermal energy and looses density at the hot region. Lower density fluid molecules then tend to move upward leaving vacancy for the heavier fluid giving rise to a circulatory convective flow

within the loop. In terms of the underlying physics, the magnitude of the destabilizing buoyant forces relative to the thermal and viscous restoring forces acting in opposition can be expressed in terms of a dimensionless *Rayleigh number*.

$$Ra = \frac{g\beta(\Delta T)r^3}{\nu\kappa} \tag{5.1}$$

Here, g is the acceleration due to gravity, ΔT is the imposed temperature difference, r is the tube radius, L is the loop length, and β, κ and ν are fluid properties (thermal expansion coefficient, thermal diffusivity, and kinematic viscosity, respectively). In convective loops, the critical value of Ra at the onset of flow is low, meaning that only small temperature gradients are required to initiate fluid motion. Thus, at a given ΔT, the overall cycle time and residence time within each temperature zone can be precisely determined by selecting appropriate loop geometry (i.e., r and L).

5.2 Basic equations

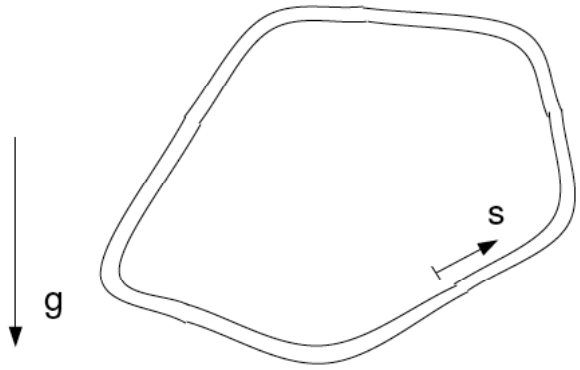

Figure 5.2 Schematic of an arbitrary closed-loop geometry

A loop of arbitrary configuration of length L and constant cross-sectional area A with orientation parallel to the vertical plane is considered (Figure 5.2). The loop is heated at certain locations while cooled at others. We assume the fluid to be incompressible and that the fluid density remains constant other than the buoyancy term (Boussinesq approximation $\rho = \rho_0 [1-\beta(T-T_0)]$). The spatial coordinate s runs counterclockwise from an arbitrary origin around the entire loop. We also assume that velocity u and temperature T remain constant across any cross-section of the loop. Since this is a closed loop system, mass conservation implies that the fluid velocity u will be constant through out the loop and will only be a function of time so that $u = u(t)$.

5.2.1 Mass balance

Consider a control volume within the arbitrary loop as shown below in Figure 5.3.

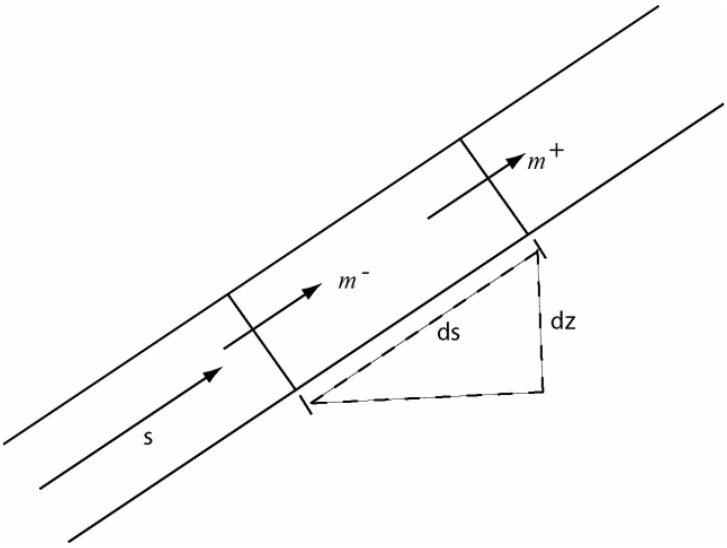

Figure 5.3 Schematic of mass flows in an elemental control volume within an arbitrary closed-loop. *"s"* represents directional coordinates

The mass fluxes in and out are:

$$m^- = \rho_0 uA \tag{5.2}$$

$$m^+ = m^- + \frac{\partial m^-}{\partial s} ds \tag{5.3}$$

Since the fluid is assumed to be incompressible, there will be no accumulation of mass within the control volume and therefore the mass flow rate in and out of the control volume will be equal.

$$m^- = m^+ \tag{5.4}$$

This suggests that over the entire loop of constant cross-section, fluid velocity will also be constant and hence u will only be a function of t and independent of the spatial coordinate s.

5.2.2 Momentum balance

Again considering a small elemental control volume of length ds as shown in Figure 5.4 such that the corresponding forces acting on this elemental length are the viscous force (f_v), the pressure (f_p) and the gravitational force (f_g) in the positive s direction.

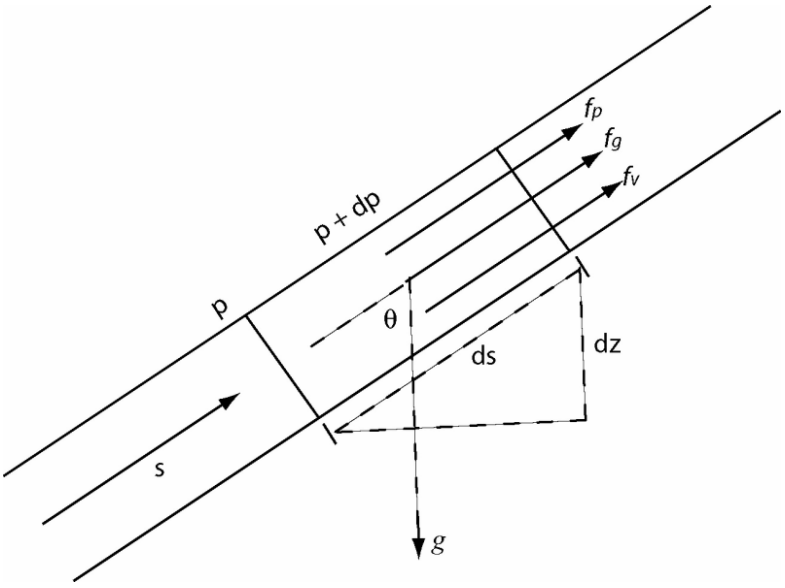

Figure 5.4 Schematic of various forces on fluid elements in the control volume within an arbitrary closed-loop

Thus, we can write the local component of gravity as:

$$\tilde{g}(s) = g\cos(\theta) \tag{5.5}$$

$$\tilde{g}(s) = g\frac{dz}{ds} \tag{5.6}$$

$$\int_0^L \tilde{g}(s)ds = 0 \tag{5.7}$$

Where $\tilde{g}$ is the local component of gravity along s whose integral around the loop diminishes to zero.

We can write the force equations as:

$$f_v = -\tau_w P ds \tag{5.8}$$

$$f_p = -A\frac{\partial p}{\partial s}ds \tag{5.9}$$

$$f_g = -\rho A ds \tilde{g} \tag{5.10}$$

Where, τ_w is the wall shear stress, p is the pressure in the fluid, A the cross-sectional area of the tube and P is the tube perimeter. For simplicity, we will assume a linear relationship between the wall shear stress and the mean fluid velocity, i.e. $\tau_w = \alpha u$. For Poiseuille pipe flow, (this is not the case here but gives an order of magnitude):

$$\alpha = \frac{8\mu}{D} \tag{5.11}$$

Where μ is coefficient of viscosity and D is the pipe diameter.

The density in the gravity force term will be taken to decrease linearly with temperature, so that:

$$\rho = \rho_0 [1-\beta(T-T_0)] \tag{5.12}$$

Since the mass of the element is $\rho_0 A\, ds$, the momentum equation can be expressed as:

$$\rho_0 A ds \frac{du}{dt} = f_v + f_p + f_g \tag{5.13}$$

The above equation when integrated over the entire loop yields:

$$\frac{du}{dt} + \frac{P\alpha}{\rho_0 A} u = \frac{\beta}{L} \int_0^L T\tilde{g}(s) ds \tag{5.14}$$

Where $u = u(t)$ and $T = T(s,t)$.

5.2.3 Energy balance

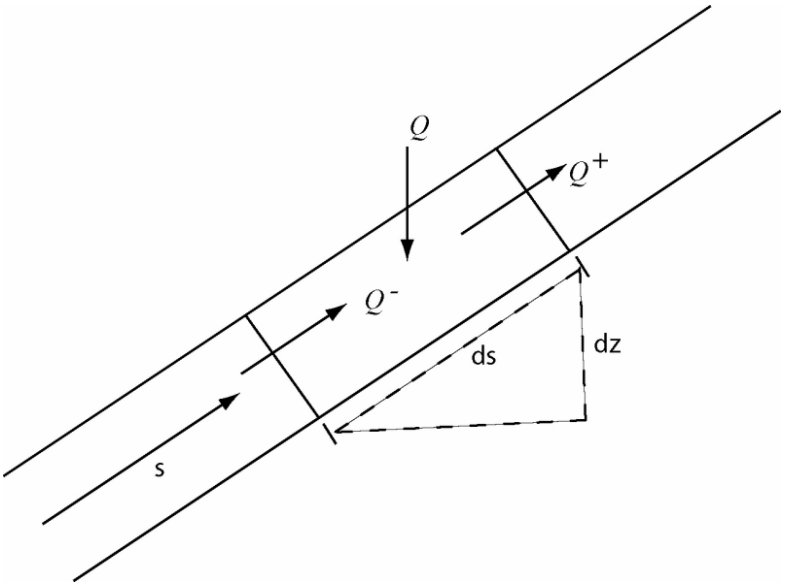

Figure 5.5 Schematic of heat transfer rates in and out of the elemental control volume within an arbitrary closed-loop

The Figure 5.5 above shows the heat transfer rates into and out of the control volume. The rate of heat in and out can be respectively written as:

$$Q^{-} = \underbrace{\rho_0 A u C_P T}_{\text{Advective}} \underbrace{- kA \frac{\partial T}{\partial s}}_{\text{Conductive}} \tag{5.15}$$

$$Q^{+} = Q^{-} + \frac{\partial Q^{-}}{\partial s} ds \tag{5.16}$$

Where *Cp* is the specific heat at constant pressure and *k* is the coefficient of thermal conductivity. Furthermore, heat is also gained from the side at a rate *Q*, which can be written as:

$$Q = q\, ds$$

Where q is the rate of gain of heat per unit length of the loop. An energy balance for the elemental control volume gives:

$$Q^{-} + Q = Q^{+} + \underbrace{\rho_0 A ds C_p \frac{\partial T}{\partial t}}_{\text{Rate of accumulation}} \tag{5.17}$$

Substituting the above equations give the overall energy equation

$$\frac{\partial T}{\partial t} + u\frac{\partial T}{\partial s} = \frac{q}{\rho_0 A C_p} + \frac{K}{\rho_0 C_p}\frac{\partial^2 T}{\partial s^2} \tag{5.18}$$

5.3 Modeling of loops of known symmetric geometries

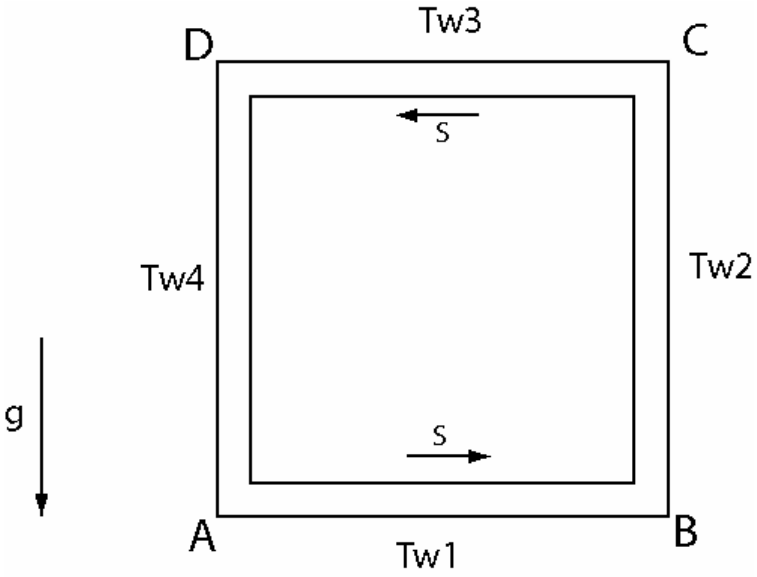

Figure 5.6 Schematic of a square loop of length L and tube perimeter P. Directional coordinate s runs from an arbitrary origin A in the counterclockwise direction. The loop is inclined parallel to the vertical plane. *Tw1, Tw2, Tw3* and *Tw4* are the wall temperatures of the four legs of the loop

Consider a square loop as shown in Figure 5.6. The loop is heated on the two vertical sides while maintaining the two horizontal sides at a lower temperature. The transport is convective with known wall temperature *Tw(s)* and heat transfer coefficient *h*.

Therefore,

$$q = hP(T\text{-}Tw) \tag{5.19}$$

Neglecting axial conduction, equations (5.14) and (5.18) yield:

$$\frac{P\alpha}{\rho_0 A}u = \frac{\beta}{L}\int_0^L T(s)\tilde{g}(s)ds \tag{5.20}$$

$$u\frac{dT}{ds} = \gamma[T - T_w(s)] \tag{5.21}$$

Where, $\gamma = -hP/\rho_0 AC_p$. Assuming point 'A' as the arbitrary origin, we solve equations (5.20) and (5.21) for each branch of the square loop by taking the continuity of temperature at points A, B, C and D as boundary conditions.

Energy equation in each branch, $0 \le s \le L/4$.

$$u\frac{dt}{ds} + \gamma T = \gamma T_W \tag{5.22}$$

$$T(s) = Ce^{-\gamma s/u} + T_W \tag{5.23}$$

Boundary condition $T = T(0)$ at $s = 0$

$$C = T(0) - T_W \tag{5.24}$$

$$T(s) = \left[T(0) - T_W\right] e^{-\gamma s/u} + T_W \tag{5.25}$$

Thus,

$$T\left(\frac{L}{4}\right) = \left[T(0) - T_W\right] e^{-\gamma L/4u} + T_W \tag{5.26}$$

Continuity of temperatures at A, B, C and D

$$T_A = \left[T_D - T_{W4}\right] e^{-\gamma L/4u} + T_{W4} \tag{5.27}$$

$$T_B = \left[T_A - T_{W1}\right] e^{-\gamma L/4u} + T_{W1} \tag{5.28}$$

$$T_C = \left[T_B - T_{W2}\right] e^{-\gamma L/4u} + T_{W2} \tag{5.29}$$

$$T_D = \left[T_C - T_{W3}\right] e^{-\gamma L/4u} + T_{W3} \tag{5.30}$$

Equation (5.30) - Equation (5.28):

$$T_D - T_B = \left(T_C - T_A + T_{W1} - T_{W3}\right)e^{-\gamma L/4u} + \left(T_{W3} - T_{W1}\right) \tag{5.31}$$

Equation (5.30) - Equation (5.28):

$$T_C - T_A = \left(T_B - T_D + T_{W4} - T_{W2}\right)e^{-\gamma L/4u} + \left(T_{W2} - T_{W4}\right) \tag{5.32}$$

Substitute (5.32) into (5.31):

$$T_D - T_B = \left[\left(T_B - T_D + T_{W4} - T_{W2}\right)e^{-\gamma L/4u} + \left(T_{W2} - T_{W4}\right) + \left(T_{W1} - T_{W3}\right)\right]e^{-\gamma L/4u} + \left(T_{W3} - T_{W1}\right) \tag{5.33}$$

Simplifying Equation (5.33),

$$T_D - T_B = \frac{\left[\left(T_{W2} - T_{W4}\right)e^{-\gamma L/4u} + \left(T_{W3} - T_{W1}\right)\right]\left[1 - e^{-\gamma L/4u}\right]}{1 + e^{-\gamma L/2u}} \tag{5.34}$$

Momentum equation:

Neglecting the two terms associated with the horizontal legs for which $\theta = 90°$ where θ is the angle with vertical plane and hence $cos(\theta) = 0$.

$$u = \frac{\beta \rho_0 A g}{P \alpha L}\left[\int_0^{L/4}\left\{(T_B - T_{W2})e^{-\gamma s/u} + T_{W2}\right\}ds - \int_0^{L/4}\left\{(T_D - T_{W4})e^{-\gamma s/u} + T_{W4}\right\}ds\right] \tag{5.35}$$

$$u = \frac{\beta \rho_0 A g}{P \alpha L}\left[\frac{u}{\gamma}(T_B - T_{W2})\left(e^{-\gamma L/4u} - 1\right) + T_{W2}\frac{L}{4} + \frac{u}{\gamma}(T_D - T_{W4})\left(e^{-\gamma L/4u} - 1\right) - T_{W4}\frac{L}{4}\right] \tag{5.36}$$

$$u = \frac{\beta \rho_0 A g}{P \alpha L}\left[\frac{L}{4}(T_{W2} - T_{W4}) + \frac{u}{\gamma}\left(e^{-\gamma L/4u} - 1\right)\left(\underbrace{T_D - T_B}_{from(5.34)} + T_{W2} - T_{W4}\right)\right] \tag{5.37}$$

$$u = \frac{\beta \rho_0 A g}{P \alpha L}\left[\underbrace{\frac{L}{4}(T_{W2} - T_{W4})}_{Term\text{-}1} + \underbrace{\frac{u}{\gamma}\left(e^{-\gamma L/4u} - 1\right)\left\{\frac{\left[(T_{W2} - T_{W4})e^{-\gamma L/4u} + (T_{W3} - T_{W1})\right]\left[1 - e^{-\gamma L/4u}\right]}{1 + e^{-\gamma L/2u}} + T_{W2} - T_{W4}\right\}}_{Term\text{-}2}\right] \tag{5.38}$$

By substituting numerical values of the corresponding parameters in term-1 and term-2, we observe that the magnitude of term-2 is negligible as compared to term-1 and hence the whole term can be neglected. Therefore, we have:

$$u \propto \frac{\beta \rho_0 A g}{P \alpha L}\frac{L}{4}(T_{W2} - T_{W4}) \tag{5.39}$$

Rearranging and expanding equation (5.39) by substituting:

$$A = \frac{\pi D^2}{4}$$

$$P = \pi D$$

$$\Delta T = \left(T_{W2} - T_{W4}\right)$$

$$\alpha = \frac{8\mu}{D}$$

$$\nu = \frac{\mu}{\rho_0}$$

We get:

$$u \propto \frac{\beta\rho_0\left(\frac{\pi D^2}{4}\right)g}{\pi D\left(\frac{8\mu}{D}\right)L}\frac{L}{4}\left(\Delta T\right) \tag{5.40}$$

$$u \propto \frac{1}{8}\frac{\beta g D^2 \Delta T}{\nu} \tag{5.41}$$

From the definition of Rayleigh number:

$$Ra = \frac{\tilde{g}\beta\Delta T D^3}{\nu\kappa} \tag{5.42}$$

Therefore from (5.41) and (5.42), we get:

$$u \propto Ra\frac{\kappa}{\nu}$$

$$Ra \propto \frac{uD}{\kappa} \tag{5.43}$$

In terms of cycle time, we substitute $u=L/t$ to get:

$$t \propto \frac{uD}{\kappa Ra} \tag{5.44}$$

Therefore, we obtain a general expression in terms of the geometric and well as heat transfer parameters describing natural convection of incompressible fluids. An interesting outcome of this analysis has been discussed in later sections where expression (5.43) reflects its significance in the designing of convective closed loop thermocycling systems such that when the curve *Ra* VS uD/κ is plotted, a straight line is

obtained irrespective of the loops geometry as long as the geometry is symmetric. We verified this outcome by plotting the curves for a square loop as well as a triangular loop and plotted values of *Ra* (from empirical data) versus calculated uD/κ and obtained collapsing curves for both geometries. Replacing the fluid velocity *u* by *L/t,* we obtain a similar correlation in terms of cycle time and other relevant variables associated with the convective flow loop design.

CHAPTER VI

INSTRUMENTATION AND EXPERIMENTAL TOOLS*

6.1 Triangular closed loop thermocycler construction

We have developed a closed loop thermocycler (CLTC) consisting of a triangular flow geometry designed to replicate the three steps in a PCR cycle (i.e., denaturing, annealing, and extension). To construct the contact heating type convective flow devices, we took advantage of thermoelectric Peltier heaters (Catalog # HT4-6-21X43, Melcor Corporation) because of their fast response to the applied currents. These Peltier heaters can attain 95°C from room temperature within 8-10 s. Convective flow loop reactors are constructed using 9 cm lengths of thin wall fluorinated ethylene propylene (FEP) tubing (Zeus Industrial Products, Inc.). Loops were constructed from three different tubing diameters: 320, 400, and 510 μm inside diameter (28, 26, and 24-gauge sizes), corresponding to reactor volumes of 10, 16, and 25 μL, respectively. The choice of FEP tubing was motivated by its attractive combination of properties including low cost, mechanical flexibility, optical transparency, and biocompatibility. Moreover, FEP possesses excellent ultraviolet transmission capabilities allowing real-time monitoring capabilities using UV radiations to excite SYBR Green I molecules. Detailed properties of the FEP are summarized in APPENDIX B. Lengths of tubing were filled with PCR

---

* Part of the data reported in this chapter is reprinted with permission from "A buoyancy-driven compact thermocycler for rapid PCR" by Agrawal, N. & Ugaz, V.M., (2006) *Journal of the Association for Laboratory Automation*, **11**, 167-284. Copyright 2006 by Elsevier, Inc.

reagents, after which the two open ends were joined together using a short sleeve of PVC tubing (PVC offers greater mechanical flexibility, ensuring a good seal). Slightly overfilling the tubing allowed the ends to be joined without trapping air pockets inside the loop.

After loading, the loops were mounted on a fixture incorporating two independently controlled thermoelectric Peltier heaters positioned on an aluminum scaffold designed to create a triangular flow path as shown in Figure 6.1. The flow loops were affixed directly to the heater surfaces using aluminum adhesive tape (Axygen Scientific) to ensure thermal contact and a uniform temperature distribution.

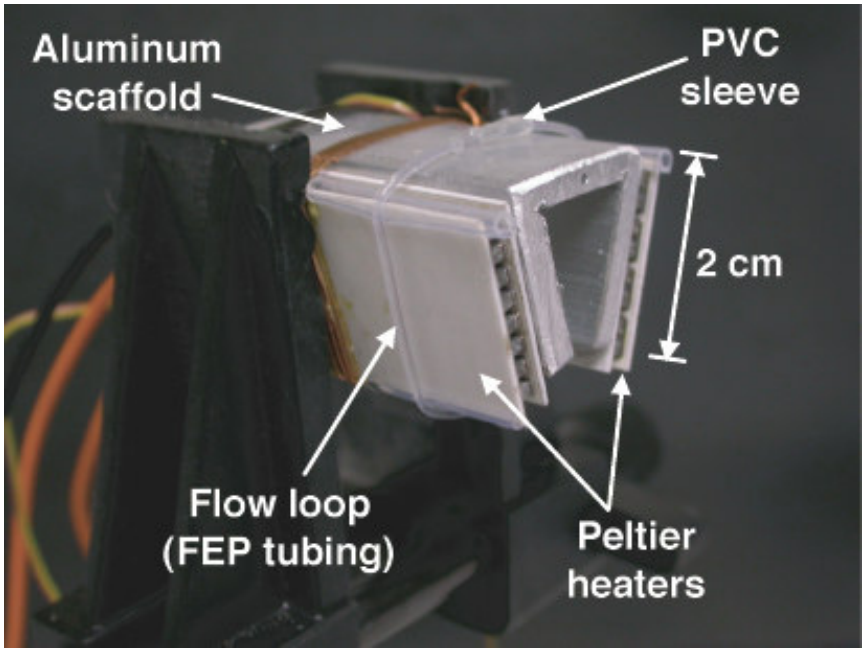

Figure 6.1 Photograph of closed-loop thermocycler assembly incorporating two Peltier heaters mounted on the two inclined legs of the triangular aluminum scaffold. The complete assembly is supported by a stand. Flat thermocouple probes are affixed on the Peltier surface. A 9cm loop of FEP tubing is wrapped around the scaffold. A small hole on the horizontal leg of the scaffold is made to insert thermocouple probe for temperature sensing

As stated previously, the use of thermoelectric heaters is advantageous because of the ability to achieve high ramping rates that help minimize the initial transient period required for the system to reach steady-state PCR temperature conditions. Flat thermocouple probes (Model # SA1-(K), Omega Engineering, Inc.) were affixed to the heater surfaces to monitor their temperature. When one of the heaters is maintained at 94°C (denaturing) and the other at 72°C (extension), the third side of the scaffold passively attains 55-60°C (annealing). This arrangement provides sufficient driving force to initiate circulation of PCR reagents through the loop. However, temperatures could also be maintained by coupling a temperature controller to the setup. The denaturing and annealing processes occur almost instantaneously, while extension proceeds at the rate of about 60 bases per second (61). Based on these considerations, the triangular geometry should be designed such that the extension leg of the loop is sufficiently long to allow replication of the target fragment of interest. At an ambient temperature of 22°C, the input power requirement was 3.1 V at 660 mA and 1 V at 460 mA for heaters at 95°C and 72°C, respectively. A ceramic fiber insulation strip was wrapped around the triangular assembly to reduce heat loss and to insulate the loop from ambient temperature fluctuations. Eventually, the entire assembly is mounted on a stand to perform thermocycling operation.

6.2 PCR conditions

Amplification performance was characterized using several reaction systems. Reagents for reactions involving amplification of the following targets were supplied in kits from Maxim Biotech, Inc.:

(i) A 191 bp target associated with the membrane channel proteins M1 and M2 of the influenza-A virus from a 3.9 kb template,

(ii) A 242 bp target associated with the human L32 gene from a genomic DNA template

(iii) A 474 bp target associated with the human β-Actin gene from a genomic DNA template.

(iv) A multiplex system incorporating a primer mix for amplification of 5 different respiratory infection associated virus targets (264 bp respiratory syncytial virus (RSV), 315 bp corona virus, 390 bp influenza virus, 484 bp adenovirus, and 547 bp rhino virus).

Standard 50 µL reaction mixes contained 30 µL of optimized buffer/dNTP mix, 10 µL of primer mix, 8.75 µL of ddH_2O, 1 µL of template DNA and 0.25 µL of 5 units/µL Ampli*Taq* polymerase. After reactions were complete, products were aspirated from the flow loops, run on a 2% agarose gel at 60 V for 1 hour, and stained with SYBR Green I.

A kit for amplification of a 1.3 kb target from a λ-DNA template was also used (Phusion High-Fidelity PCR Kit; New England Biolabs, Inc.). Standard 50 µL reaction

mixes contained 34μL of H_2O, 10μL of 5x Phusion HF buffer, 1μL of 10 mM dNTPs, 2.5μL of primers, 2μL of control template DNA and 0.5μL of Phusion DNA polymerase (2 units/μL). The remainder of the reaction protocol was identical to that used with the other systems.

6.3 Flow visualization methods

Flow visualization studies were performed by loading the loops with aqueous suspension of 6 μm fluorescent latex microspheres (Polysciences, Inc.). The closed loop was wrapped around the CLTC assembly and securely adhered to the periphery of the CLTC using an adhesive aluminum tape to ensure good thermal contact and uniform heat distribution around the loop. A small window was created by peeling off the covering aluminum tape to expose tubing at the desired location for imaging purposes. Flow profiles were closely monitored by observing microsphere motion using a microscope equipped with a mercury arc illumination source and CCD camera. Excited microspheres were monitored in real-time on the television screen connected to the CCD. Flow velocities were measured by marking the exposed tube at 2mm gap and then recording the time taken by individual microspheres to travel through the gap (motion monitored on TV screen). The microscope was aligned such that the desired location of the flow loop could be focused perpendicular to the objective lens. Microsphere movement initiated at temperature gradient as little as 1°C and the velocity increased with subsequent increase in temperature gradient. In order to identify the effect of any

possible viscous drag forces acting on the microspheres, we loaded the loops with a solution containing both 2 μm and 6 μm fluorescent beads and it was observed that at lower temperature gradients when the flow rates were significantly slower, the 2μm microspheres appeared to be moving faster than the fastest moving 6μm beads. However, at higher temperature gradients such as at PCR temperature conditions (where the temperature gradient is about 22-40°C), the 2 μm spheres moved at significantly faster rates and were difficult to monitor due to limited speed and resolution of the camera (30 frames per second) used in our experiments. Although, it appeared that after a certain absolute temperature on the hot side (when the density of the fluid was reduced), both sized microspheres started moving at comparable speeds. Therefore at higher temperatures, the flow rates were monitored by observing the 6 μm microspheres while at lower temperatures, it was done by observing the smaller microspheres. The parabolic laminar flow profile inside the tube was illustrated from the two dimensional visualization as particles close to the walls of the tube appeared moving slower than those moving near the center line.

6.4 Product purification and quantification

Amplified PCR products were purified to remove unused nucleotides, primers and other low molecular weight components followed by the quantitative analysis step. For purification using a microcentrifuge, the QIAquick PCR purification kit (QIAGEN Inc. – USA, Catalog # 28104) was used. The QIAquick system uses the spin-column

technology utilizing the selective binding properties of a uniquely-designed silica-gel membrane (62). In the presence of high salt concentration, DNA gets adsorbed to the silica-membrane while allowing the contaminants to pass through the column. Impurities are efficiently washed away, and the pure DNA is eluted with water or Tris buffer provided with the kit. The silica-gel membrane in each column is designed to bind up to 10μg DNA under precise salt concentration and pH environment. The high concentration of chaotropic salts modifies the structure of water and facilitates the adsorption of nucleic acids to the silica-gel surfaces. The pH dependence of DNA adsorption to silica is also critical and the adsorption is typically 95% if the pH is ≥7.5, and reduces drastically at higher pH values. This PCR purification system can be used to extract 100 bp to 10 kb fragments of single or double stranded PCR products.

The purification protocol involves addition of high salt buffer to the PCR sample followed by a 60s centrifugation. During this step, the desired DNA to be extracted binds to the silica membrane inside the purification column and the other contaminants pass through. The columns were centrifuged using a microcentrifuge instrument at 13000 rpm to ensure maximum extraction. Then the column is again washed with buffer and centrifuged to remove any residual impurities adhered to the walls of the column. Finally, the column is washed with an elution buffer or simply water and centrifuged to recover the DNA products. Product yield depends on the amount of elution buffer used to recover DNA, therefore, equal amounts of elution buffer was used for each product to maintain consistency.

Reaction yields were also measured from purified PCR products using a NanoDrop ND-1000 spectrophotometer and were compared with the yields obtained from a traditional benchtop thermocycler. The product yield results are discussed in the next section.

CHAPTER VII

RESULTS AND DISCUSSION

7.1 Robustness and amplification speed

The ability to perform rapid amplification is critically important in many applications (e.g., medical diagnostic and pathogen detection assays). We investigated this by performing series of experiments to characterize amplification efficiency of CLTC using 10, 16, and 25 μL closed loop FEP reactors with corresponding cycling times of 102, 69, and 42 seconds, respectively (flow velocities in the loops scale with tubing diameter).

We demonstrated the functionality of the prototype CLTC by successfully amplifying a 191 bp target associated with the M1 and M2 channel proteins of the influenza-A virus within 50 minutes (inside a closed loop reactor of 320 μm inner diameter and 10 μL volume). To determine the minimum reaction time required to replicate the target amplicon (191 bp) for this specific loop geometry, we performed a series of reactions with reaction times ranging from 20-55 minutes. As expected, the electrophoresis results of the amplified products show a reduction in the product band intensity as the reaction time is decreased. (Figure 7.1 (A)). Robustness of the simplified thermocycler design was investigated by performing a series of reactions for varying denaturing temperatures ranging 90-96℃.

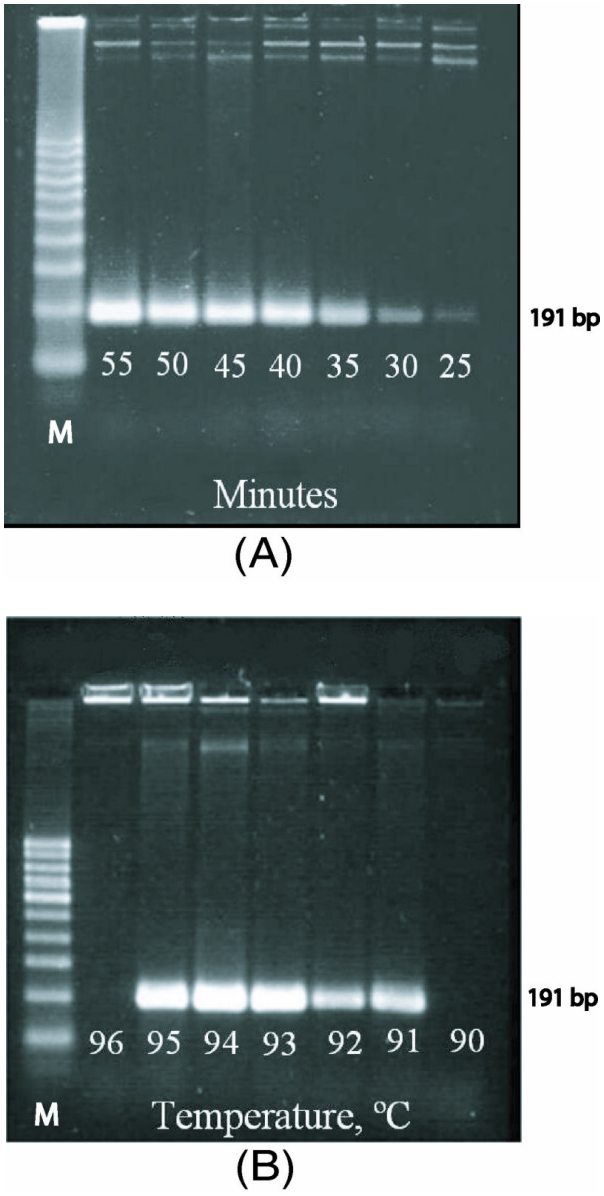

Figure 7.1 (A) Gel picture of 191 bp influenza-A target amplification for different times ranging from 25-55 minutes inside CLTC reactor. Lane M represents the 100 bp marker lane. As the reaction time decreases, number of cycles also decreases which is illustrated by decreasing band intensities of the amplified products. (B) Gel picture showing successful amplification for different temperatures ranging from 91-95℃. This implies that extremely precise temperature control is not required for achieving a successful amplification in the simplified CLTC device

It is evident from Figure 7.2(B) that the reaction works consistently over a range of denaturing temperatures and illustrating the robust functionality of the CLTC without requiring intricate electronic circuitry for precise dynamic temperature control.

We continued working with the 191 bp target amplification experiments and to identify the amplification speed limits, reactions were carried out for total reaction times differing by 5 minute intervals. For example, in case of 25 µL loop, a set of three reactions were performed for reaction times of 20, 15 and 10 minutes. Identical reactants were used for all three reactions in each case. The rapid thermocycling capability of CLTC was demonstrated by using the 25 µL loop to amplify 191 bp target and the product band was detectable by agarose gel analysis after reaction times as short as 10 minutes (Fig. 7.2(A)). While for the other two longer reaction times (15 and 20 minutes), the product band intensities were significantly brighter than the first one. As expected, the band intensity was brightest for the 20 minutes reaction while lowest for the 10 minutes reaction. Subsequently, quantitative analysis of the product yields was also performed to investigate the amplification efficiency of CLTC as compared to the benchtop thermocyclers.

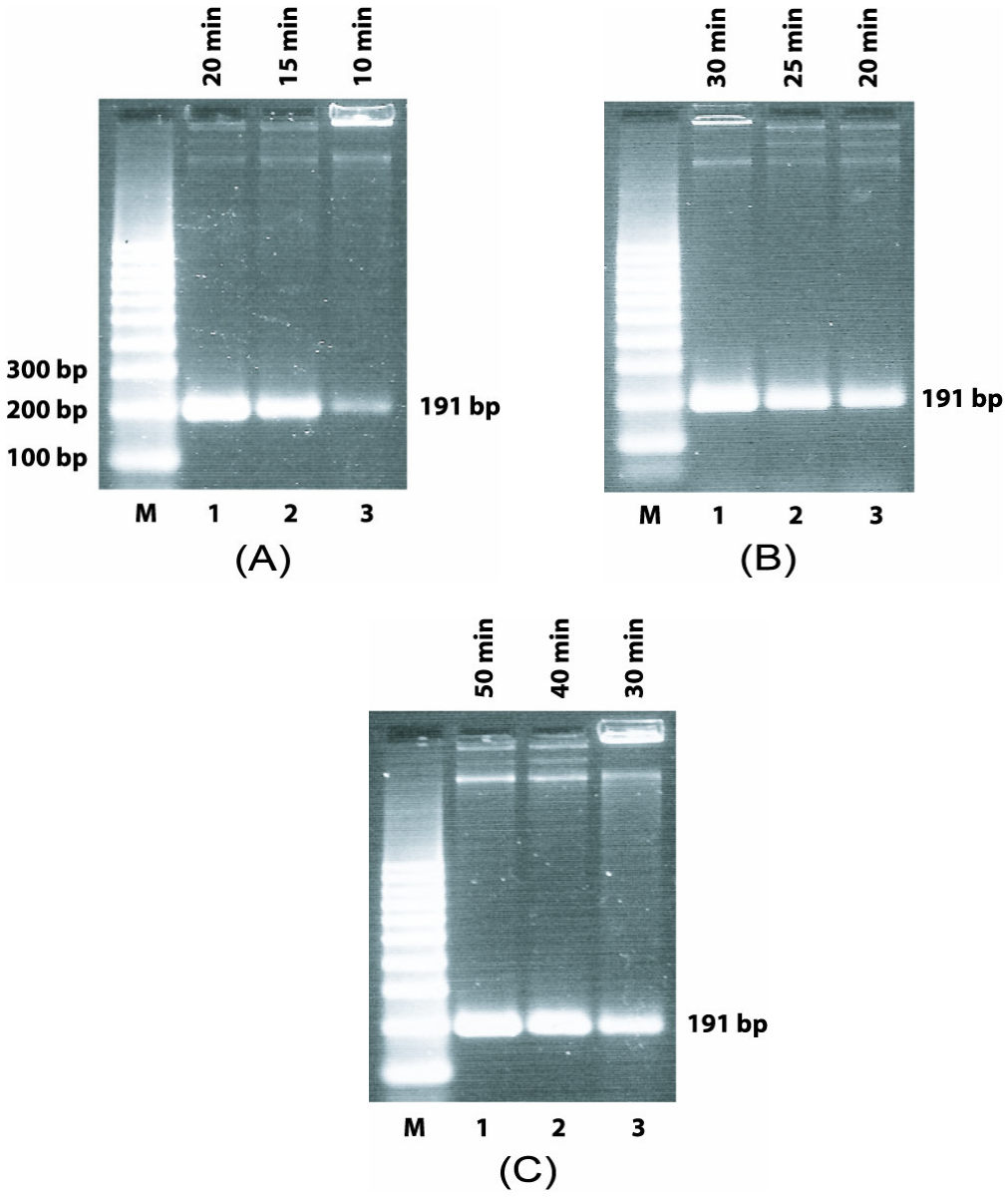

Figure 7.2 (A) Electrophoresis gel picture of PCR amplification of 191 bp influenza-A virus target inside a 9cm loop of 510 µm inside diameter tubing. Lane 1, 2 and 3 shows the amplified product bands for reaction times of 20, 15 and 10 minutes respectively. Lane M represents a 100 bp marker lane. (B) Gel picture of amplified products for CLTC geometry similar to (A) however, in this case, lane 1, 2 and 3 represents product bands for reaction times of 30, 25 and 20 minutes respectively. (C) Similar to (A) and (B) here lane 1,2 and 3 represents amplification of 191 bp target within 50, 40 and 30 minutes of reaction times.

The three gel pictures illustrate that the cycling/reaction time decreases as the tube diameter increases

From the flow characterization data (discussed in the following section), it was evident that the flow rate in a closed loop reactor increases with increasing temperature gradient and also with increasing tube diameter. To analyze the effect of flow rate on amplification speed, a series of three reactions were again carried out for smaller volume flow loops i.e., constructed from smaller diameter tubing delivering longer cycling times. Under similar PCR conditions, the 16 µL loop (400 µm inside diameter) produced detectable products in 20-30 minutes while the 10 µL loop (320 µm inside diameter) produced detectable products in 30-50 minutes (Figure 7.2 (B) and (C)). In each case, product band intensity increased with increasing reaction time. This level of performance is significant because these cycling times approach those demonstrated in the most rapid thermocycling systems to date (63,64), but in a device format incorporating an unprecedented level of mechanical and electronic simplicity.

7.2 Duplex, multiplex and long target amplification

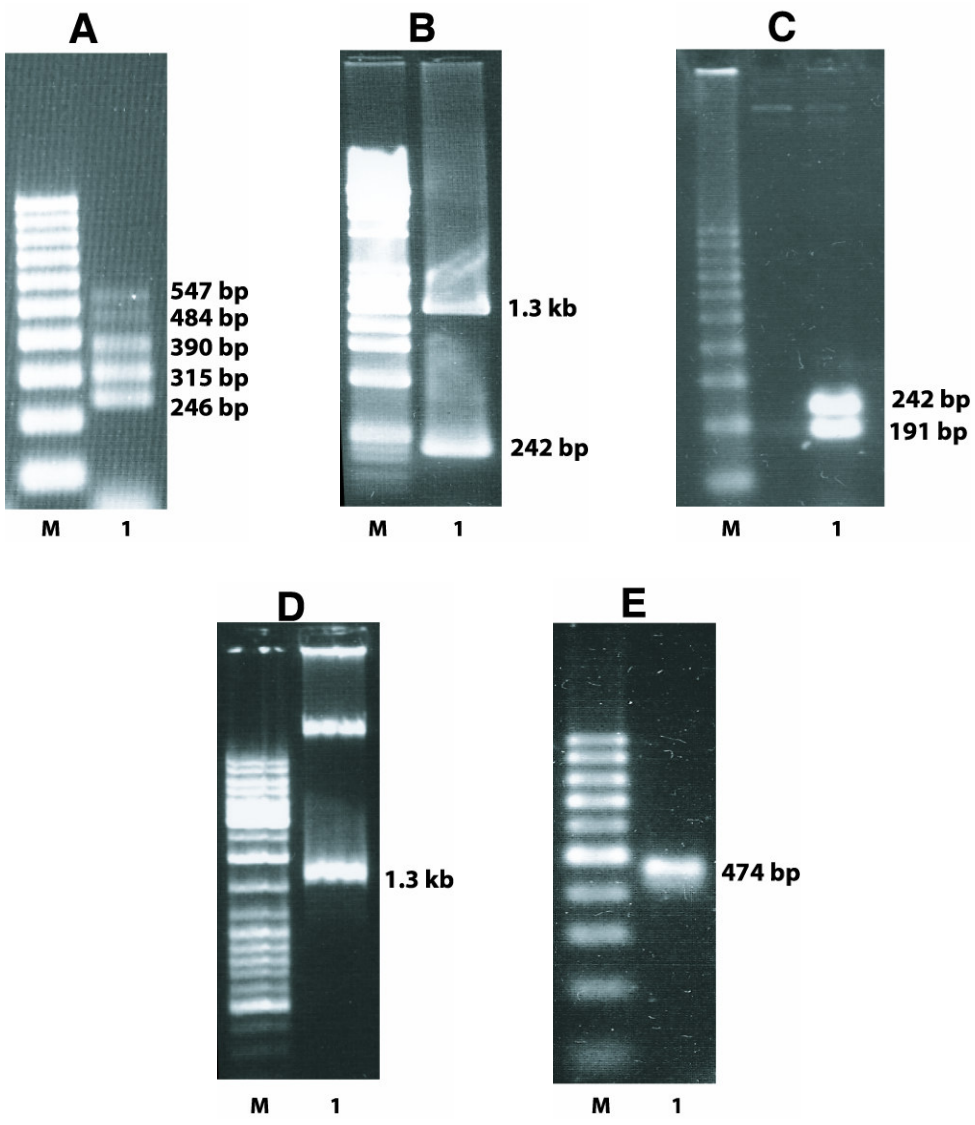

Figure 7.3 Gel pictures of a variety of targets amplified in single, duplex and multiplex formats. All these reactions were carried out in a 9 cm triangular closed loop reactor of 400 μm diameter tubing (16μL reaction volume) and for 50 minutes of reaction time. (A) Multiplex amplification of 5 different human respiratory virus targets ranging from 246-547 bp. (B) Duplex PCR for a mixture containing primers and template for a 1.3 kb target from a λ-DNA template and a 242 bp human L32 gene target. (C) Duplex PCR for a mixture of 191 bp influenza-A amplicon and 242 bp human L32 gene target.(D) Amplification of 1.3 kb target from a λ-DNA template done in a 320 μm diameter tubing and (E) Amplification of 474 bp human β-Actin target inside 320 μm diameter tubing

An ideal PCR system should be capable of rapidly amplifying a wide range of target lengths including long targets (>1 kb) not only individually but also in multiplex formats. Multiplex PCR assays allow co-amplification of several target sequences so that multiple genomic signatures can be simultaneously detected. We investigated the versatility of this CLTC system by performing several co-amplification reactions containing up to five different target sequences. The following multiplex reactions were carried out:

(i) A multiplex PCR mixture containing targets associated with 5 different respiratory viruses amplifies within 50 minutes using a 16 μL flow loop reactor. A PCR kit was used for this reaction and 5 distinct bands were obtained from the electrophoresis results as shown in Figure 7.3(A).

(ii) Simultaneous co-amplifications in mixture containing primers and template for a 1.3 kb target from a λ-DNA template and a 242 bp human L32 gene target. Both reaction mixtures were prepared individually and then mixed together to perform the co-amplification (Figure 7.3(B)). This further demonstrated the robustness of the CLTC as the presence of multiple primers and templates doesn't show any interference or binding interactions with each other.

(iii) Similarly, a solution containing individually prepared mixtures of 191 bp influenza-A virus and 242 bp human L32 gene targets was also amplified within 50 minutes using a 16 μL loop (Figure 7.3(C)).

(iv) The ability to handle a broad range of target lengths is further demonstrated by using a 10 μL loop to amplify a 1.3 kb target from a λ-DNA template (Figure 7.3(D)), and a 474 bp human β-Actin target (Figure 7.3(E)) in 50 minutes.

This level of versatility has yet to be approached in either miniaturized or convective flow thermocycling systems. It is also notable that no modifications were made to the reagent mixtures used in conventional thermocycler-based protocols in order to perform PCR in the convective flow loop system. This is primarily because the fluoropolymer tubing used to construct the flow loops is chemically inert and thus exhibits a low susceptibility to non-specific binding interactions. Consequently, none of the surface pre-treatment processes required in many miniaturized PCR systems (32) needs to be applied here.

7.3 Quantitative analysis of the amplified products

In order to quantitatively verify PCR performance in the CLTC, product purification was carried out to remove unused primers and lower molecular weight components followed by spectrophotometric measurement of the final nucleotide concentration. Product yields obtained from CLTC reactions (from series of reactions discussed earlier in section 7.1) were measured by a spectrophotometer and compared with the products obtained from a standard benchtop thermocycler using the same reagents as in CLTC. A standard cycling protocol was used in the benchtop thermocycler providing 1 minute residence time at each temperature step. From the yield

comparison table, it is evident that the CLTC performance is over 5 times better than the conventional benchtop thermocyclers both in terms of yield as well as reaction times. Table 7.1 summarizes the product yields obtained for the reactions performed in CLTC for three different reactors and for different reaction times.

Table 7.1 Amplification yields obtained from the quantification of the purified PCR products from different diameter tubing reactors in CLTC as well as from the benchtop thermocycler

	28 AWG (320 μm) (ng/μL)	**26 AWG (400 μm) (ng/μL)**	**24 AWG (510 μm) (ng/μL)**	**Benchtop Thermocycler (ng/μL)**
10 mins	-	-	3.96	2.1
15 mins	-	-	4.8	1.8
20 mins	-	5.03	7.37	1.9
25 mins	-	6.97	-	2.03
30 mins	6.97	8.57	-	2.13
40 mins	8	-	-	2.03
50 mins	8.9	-	-	2.8
2.5 hrs	11.07	-	-	12.0

7.4 Flow measurements and thermocycler modeling

We measured velocities in convective flow loop reactors by observing the motion of an aqueous suspension of 6 μm-diameter fluorescent latex microspheres over a wide range of temperature conditions. Due to the laminar parabolic flow profile throughout the loop, microspheres near the tube wall travel more slowly than those near the centerline. In order to account for this velocity distribution, we averaged an ensemble of successive measurements of the time required for microspheres to traverse a fixed distance along the loop. As expected based on Equation (5.1), these data show that fluid velocity increases (i) with increasing temperature gradient, and (ii) with increasing tube diameter (Figure 7.4). In addition, the onset of fluid motion occurs upon application of a very small temperature difference (ΔT ~ 1°C). Under PCR conditions, average flow velocities of approximately 0.9, 1.3, and 2.1 mm/sec were obtained in 320, 400 and 510 μL diameter loops, respectively.

To verify and compare the proximity of the experimental results with simulated data, we used Fluent simulation software and obtained flow velocity data for exactly the same input conditions as the experimental setup. Under PCR conditions, average flow velocities of 1.0, 1.6, and 2.8 mm/sec were obtained from simulation data for 320, 400 and 510 μL diameter loops, respectively. The simulation data appears to be in close agreement with the empirical values and the slight variation could be accounted for the experimental measurement errors. Although the flow rate data illustrates the influence of temperature and geometry on velocities inside the convective loop reactors, determination of cycling parameters is not entirely straightforward because each unique

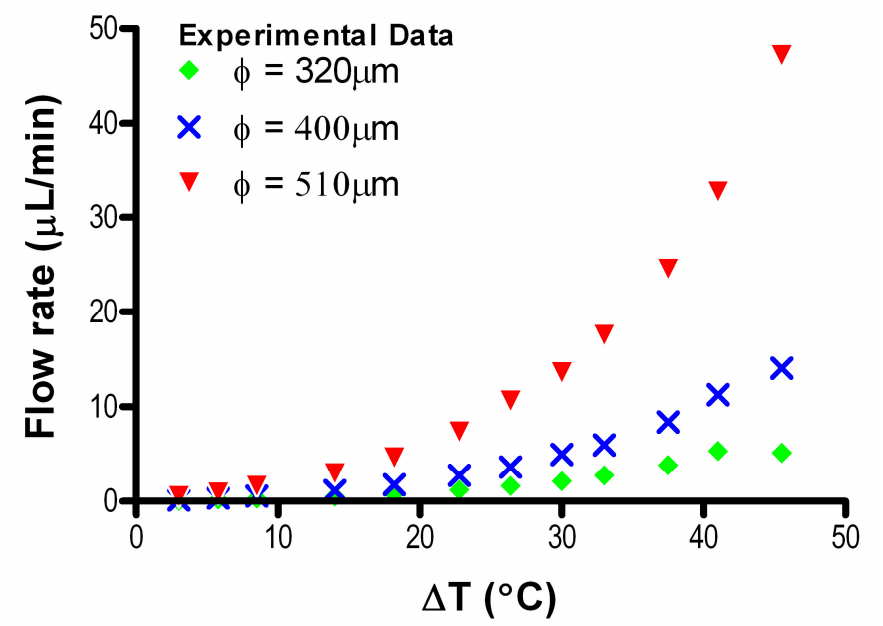

(A)

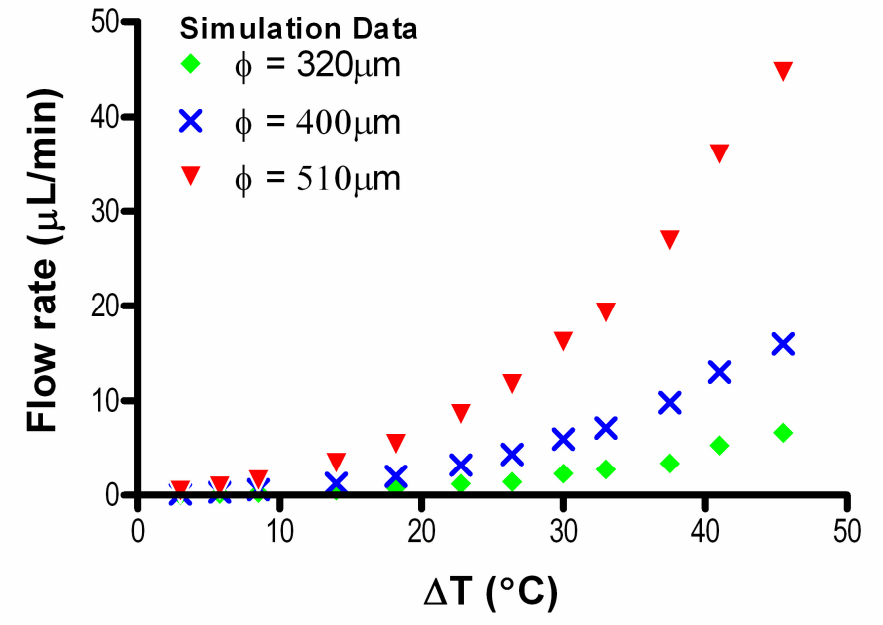

(B)

Figure 7.4 (A) Curves showing increase in flow rate with increase in temperature gradient. Also higher diameter tubing has higher flow rate at any given ΔT. (B) Similar to figure (A) but for simulation data obtained using Fluent

loop geometry (i.e., combination of r and L) will be characterized by its own corresponding flow curve analogous to those shown in Figure 7.4.

The analysis of the momentum and energy balance equations, however, suggests that equation (5.38) emerges as a natural physical scaling parameter. Remarkably, when velocities from the flow rate data in Figure 7.4 are combined with other scaling parameters and plotted versus Ra (where the local component of gravity $\tilde{g}(s) = g\cos(\theta)$ and the temperature dependence of fluid properties β, ν and κ are taken into account), the data for all three tube diameters collapses onto a single straight line *master curve* (Figure 7.5 (A)). As before, simulation data points for three different diameters were plotted (Ra VS uD/κ) based on the derived mathematical model and similar curves were obtained as for the experimental data (Figure 7.5 (B)). To compare the closeness of the simulation data with experimental values, both results were plotted simultaneously on a single chart and an excellent agreement was observed between experimental and simulation results where all six curves (three for experimental results and three for simulation) collapsed within a narrow band as shown in Figure 7.6.

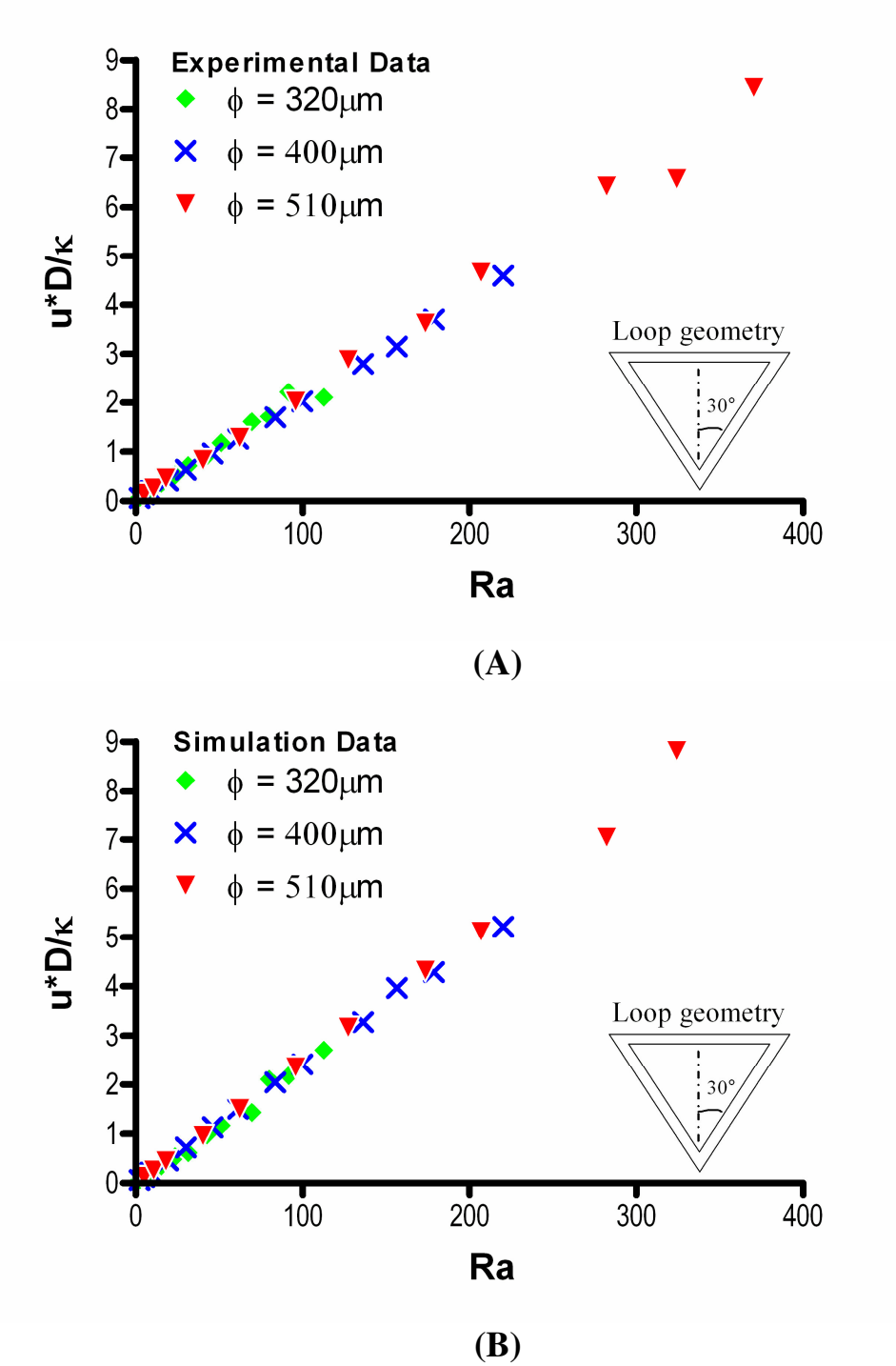

Figure 7.5 Master curves for flow data in equilateral triangular loop geometry for (A) Experimental data showing agreement with mathematically derived correlation. (B) Simulation data obtained from Fluent also showing similar agreement with mathematical model

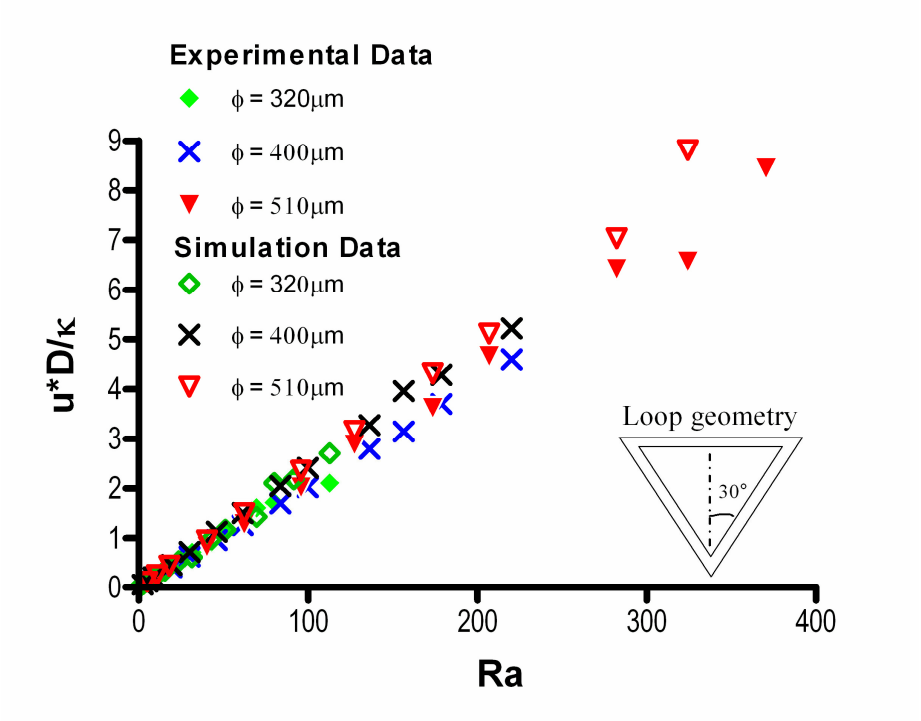

Figure 7.6 Same data points plotted in figure 7.5 (A) and (B) however, plotted here together in order to compare the proximity of experimental data with simulation results. All six curves seem to collapse within a narrow band showing close proximity

This correlation makes the reactor design process extremely straightforward because it allows cycling parameters to be predicted for any loop geometry without the need for flow experiments. This simple procedure can be applied to design reactor geometries satisfying virtually any combination of reagent volume and cycling parameters.

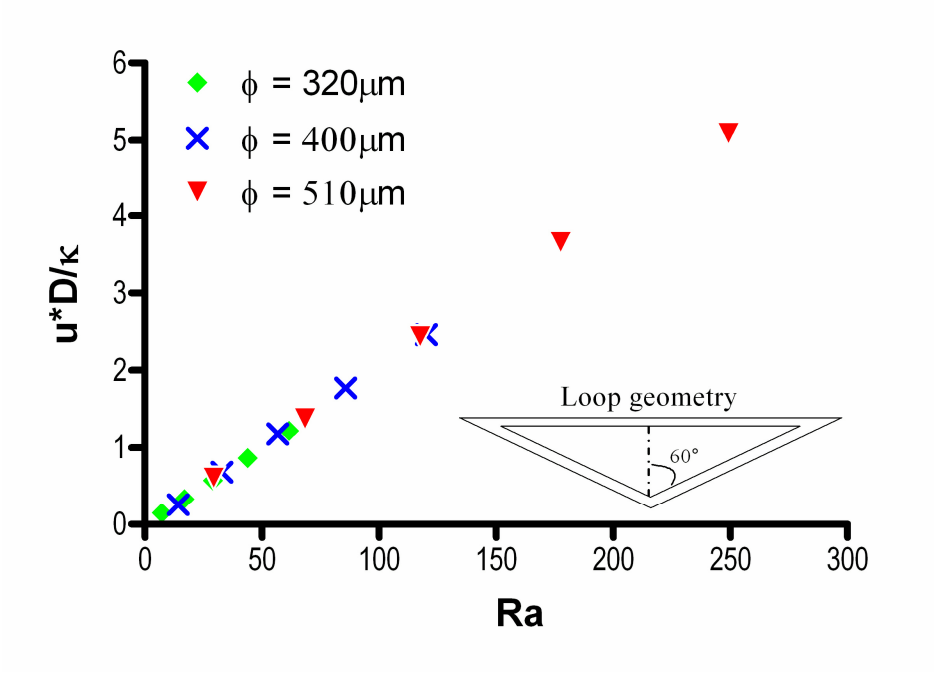

(A)

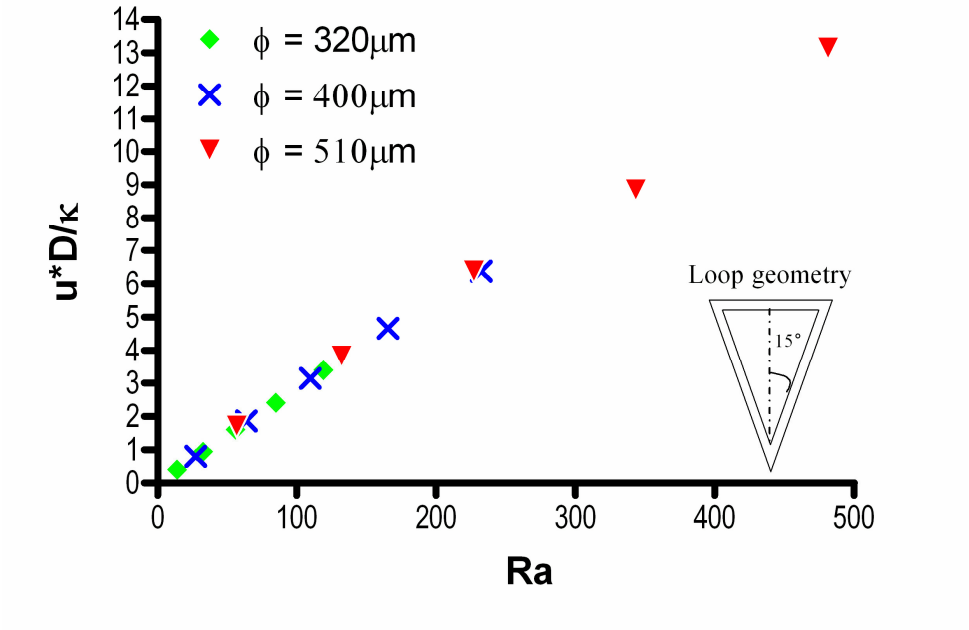

(B)

Figure 7.7 (A) Curves for triangular loops of same length but with sides inclined at 60° with vertical plane and plotted from simulation data obtained using fluent software. (B) Same as (A) however with sides inclined at 15° with vertical plane

To extend the applicability of this model for other loop geometries, we obtained simulation data for symmetric triangular loops of the same lengths, however with a different slope of the inclined legs of the triangle. While, previously for the data in Figure 7.5, the loop was inclined at 30° with respect to the vertical plane. We plotted Rayleigh number Vs uD/κ for two other geometries with inclination angle of 60° and 15° of the triangular sides with vertical plane. We obtained an interesting result showing that for both of these triangular models, the curves for velocities obtained in tubes of different diameters (320, 400 and 500 μm) collapsed analogous to the equilateral triangular geometry and in similar agreement with the experimental data (Figure 7.7). This evidently verifies the robustness of this model to design closed loop thermal cyclers without performing experiments.

To further simplify the utility of this model for convective PCR reactor designing, we rearranged equation [5.43] and obtained a new expression in terms of cycle time directly correlated to other scaling parameters as given by equation [5.44]. When we plotted twelve different results (3 for experimental data for 30° triangle and 9 for simulation data for 60°, 30° and 15° triangular loops respectively), the log-log plot of cycle time VS $LD/\kappa Ra$ provides a *master curve* where all 12 individual curves collapse together (Figure 7.8). This *master curve* can be reliably used to obtain any combination of L and D for the desired cycle time at PCR conditions and vice versa. Therefore, one can use this model to construct a closed loop thermocycler offering either the desired cycle time or the desired reaction volume (any combination and D and L) without performing individual experiments for each case.

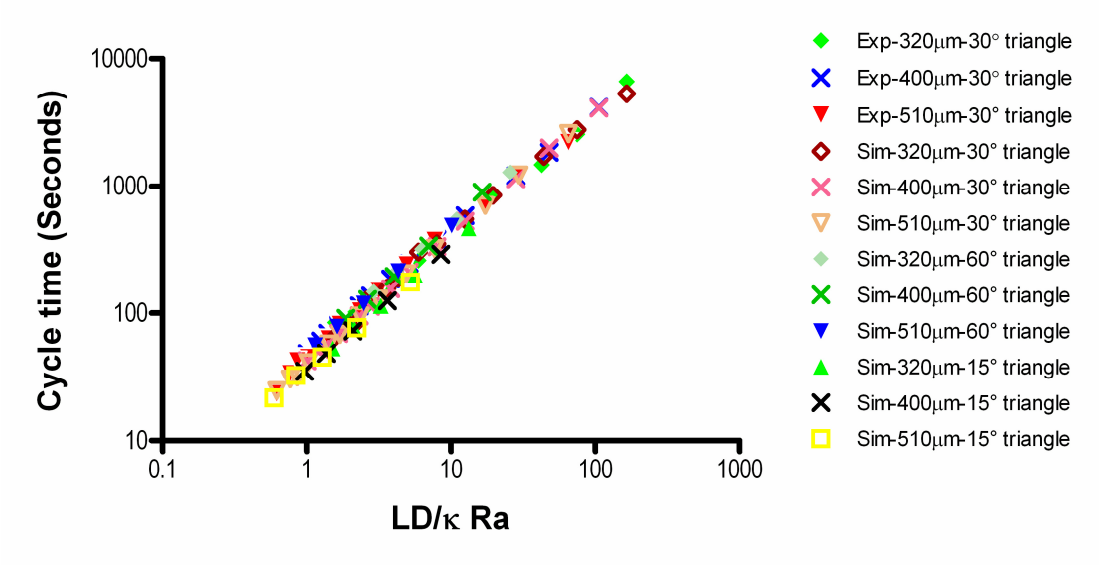

Figure 7.8 Curves representing 4 cases with each case plotted individually for three different tube diameters. The 1st case represents the experimental data while the other three are plotted from simulation data. Total of 12 curves for triangular loops of same length but with varying geometries having sides inclined at 30°, 60° and 15° respectively with vertical plane. This plot can be used to design closed loop thermocycler with any combination of cycle time, tube diameter and the loop length as desired

In addition to adjusting the global loop geometry, it is also possible to incorporate local modifications in order to deliver different residence times under denaturing, annealing, or extension conditions. For example, flow loops incorporating a larger diameter in the extension zone than in the rest of the loop can be employed in order to increase residence times during that part of each cycle. Horizontal segments can also be added to the flow path to locally increase loop length so that the residence time in a desired temperature zone can be increased (9).

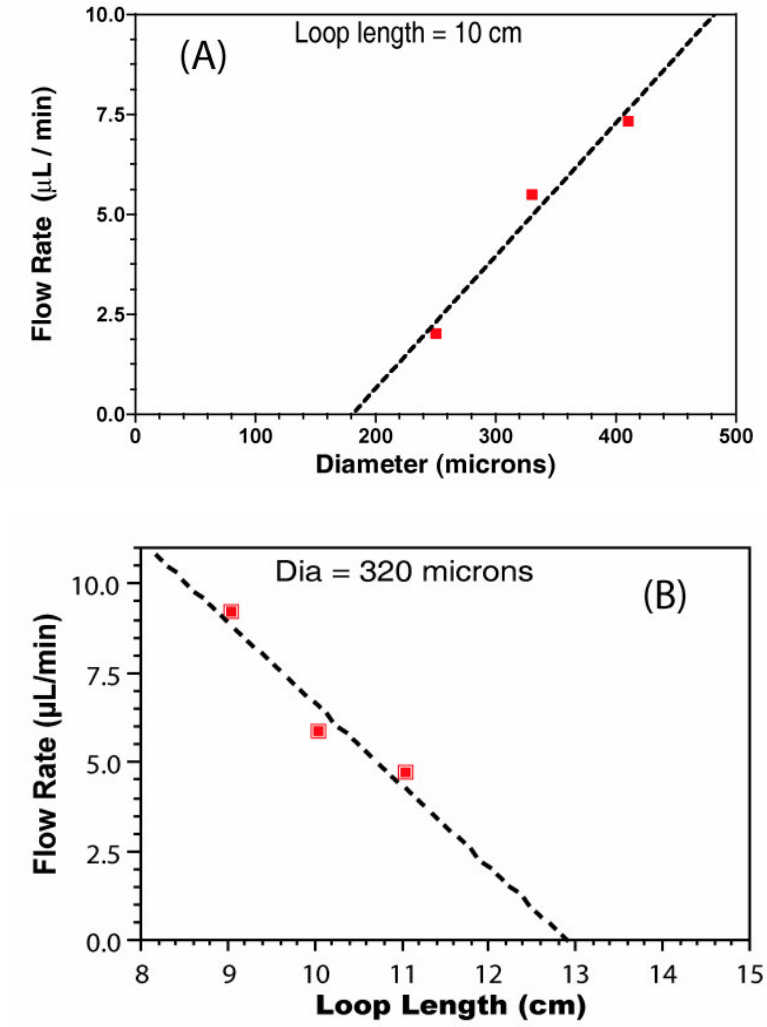

Figure 7.9 (A) Extrapolation curve showing miniaturization limits of a closed loop reactor in terms of channel diameter identifying the minimum diameter at which flow rate would cease for a specified loop length. (B) Extrapolation curve identifying the minimum length at which channel will offer drag resistance enough to stop the flow in a channel of fixed diameter

A few general guidelines for the scale-down of convective flow systems in miniaturized loops can be derived. We can use the flow rate data in Figure 7.4(A) to extract a rough estimate of the minimum channel diameter for flow to occur by extrapolating to the conditions corresponding to zero flow rate. This analysis indicates

that channel diameters can be scaled down to at least 180 μm at this tubing diameter (28 gauge) for a particular loop length, maintaining a temperature difference of 35 °C between annealing and denaturing temperatures (Figure 7.9 (A)). This minimum diameter can be further reduced through the use of shorter flow loops because the corresponding decrease in hydrodynamic resistance allows higher flow rates to be achieved under the same thermal driving force. Similarly, plotting the flow rates for different lengths of a closed loop and extrapolating the curve gives the limit up to which the loop length can be increased keeping the diameter fixed. In this case, the loops of up to around 13 cm length can be made for a 320 μm diameter channel under specified temperature gradient conditions (Figure 7.9 (B)).

Finally, we note that the parabolic velocity profile inside the flow loop implies that some variation in flow velocity exists over the tube cross section, with slower velocities present near the wall and faster speeds near the centerline. These effects, however, are counteracted by both lateral molecular diffusion of reagents across streamlines and perturbations to the streamlines due to centrifugal effects generated at the curved locations as the flow travels through the abrupt corners of the square/triangular shaped loops.

CHAPTER VIII

PORTABLE BATTERY POWERED THERMAL CYCLERS

With continued research and recent advancements in the development of more efficient PCR amplification systems, sufficient knowledge is available to construct miniaturized thermocyclers. However, until recently, no such design has been proposed or developed that is inexpensive, robust and at the same time portable enough to be carried over and used anywhere depending on the requirement. With the essence of PCR technology being utilized these days in numerous applications including advanced forensics and pathogen detection during a warfare, development of portable analysis systems are of immense importance. Combining the various techniques developed in late 90's including the PCR microchips developed by Northrup et al. earlier, microtechnology center at the Lawrence Livermore National Laboratory (LLNL) developed the first prototype of a portable DNA amplification and detection system (65). The miniature analytical thermal cycler instrument (MATCI) (12 cm x 27 cm x 14 cm) contained a laptop computer and utilized a PCR microchip (0.6 cm x 2.2 cm x 0.2 cm), a solid-state optics system for real-time fluorescent detection and an electronic controller for computer interfacing. The PCR unit was operated by 13 NiCd batteries, and the entire The entire MATCI unit and the laptop computer were fitted in medium sized briefcase of dimensions 33 cm x 54 cm x 18 cm and altogether weighed 35 pounds (Figure 8.1(A)). In this report, the MATCI was applied to perform human identity testing. In their continued efforts, the same group then utilized MATCI to generate

products for human identity testing and demonstrated the applications of portable analysis systems applied to forensic science (66).

(A)

(B) **(C)**

Figure 8.1 Pictures of portable and advanced nucleic acid analyzers developed by Lawrence Livermore National Laboratory. (A) A miniature analytical thermal cycler instrument (MATCI), first prototype portable thermocycler developed by LLNL. Picture adapted from (65) (B) Advanced nucleic acid analyzer (ANAA) is the modified version of MATCI containing an array of 10 silicon chambers for multiple sample handling. Picture adapted from (49) (C) Bio-Seeq, the first commercial handheld nucleic acid analyzer (HANAA) developed by Smiths Detection-Edgewood (SDE), Inc.. Picture adapted from www.arrowtechinc.com

The MATCI proved challenging towards the development of portable analysis instruments and LLNL continued their efforts and developed a modified version of MATCI with multiple sample handling capability utilizing an array of 10 silicon reaction chambers (49). They called the instrument an advanced nucleic acid analyzer (ANAA) (Figure 8.1(B)) and the detection of microbes was demonstrated in as little as 16 min with detection limits of 10^5–10^7 organisms/L (10^2–10^4 organisms/mL).

Subsequently, the first hand-held advanced nucleic acid analyzer (HANAA) was developed by the Lawrence Livermore National Laboratory in 1999 based on their previous model of the nucleic acid analyzer ANAA (67). The PCR process used by HANAA was also utilizing the *Taq*Man real-time PCR technology. HANAA weighed around 2 pounds operating for up to 5.5 hours depending on the usage and represented great sensitivity (capability of detecting 200 organisms per milliliter). HANAA has been commercialized by Smiths Detection-Edgewood (SDE), Inc. as Bio-Seeq (a hand-held nucleic analyzer) capable of detecting pathogens including anthrax, orthopox, tularemia and plague (Figure 8.1(C)).

In an attempt to harness the technologies recently developed to utilize convectively driven flows in combination with the microfluidic approach, we have designed an advanced version of CLTC that can be operated using just two “AA” size batteries. The complete thermocycler hardware can be enclosed inside a small handheld unit of the size of a small cell phone. Preliminary results show that the battery operated device is capable of performing high-speed PCR with reduced reaction volumes. The

greatly simplified design of this system incorporates three aluminum blocks maintained at each of the three PCR temperature zones as shown in Figure 8.2.

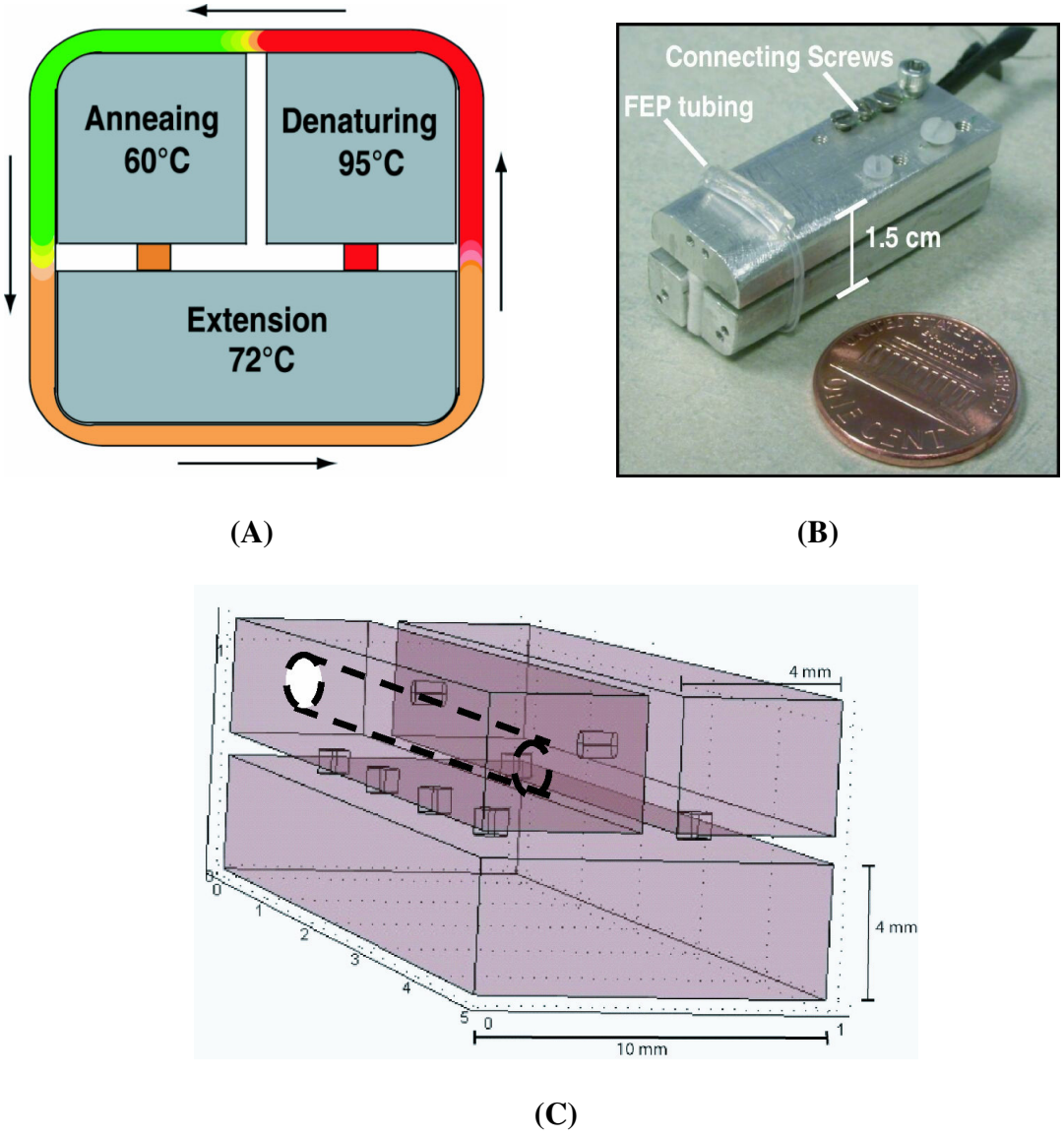

(A) **(B)**

(C)

Figure 8.2 (A) Schematic of the 3-block battery operated thermal cycler design showing plan view of the three aluminum blocks interconnected by threaded screws. The flow loop is wrapped on the aluminum block assembly. Only by heating one of the blocks, the other blocks attain their respective temperatures due to heat conduction through the connecting screws

One of the blocks is drilled with a bore from one side and a resistance heater cartridge is inserted to heat the block. While on the other side, small holes are provided to insert thermocouple probes for temperature monitoring. All three blocks are interconnected with each other sideways using threaded screws such that when only one block is heated to 95°C (denature), the other blocks are passively maintained at 72°C (extension) and 60°C (anneal) by heat conduction through the connecting screws. Air gap is provided between the individual blocks to provide maximum insulation between the block surfaces and to ensure that heat conduction only occurs through the connecting screws. Because only one block needs to be heated using a single heater, power consumption is minimal and the whole setup (including temperature controller) can be operated on two 'AA' size batteries (Figure 8.3 (A)).

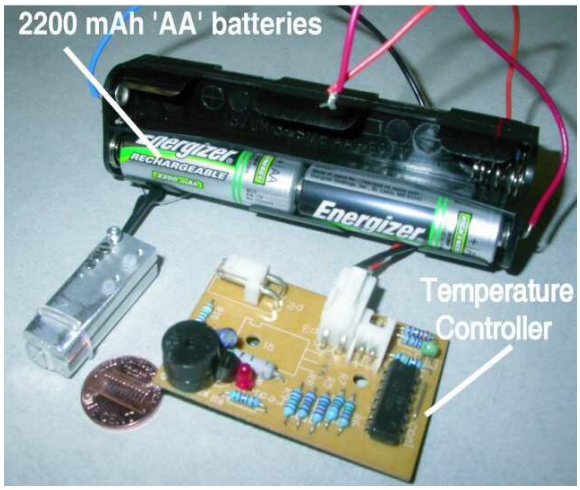

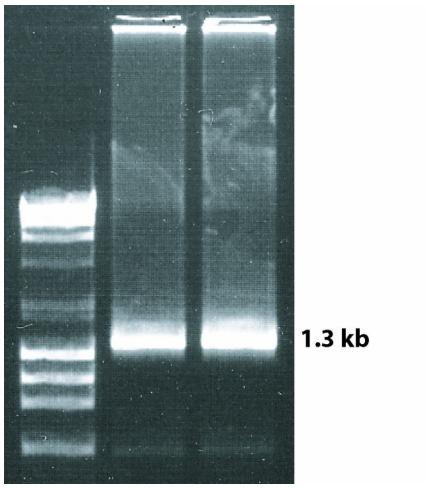

(A) **(B)**

Figure 8.3 (A) Photograph of the complete 3-block thermal cycler assembly showing the aluminum block device, a battery holder and a simple on/off type temperature controller to maintain the temperature of one of the blocks at constant 95℃. (B) Electrophoresis gel picture of the 1.3 kb target amplified in 3-block thermocycler using 2 'AA' batteries within 50 minutes

Temperatures in all zones can be easily and independently adjusted by altering the number of screws connecting the blocks or by using screws of different diameters. Additional precision and control can be obtained by using screws of appropriate thermal conductivities.

We have successful demonstrated amplification of a 1.3kb amplicon of λ-DNA incorporating only 6-8μL reaction volume and for reaction times of 50 minutes. This is only a prototype design and can be further optimized for greatly enhanced level of performance. This low cost portable device can be invaluable to soldiers, doctors, forensics and many other applications requiring an immediate onsite analysis of the collected DNA samples.

The CLTC offers advantages over conventional benchtop thermocyclers in terms of speed, portability, and cost. A format equivalent to the multiwell arrangement in benchtop thermocyclers can also be achieved by using an array of multiple loop reactors arranged in parallel on the triangular scaffold. In terms of power consumption, the dual thermoelectric heater design used in this prototype draws about 3.5 W, with each 4-cm-long heating element capable of comfortably accommodating 10-12 tubing loops (including both the tubing outside diameter and the larger diameter PVC sleeve used to join the free ends, and accounting for a 2-cm-long inactive area occupied by temperature sensors and mounting hardware). Based on these results, a scaled-up design capable of accommodating 96 loops would require a heating element of about 18 cm in length (calculated using a basis of 12 loops per 2 cm heater length, plus a 2-cm-long inactive zone) that would be expected to consume about 16 W of power (calculated using a basis

of 3.5 W per 4 cm heater length). Even considering the case where all three temperature zones are actively controlled (power consumption would increase to about 24 W), this analysis implies a power requirement of 100 W or less for a 384-reactor array. For comparison, the conventional benchtop thermocycler used in our control studies (TGradient, Biometra) lists a 310 W maximum power rating. Although these power consumption values are approximate, they can serve to establish an order of magnitude estimates for comparison. Finally, we note that the FEP loops are inexpensive and disposable, and the entire system is suitable for use in a variety of applications including cycle sequencing and real-time PCR assays.

CHAPTER IX

OTHER APPPLICATIONS OF CONVECTIVE THERMAL CYCLING SYSTEMS

Before getting the idea of using FEP tubing to perform thermocycling for DNA analysis applications, we constructed various flow loop devices using a melt processable thermoplastic elastomer and Plexiglas blocks. Microfluidic flow channels were constructed by molding a soft aluminum wire between the two sheets of the polymer material. After sandwiching the wire, slightly heating the polymer facilitates the two polymer sheets to bond together. The aluminum wire is then pulled out closing the upper open end of the rectangular loop. Figure xxx shows a rectangular flow loop channel of 250 μm diameter constructed using the above procedure. Similarly closed flow loops can also be fabricated by drilling holes in the Plexiglas blocks and subsequently closing the open ends by filling epoxy. Only two ends are left open at the top as inlet and outlets. Threads are etched on the inner surface of the open ends to provide an alternative way of closing the channels using threaded screws.

Figure 9.1(B) shows a rectangular flow loop of 960 μm diameter. These closed loops were developed as our preliminary efforts towards developing a simplified and optimized system. However, these microfluidic circuits can also be used in many other applications few of them are described as follows.

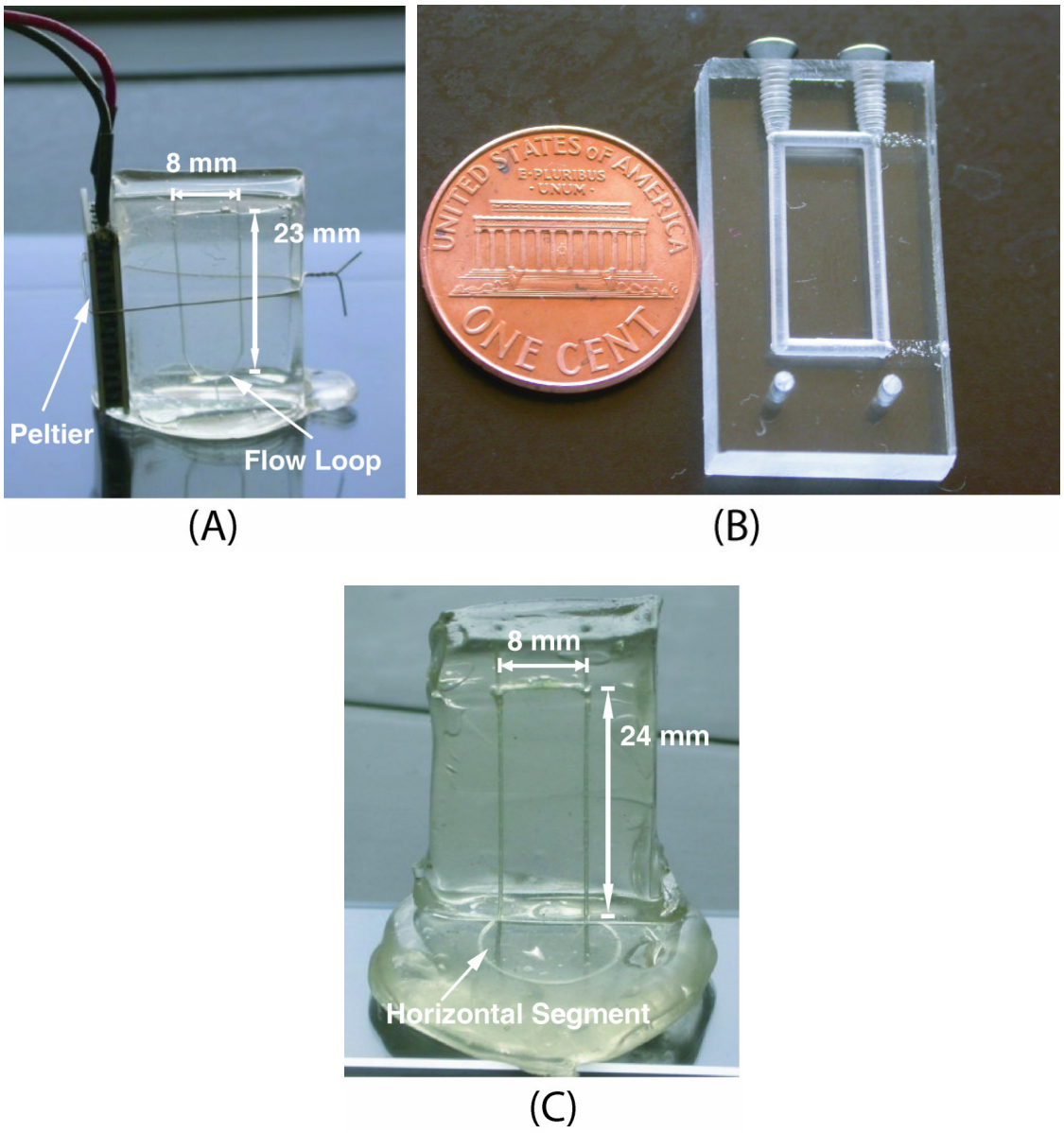

Figure 9.1 (A) A 6 cm long rectangular flow loop molded in a thermoplastic polymer using a 250 µm diameter flexible aluminum wire. A Peltier heater attached on one side of the block is used to heat the loop legs while maintaining the other side at room temperature. (B) A 960 µm inner diameter channel drilled in a Plexiglas block and sealing the open end by filling with epoxy. Two ends at the top are left open as inlet and outlet. (C) A 3-dimentional flow loop constructed by joining two separate semi-loops perpendicular to each other. When a temperature gradient is maintained across the vertical legs of the loop, similar flow rates are generated in the horizontal segment as well demonstrating the capability of these devices to pump fluids inside microfluidic devices

9.1 Recirculating extensional flows

In addition to performing biochemical reactions, these devices can also be used to generate extensional flow fields in cross-slot geometry or to perform on chip pumping and thermocycling operations when integrated with microfluidic systems. Extensional flows are often difficult to generate, but are of considerable interest in the area of complex fluid rheology. A typical geometry used to generate extensional flow consists of a cross-slot arrangement in which a stagnation flow is generated between two impinging liquid streams. In this configuration, a planar extensional flow occurs in the vicinity of the stagnation point such that:

$$V_x = \dot{\varepsilon} x \qquad \text{and} \qquad V_y = -\dot{\varepsilon} y$$

Where, $\dot{\varepsilon} = V_x / x = -V_y / y$ is a constant called the extension rate. V_x and V_y are fluid velocities at in 'x' and 'y' directions at distances x and y respectively from the stagnation point. Figure 9.2 shows a closed cross-slot channel network fabricated in a Plexiglas block which, when heated from any two opposite sides while keeping the other two sides at a lower temperature, can generate extensional flow patterns at the stagnation point of the cross-slot. Flow visualization using fluorescent spheres confirmed that microspheres become trapped at the stagnation point for 2-3 seconds experiencing elongational forces before they start accelerating in the x-direction. Under these conditions, extension rates in the vicinity of 3 s^{-1} could be achieved. These non-pulsatile continuous flow fields can be harnessed to stretch DNA/polymers and to study single molecule behavior.

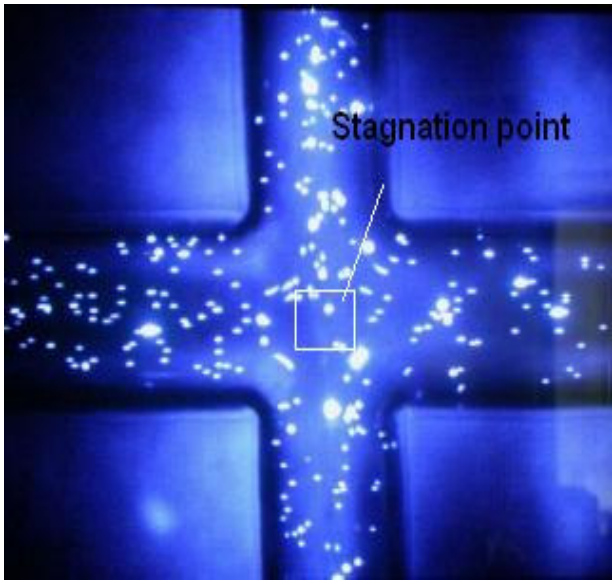

(A)

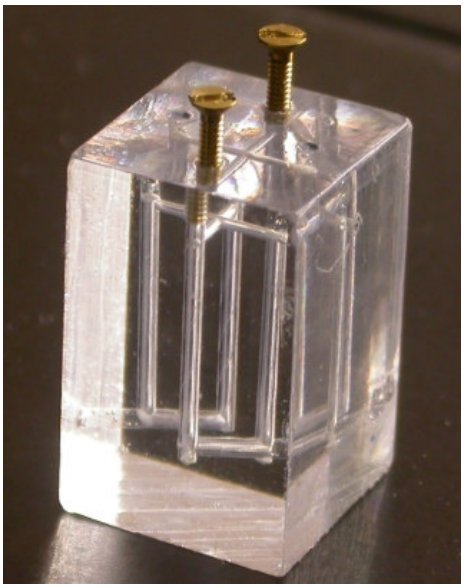

(B)

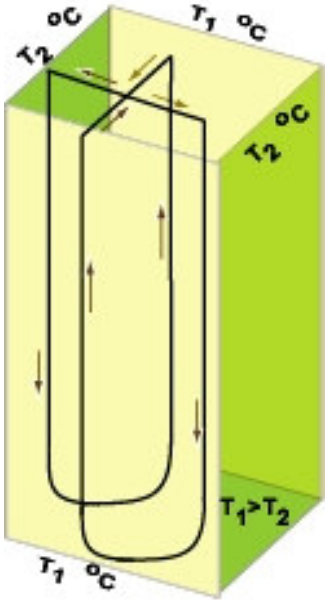

(C)

Figure 9.2 (A) Top view of the cross-slot channel filled with 6 µm fluorescent beads. While circulating through the channel network, the movement of fluorescent beads ceases for a few seconds at the stagnation point due to the effect of opposing forces acting at the stagnation point. At this point, the particles experiencing a net extensional force as long as trapped within the stagnation location. (B) Picture of the cross-slot channel network constructed inside a Plexiglas block by drilling holes. (C) Schematic of the fluid flow scheme within the cross-slot network

9.2 Convectively driven micropumps

We have also investigated the use of these flow loops to pump fluids in the horizontal plane by constructing devices where the lower horizontal segment of the loop is replaced by a longer segment creating a 3-D flow path (Figure 9.1(C)). Similar flow rates are observed in these devices, indicating that sufficient pumping capacity exists to drive flows in a variety of microfluidic channel networks.

CHAPTER X

CONCLUSION

With this work, we hope to show that convective flow thermocycling systems have advanced beyond the proof-of-concept phase of development, and are now capable of seriously competing with existing mainstream instrumentation. We have shown that convective flow thermocycling systems are capable of offering a level of performance comparable to existing instrumentation, with the added benefits of (i) faster cycling times, (ii) low cost, and (iii) compatibility with existing laboratory protocols.

In terms of cost, the complete system shown in Figure 6.1 can be assembled for well under $200 US (excluding the power supply units). Since the majority of this cost is attributable to the power supply, it is feasible to expect an additional order of magnitude in cost reduction for an instrument manufactured in commercial quantities and designed for battery powered operation. Whereas the battery operated 3-block thermal cycling device shown in Figure 8.2(B) and Figure 8.3(A) can be constructed (in a lab) for less than $10 including the batteries and the temperature controller. In terms of adaptability, it is notable that all of the amplification reactions reported here were performed with no modification to standard protocols used in conjunction with a conventional benchtop thermocycler. The tubing-based format can also be straightforwardly coupled with an automated fluidic interface to perform sequential sample loading, product recovery, and downstream analysis (e.g., capillary electrophoresis). Moreover, the flow loop design is readily adaptable for use in real-time PCR and cycle sequencing applications. The

attractive combination of performance and simplicity offered by these devices addresses many of the shortcomings of current technology, ultimately making it feasible to greatly expand the use of PCR-based assays. A reduced level of overall power consumption and elimination of the need for dynamic temperature control also makes these systems ideal for use in portable battery operated applications.

CHAPTER XI

FUTURE WORK: DOWNSTREAM ANALYSIS PROCEDURES

11.1 Real-time PCR

Although real-time PCR is not actually a downstream process, it obviates the requirement of "gel electrophoresis" which is usually the immediate post PCR analysis process. PCR has proved to be a powerful technique in analyzing the genetic material, though the speeds associated with the overall process are still dictated by several steps involved in the entire process. While we have developed novel techniques to overcome one of the rate limiting step (DNA amplification step), the downstream analysis steps still remain an important issue to address requiring considerable amount of research. One of the relevant post PCR steps is gel electrophoresis that is required to isolate individual amplified products from each other and from the other impurities. As discussed in the earlier sections, gel electrophoresis is a time consuming yet extremely important step of the overall analysis process. In some cases For example, during pathogen detection studies, it is often required to ensure whether the sample contains the template DNA associated with the primers used for amplification and the actual end products are irrelevant. Whereas in other cases such as study of gene expression, investigating the initial amount of available template is of utmost importance. For instances such as these, a powerful technique called real-time PCR has been developed that monitors the amplification process as it proceeds.

11.1.1 Significance of real-time PCR

Real-time monitoring of PCR has simplified and accelerated PCR laboratory procedures and has increased information obtained from specimens including routine quantification of amplification products. This combines the nucleic acid amplification and detection steps into one homogeneous assay and obviates the need for gel electrophoresis to detect amplification products (68) allowing the sensitive, specific and reproducible quantization of nucleic acids. In a traditional PCR reaction as the reaction progresses, the reagents are consumed as a result of amplification. Due to this reagent constraint after a certain point after about 30-35 cycles), all DNA templates are not replicated during the PCR cycle. This depletion occurs at different rates for each replicate. Until about 8-10 cycles, amplification of the target DNA amplicon is in the initial phase which is almost negligible because there are very few copies of the exact target DNA while most others also include flanking DNA regions. Subsequently after about 8-10 cycles, there is a sudden rise in the amplification rate and the amplified products begin to diverge in their quantities within the linear amplification phase. Eventually, the sample gets depleted of the reactants (primers, nucleotides, enzymes) and the amplification rate significantly diminishes and enters the plateau phase. The plateau for different samples may differ due to the different reaction kinetics for each sample. It is in this phase where traditional PCR is analyzed, also known as the end-point analysis. This end-point detection suffers from certain issues such as low resolution, poor precision, low sensitivity and the need for post PCR processing. Also, the results of this detection are not expressed quantitatively and often require additional

purification and quantification steps. On the other hand, real-time PCR allows the detection of PCR products during the early phases of the reaction. This ability of measuring the reaction kinetics in the early phases of PCR provides a distinct advantage over traditional PCR detection.

The fluorescence based real-time PCR techniques has completely revolutionized the approach to PCR-based quantification of DNA and RNA and is easy to perform, has high sensitivity, more specificity, and provides scope for automation. This technology has enabled the shift of molecular diagnostics toward a high-throughput, automated technology with lower turnaround times.

11.1.2 Real-time PCR principle

Real-time PCR is based on the detection of the fluorescence produced by a reporter molecule which increases, as the reaction proceeds. The fluorescence emitted by the reporter molecule multiplies as the PCR product accumulates with each cycle of amplification. By recording the amount of fluorescence emission after each cycle, it is possible to monitor the PCR reaction during exponential phase where the first significant increase in the amount of PCR product correlates to the initial amount of target template. The increasing number of probes and platforms available for real-time PCR has significantly reduced its overall cost making this an increasingly attractive technique (69). There are several types of detection system available to carry out real-time PCR including dual labeled probes (often known as *Taq*Man probes), minor groove binding (MGB) probes, molecular beacons, intercalating dyes (SYBR Green I) and fluorescence

energy transfer (FRET) probes and more recently developed fluorescent labeled primers such as Sunrise, Lux or Scorpion primers (69-72).

11.1.3 Determination of critical (Ct) value for controls

For real-time PCR assays, addition of suitable standard quantitative controls to the assay is required. The quantitative standards (oligos or plasmids) are prepared in bulk, tested for acceptable linearity and slope (−3.33) for a good 10-fold dilution series. It is essential to track the C_T values of the controls to check that the assay is performing satisfactorily, and to enable a smooth transition to a new control set when required. A fluorescence threshold is determined in the linear part of the curve, corresponding to the phase with the best efficiency of amplification. A *'C_t'* is defined as the number of cycles necessary to reach this threshold of fluorescence. $C_t = f(\log_{10})$ initial concentration of the specific target). Newly prepared standards must have C_t values falling within two standard deviations of the mean value determined for the standards previously in use. The correct placing of the threshold line is essential to allow accurate C_t measurement. Some of the computer software available with current real-time PCR formats can automatically place the threshold line during result analysis. Any sample with fluorescence above this line will be regarded as positive by the computer. An alternative is to use a fixed threshold line. The use of such a system will ensure the real-time assay is directly comparable to previous runs.

Preparation of calibration curve: A calibration curve is drawn from parallel runs using known initial amounts of the specific target. This allows the calculation of the amount of the target product present in a given sample of interest.

Prevention of evaporation of samples: Real-time thermocycling reactors should be sealed properly to avoid evaporation of PCR reagents during cycling. Evaporation of samples during reaction may result in a curve mimicking a positive PCR reaction.

11.1.4 Signal drift

Signal drift (traces that increase in fluorescence as the PCR progresses but are not exponential) often occurs towards the end of the PCR reaction. True positive samples may show signal drift because of sub optimal PCR conditions, inhibition and primer mismatches. However, negative samples may also show signal drift due to probe breakdown resulting in a fluorescence increase. Some platforms allow multicomponent analysis of weak positive traces. This allows users to assess the changes of each fluorescent label in the reaction. True positive samples show an exponential increase in the fluorescent signal whereas signal drift is observed due to a change in the normalization dye and is not exponential.

11.1.5 Non –specific and specific detection of DNA

Based on the molecule used for the detection, the real-time PCR techniques can be of two types: The detection of PCR products can be either non-specific detection using DNA binding dyes or specific detection using target specific probes. DNA binding dyes are used as fluorescent reporters to monitor the real-time PCR reaction. Double-stranded DNA-binding dyes provide the simplest and cheapest option for real-time PCR. In the simplest and most economical format, that reporter is the double-strand DNA-specific dye SYBR Green I (molecular probes). SYBR Green I is the most widely used double-strand DNA-specific dye reported for real-time PCR. SYBR Green I remains stable under PCR conditions and in the solution, the unbound dye exhibits very little fluorescence. SYBR Green I binds minor groove of double-stranded DNA, and upon excitation emits light. Thus, as a PCR product accumulates, fluorescence increases.

All real-time PCR systems rely upon the detection and quantization of a fluorescent reporter, the signal of which increases in direct proportion to the amount of PCR product in a reaction. If a graph is drawn between the log of the starting amount of template and the corresponding increase the fluorescence of the reporter dye fluorescence during real-time PCR, a linear relationship is observed. The disadvantage is that SYBR Green I will bind to any double-stranded DNA in the reaction, including primer-dimers and other non-specific reaction products, which results in an overestimation of the target concentration. For single PCR product reactions with well designed primers, SYBR Green I can work extremely well, with spurious non-specific background only showing up in very late cycles. The two most popular alternatives to

SYBR Green I are *Taq*Man and molecular beacons, both of which are hybridization probes relying on fluorescence resonance energy transfer (FRET) for quantization.

11.1.6 Multiplex real-time PCR

Real-time PCR can be performed in a "multiplex" format which means that more than one PCR product can be detected in a single reaction tube. For each sequence, there is a unique color of fluorescent dye and therefore, each PCR product is associated with its own color which is detected by the real-time PCR machine.

11.1.7 Limitations of real-time PCR

Despite numerous advantages, real-time PCR has some limitations. Since it is performed on small DNA fragments, real-time quantitative PCR might fail to detect biologically relevant processes like alternative splicing or partial transcript degradation occurring during post-transcriptional gene silencing events (73). Most evidently, real-time PCR development is still limited by the high costs of the machine and reagents, but hopefully, future will make this technology economically more widely accessible.

11.1.8 Utilization of convective CLTC for real-time PCR application

The CLTC is well suited to perform simultaneous detection due to transparent nature of the FEP loop reactor. This can be simply done by positioning a photo-detector

at a location immediately after the extension zone since the SYBR Green I dye expresses fluorescence only when bound to the double stranded DNA molecule (Figure 11.1).

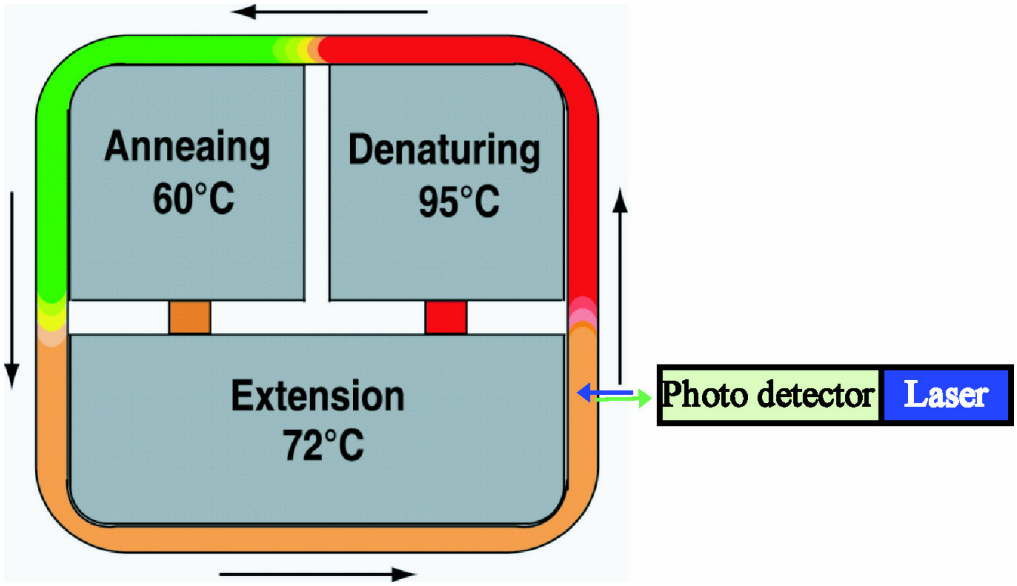

Figure 11.1 Schematic of the closed loop thermal cycler demonstrating its adaptability to perform real-time PCR by aligning a photodetector at the location just before the initiation of denaturation step

Hence, detection step must be performed before the initiation of denaturation cycle. We will further explore and characterize the capability of CLTC to perform real-time detection, which will be eventually useful to develop portable pathogen detection systems.

The transparency of the thin walled FEP tubing used here as PCR reactors makes this system ideally suited for real-time applications since a part of the tubing is already kept exposed for the detection window. The same detection window can be used for real-time fluorescence imaging. We performed preliminary experiments and detected weak fluorescence using a simple optical microscope equipped with a CCD camera. However,

further characterization of this technique needs to be done in order to get optimized performance.

11.2 DNA sequence analysis (Sanger cycle sequencing)

In recent years, DNA sequencing has emerged as an important molecular biological technique allowing thorough analysis of DNA because it provides the most basic information of the sequence of nucleotides. DNA sequencing is the process of determining the exact order of the bases A, T, C and G in a fragment of DNA. The DNA is used as a template to generate a set of fragments that differ in length from each other by a single base. The fragments are then separated by size, and the bases at the end are identified, recreating the complementary sequence of the original DNA. The most commonly used method of sequencing DNA - the dideoxy or chain termination method was developed by Frederick Sanger in 1977 (74).

DNA Sequencing has been applied to many areas of research. For example, the polymerase chain reaction (PCR), a procedure which rapidly produces multiple copies of a desired piece of DNA, requires first knowing the flanking sequences of this piece to design primer. DNA sequencing helps in locating regulatory and gene sequences, making comparisons between homologous genes across species and identifying mutations. The amino acid sequences can be determined more easily by sequencing a piece of cDNA and finding an open reading frame. These are only a few examples that illustrate how DNA sequencing has revolutionized molecular biology.

11.2.1 Sanger cycle sequencing principle

Sanger's method of sequencing , which is also referred to as dideoxy sequencing or chain termination, is based on the use of modified bases 2',3'-dideoxynucleotide triphospates (ddNTP's) in addition to the normal deoxynucleotides (dNTP's) found in DNA. When a piece of DNA is being replicated and a dideoxy base is incorporated into the new chain, it stops the replication reaction (75). Dideoxynucleotides are essentially the same as nucleotides except they contain a hydrogen group on the 3' carbon instead of a hydroxyl group (OH). The key principle is that the concentration of ddNTP should be 1% of the concentration of dNTP. The primer plays the critical role of determining the region of the template molecule that will be sequenced. As the DNA is synthesized, nucleotides are added on to the growing chain by the DNA polymerase. However, at random occasions, a dideoxynucleotide is incorporated into the chain in place of a normal nucleotide, which results in a chain-termination. This results a series of labeled DNA with varying length. The strand synthesis does not proceed indefinitely because the reaction mixture contains small amounts of a dideoxynucleotide, which blocks further elongation because it has a hydrogen atom rather than a hydroxyl group attached to its 3′-carbon. The lengths of these strands depend on the location of the base relative to the 5' end. Thus, chain termination sequencing involves the synthesis of varying lengths of strands of DNA that are complementary to a single-stranded template. The fragments of varying length are separated by polyacrylamide gel electrophoresis (PAGE) on the basis of size, with the shorter fragments moving faster and appearing at the bottom of the gel.

11.2.2 Automated sequencing

The automated sequencing method uses PCR to incorporate dideoxynucleotides which contain fluorescent dyes in a primer extension sequencing reaction. Thermal cycle sequencing offers an alternative to the traditional methodology. The discovery of thermostable DNA polymerases, which led to the development of PCR, has also resulted in new methodologies for chain termination sequencing. In particular, the innovation called thermal cycle sequencing has two advantages over traditional chain termination sequencing. It uses double-stranded rather than single-stranded DNA as the starting material. Very little amount of DNA is needed, so the DNA does not have to be cloned before being sequenced. With the automated procedures the reactions are performed in a single tube containing all four ddNTP's, each labeled with a different color dye (76), one for each ddNTP. Thermal cycle sequencing is carried out in a similar way to PCR but just one primer is used. Because there is only one primer, only one of the strands of the starting molecule is copied, and the product accumulates in a linear fashion, not exponentially as is the case in a real PCR. The presence of the ddNTP in the reaction mixture causes chain termination. When the PCR is complete, the reaction mix contains a population of PCR fragments of different lengths, each terminating in a fluorescent-dye-containing dideoxynucleotide. Advancements in fluorescence detection and fluorescent dyes (77-79) have helped to define current fluorescence detection in DNA sequencing method.

Each dideoxynucleotide base contains a different fluorescent dye which emits a characteristic wavelength, thus the identity of the dye corresponds to the final base on

that fragment. The entire reaction is purified, then run in a single lane on a polyacrylamide gel in a sequencer, so that the fragments separate according to size. As the fragments are electrophoresed, they run past a laser detector at the bottom of the gel, and the emission wavelength of each fragment is detected. Since the four dyes fluoresce at different wavelengths, a laser then reads the gel to determine the identity of each band according to the wavelengths at which it fluoresces. The results are then depicted in the form of a chromatogram, which is a diagram of colored peaks that correspond to the nucleotide in that location in the sequence.

11.2.3 Utilization of CLTC for DNA sequencing reactions

Sequencing reactions also require thermocycling as one of the major steps in the overall process, though the sequencing protocol is different from PCR in a way that the sequencing reagent mixture also contains chain-terminator dideoxynucleotides (ddNTP) in addition to the regular dNTPs. During the last step of the PCR cycle, the polymerase adds either the dNTPs or the ddNTPs to the chain randomly. Therefore, when PCR is complete, the product contains PCR fragments of all different lengths; for whenever a ddNTP was added, the elongation stopped. Moreover, sequencing reactions involve only single type of primers associated with the target template strand. Hence, the sequencing amplification is linear unlike the PCR process that proceeds exponentially. Due to these complexities involved, cycle sequencing reaction yields less throughput compared to regular PCR amplification and requires longer reaction times to achieve detectable amplified products.

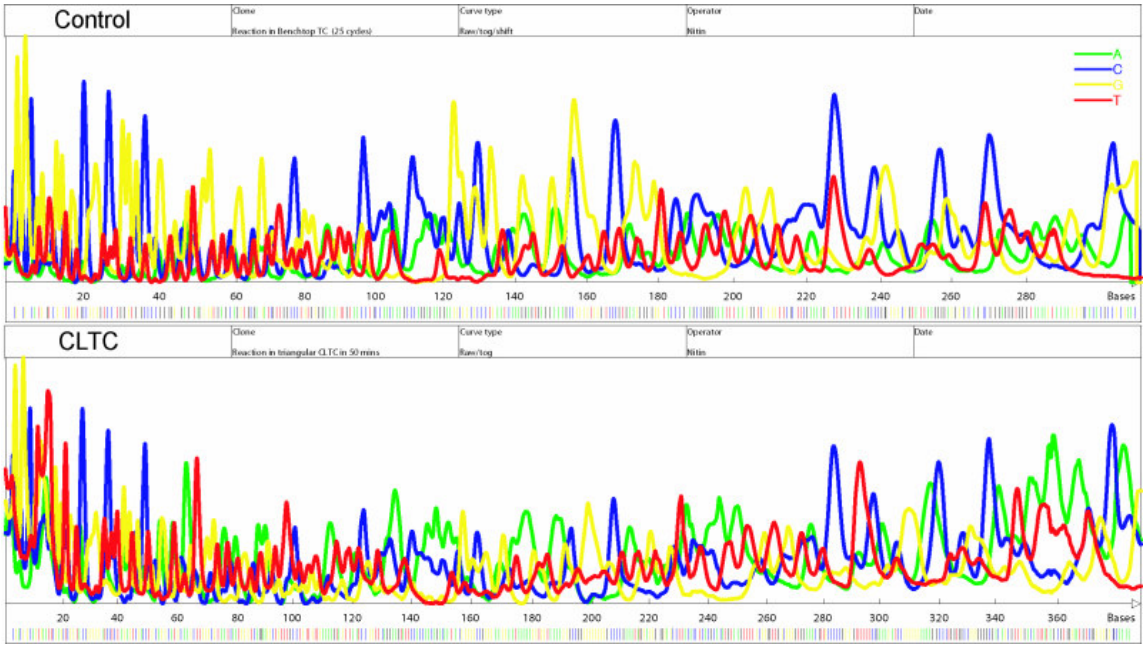

Figure 11.2 Sanger cycle sequencing picture showing peaks of sequenced nucleotides and the results of the cycling reaction from CLTC compared with those from a benchtop thermocycler (control)

The CLTC offers an inexpensive way to overcome these limitations to accelerate the time limiting thermocycling step of the sequencing process. The rapid thermocycling capabilities of CLTC make it an ideal choice to be used as a sequencing device. Though, the CLTC only performs thermocycling, it can significantly reduce the sequencing reaction times required by traditional thermocycling instruments. Moreover, the CLTC can be easily incorporated as an integral part of a micro-total analysis system and with an ability to be interlinked with other downstream separation and detection processes. We have performed preliminary experiments to demonstrate that CLTC can also be effectively used for high speed sequencing processes. We have shown preliminary by performing sequencing PCR in CLTC within 50 minutes Figure 11.2. However, further work is required to characterize and optimize the sequencing capabilities of CLTC.

REFERENCES

1. Cantor, C.R. and Smith, C.L. (1999) *Genomics: The Science and Technology Behind the Human Genome Project*. Wiley Interscience, New York.
2. Yang, S. and Rothman, R.E. (2004) PCR-based diagnostics for infectious diseases: uses, limitations, and future applications in acute-care settings. *The Lancet: Infectious Diseases*, **4**, 337-348.
3. Saferstein, R. (2004) *Criminalistics - An Introduction to Forensic Science*. Pearson Prentice Hall, Upper Saddle River, NJ.
4. Sauer, S., Lange, B.M.H., Gobom, J., Nyarsik, L., Seitz, H. and Lehrach, H. (2005) Miniaturization in functional genomics and proteomics. *Nature Reviews: Genetics*, **6**, 465-476.
5. Syvänen, A.C. (2005) Toward genome-wide SNP genotyping. *Nature Genetics*, **37**, 55-59.
6. Krishnan, M., Ugaz, V.M. and Burns, M.A. (2002) PCR in a Rayleigh-Bénard convection cell. *Science*, **298**, 793.
7. Braun, D. (2004) PCR by thermal convection. *Modern Physics Letters B*, **18**, 775-784.
8. Chen, Z., Qian, S., Abrams, W.R., Malamud, D. and Bau, H. (2004) Thermosiphon-based PCR reactor: experiment and modeling. *Analytical Chemistry*, **76**, 3707-3715.

9. Krishnan, M., Agrawal, N., Burns, M.A. and Ugaz, V.M. (2004) Reactions and fluidics in miniaturized natural convection systems. *Analytical Chemistry*, **76**, 6254-6265.

10. Wheeler, E.K., Benett, W., Stratton, P., Richards, J., Chen, A., Christian, A., Ness, K.D., Ortega, J., Li, L.G., Weisgraber, T.H. *et al.* (2004) Convectively driven polymerase chain reaction thermal cycler. *Analytical Chemistry*, **76**, 4011-4016.

11. Chandrasekhar, S. (1961) *Hydrodynamic and Hydromagnetic Stability*. Dover Publications, Clarendon, Oxford

12. Gershuni, G.Z. and Zhukovitskii, E.M. (1976) *Convective Stability of Incompressible Fluids (translated from Russian)*. Israel Program for Scientific Translations ; Springfield, VA : available from National Technical Information Service, 1976, Jerusalem

13. Greif, R. (1988) Natural circulation loops. *Journal of Heat Transfer* **110**, 1243-1258.

14. Saiki, R.K., Scharf, S., Faloona, F., Mullis, K.B., Horn, G.T., Erlich, H.A. and Arnheim, N. (1985) Enzymatic amplification of beta-globin genomic sequences and restriction site analysis for diagnosis of sickle cell anemia. *Science*, **230**, 1350-1354.

15. Mullis, K.B. and Faloona, F.A. (1987), *Methods in Enzymology*. Academic Press, San Diego, CA, Vol. 155, pp. 335-350.

16. Chong, M.D., Calloway, C.D., Klein, S.B., Orrego, C. and Buoncristiani, M.R. (2005) Optimization of a duplex amplification and sequencing strategy for the HVI/HVII regions of human mitochondrial DNA for forensic casework. *Forensic Science International*, **154**, 137-148.

17. Onofri, V., Alessandrini, F., Truchi, C., Pesaresi, M., Buscemi, L. and Tagliabracci, A. (2006) Development of multiplex PCRs for evolutionary and forensic applications of 37 human Y chromosome SNPs. *Forensic Science International*, **157**, 23-35.

18. Lu, X. and Eardman, D.D. (2006) Molecular typing of human adenoviruses by PCR and sequencing of a partial region of the hexon gene. *Archives of Virology*, **DOI 10.1007/s00705-005-0722-7**, Published online.

19. Dieffenbach, C.W. and Dveksler, G.S. (2003) *Pcr Primer: A Laboratory Manual*. 2nd ed. CSHL Press, Woodbury, NY.

20. Sambrook , J. and Russell, D.W. (2001) *Molecular Cloning: A Laboratory Manual*. 3rd ed. CSHL Press, Woodbury, NY.

21. Thorne, H.V. (1966) Electrophoretic separation of polyoma virus DNA from host cell DNA. *Virology*, **29**, 234-239.

22. Waring, M.J. (1965) Complex formation between ethidium bromide and nucleic acids. *Journal of Molecular Biology*, **13**, 269-282.

23. Wittwer, C.T., Fillmore, G.C. and Hillyard, D.R. (1989) Automated polymerase chain-reaction in capillary tubes with hot air. *Nucleic Acids Research*, **17**, 4353-4357.

24. Wittwer, C.T., Fillmore, G.C. and Garling, D.J. (1990) Minimizing the time required for DNA amplification by efficient heat transfer to small samples. *Analytical Biochemistry*, **186**, 328-331.

25. Swerdlow, H., Jones, B.J. and Wittwer, C.T. (1997) Fully automated DNA reaction and analysis in a fluidic capillary instrument. *Analytical Chemistry*, **69**, 848-855.

26. Rollo F, Amici A and R., S. (1988) A simple and low cost DNA amplifier. *Nucleic Acids Research*, **16**, 3105-3106.

27. Oda, R.P., Strausbauch, M.A., Huhmer, A.F., Borson, N., Jurrens, S.R., Craighead, J., Wettstein, P.J., Eckloff, B., Kline, B. and Landers, J.P. (1998) Infrared-mediated thermocycling for ultrafast polymerase chain reaction amplification of DNA. *Analytical Chemistry*, **70**, 4361-4368.

28. Huhmer, A.F. and Landers, J.P. (2000) Noncontact infrared-mediated thermocycling for effective polymerase chain reaction amplification of DNA in nanoliter volumes. *Analytical Chemistry*, **72**, 5507-5512.

29. Braun, D., Goddard, N.L. and Libchaber, A. (2003) Exponential DNA replication by laminar convection. *Physical Review Letters*, **91**, 158103.

30. Kricka, L.J. and Wilding, P. (2003) Microchip PCR. *Analytical and Bioanalytical Chemistry*, **377**, 820-825.

31. Roper, M.G., Easley, C.J. and Landers, J.P. (2005) Advances in polymerase chain reaction on microfluidic chips. *Analytical Chemistry*, **77**, 3887-3894.

32. Spitzack, K.D. and Ugaz, V.M. (2005) In Minteer, S. D. (ed.), *Microfluidic Techniques: Reviews and Protocols*. Humana Press, Totowa, NJ, Vol. 321, pp. Chapter 10.

33. Zhang, C., Xu, J., Ma, W. and Zheng, W. (2006) PCR microfluidic devices for DNA amplification. *Biotechnology Advances*, **24**, 243-284.

34. Northrup, M.A., Ching, M.T., White, R.M. and Watson, R.T. (1993) In Yokohama, J. (ed.), *Proceedings of the 7th International Conference on Solid-state Sensors and Actuators*, Yokohama, Japan, pp. 924-926.

35. Wilding, P., Shoffner, M.A. and Kricka, L.J. (1994) PCR in a silicon microstructure. *Clinical Chemistry*, **40**, 1815-1818.

36. Wilding, P., Shoffner, M.A., Cheng, J., Hvichia, G. and Kricka, L.J. (1995) Thermal cycling and surface passivation of micromachined devices for PCR. *Clinical Chemistry*, **41**, 1367-1368.

37. Nakano, H., Matsuda, K., Yohda, M., Nagamune, T., Endo, I. and Yamane, T. (1994) High-speed polymerase chain-reaction in constant flow. *Bioscience Biotechnology and Biochemistry*, **58**, 349-352.

38. Kopp, M.U., de Mello, A.J. and Manz, A. (1998) Chemical amplification: continuous-flow PCR on a chip. *Science*, **280**, 1046-1048.

39. Sun, K., Yamaguchi, A., Ishida, Y., Matsuo, S. and Misawa, H. (2002) A heater-integrated transparent microchannel chip for continuous-flow PCR. *Sensors and Actuators B-Chemical*, **84**, 283-289.

40. Curcio, M. and Roeraade, J. (2003) Continuous segmented-flow polymerase chain reaction for high-throughput miniaturized DNA amplification. *Analytical Chemistry*, **75**, 1-7.

41. Park, N., Kim, S. and Hahn, J.H. (2003) Cylindrical compact thermal-cycling device for continuous-flow polymerase chain reaction. *Analytical Chemistry*, **75**, 6029-6033.

42. Obeid, P.J., Christopoulos, T.K., Crabtree, H.J. and Backhouse, C.J. (2003) Microfabricated device for DNA and RNA amplification by continuous-flow polymerase chain reaction and reverse transcription-polymerase chain reaction with cycle number selection. *Analytical Chemistry*, **75**, 288-295.

43. Bu, M.Q., Tracy, M., Ensell, G., Wilkinson, J.S. and Evans, A.G.R. (2003) Design and theoretical evaluation of a novel microfluidic device to be used for PCR. *Journal of Micromechanics and Microengineering*, **13**, S125-S130.

44. Liu, J., Enzelberger, M. and Quake, S. (2002) A nanoliter rotary device for polymerase chain reaction. *Electrophoresis*, **23**, 1531-1536.

45. Chou, C.F., Changrani, R., Roberts, P., Sadler, D., Burdon, J., Zenhausern, F., Lin, S., Mulholland, A., Swami, N. and Terbrueggen, R. (2002) A miniaturized cyclic PCR device - modeling and experiments. *Microelectronic Engineering*, **61-2**, 921-925.

46. West, J., Karamata, B., Lillis, B., Gleeson, J.P., Alderman, J., Collins, J.K., Lane, W., Mathewson, A. and Berney, H. (2002) Application of magnetohydrodynamic actuation to continuous flow chemistry. *Lab on a Chip*, **2**, 224-230.

47. Bau, H.H., Zhu, J.Z., Qian, S.Z. and Xiang, Y. (2003) A magneto-hydrodynamically controlled fluidic network. *Sensors and Actuators B-Chemical*, **88**, 207-218.

48. Cheng, J., Shoffner, M.A., Hvichia, G.E., Kricka, L.J. and Wilding, P. (1996) Chip PCR. 2. Investigation of different PCR amplification systems in microfabricated silicon-glass chips. *Nucleic Acids Research*, **24**, 380-385.

49. Belgrader, P., Benett, W., Hadley, D., Long, G., Mariella, R., Milanovich, F., Nasarabadi, S., Nelson, W., Richards, J. and Stratton, P. (1998) Rapid pathogen detection using a microchip PCR array instrument. *Clinical Chemistry*, **44**, 2191-2194.

50. Wilding, P. (2003) In Cheng, J. and Kricka, L. J. (eds.), *Biochip Technology*. Taylor & Francis Books, Inc., New York, pp. 173-184.

51. Liu, R.H., Yang, J., Lenigk, R., Bonanno, J. and Grodzinski, P. (2004) Self-contained, fully integrated biochip for sample preparation, polymerase chain reaction amplification, and DNA microarray detection. *Analytical Chemistry*, **76**, 1824-1831.

52. Ugaz, V.M. and Krishnan, M. (2004) Novel convective flow based approaches for high-throughput PCR thermocycling. *Journal of the Association for Laboratory Automation (JALA)*, **9**, 318-323.

53. Hennig, M. and Braun, D. (2005) Convective polymerase chain reaction around micro immersion heater. *Applied Physics Letters*, **87**, 183901.

54. Gordon, M., Ramos, E. and Sen, M. (1987) A one-dimensional model of a thermosyphon with known wall temperature. *Heat and Fluid Flow*, **8**, 177-181.

55. Vijayan, P.K. and Austregesilo, H. (1994) Scaling laws for single-phase natural circulation loops. *Nuclear Engineering and Design*, **152**, 331-347.

56. Norton, B. and Probert, S.D. (1982) Thermosyphonic water heaters stimulated by renewable energy-sources. *Applied Energy*, **12**, 237-242.

57. Norton, B. and Probert, S.D. (1982) Natural-circulation solar-energy stimulated systems for heating water. *Applied Energy*, **11**, 167-196.

58. Agrawal, A.K., Madni, I.K., Guppy, J.G. and Weaver, W.L. (1981) Dynamic simulation of LMFBR plant under natural circulation. *Journal of Heat Transfer*, **103**, 312-318.

59. Garner, S.D. and Patel, C.D. (2001), *Proceedings of the International Electronic Packaging Technical Conference and Exhibition*, Kauai, HI.

60. Pal, A., Joshi, Y., Beitelmal, A.H., Patel, C.D. and Wenger, T. (2002), *Proceedings of the United Engineering Foundation*, Santa Fe, NM.

61. Innis, M.A., Myambo, K.B., Gelfand, D.H. and Brow, M.A.D. (1998) DNA Sequencing with Thermus aquaticus DNA polymerase and direct sequencing of polymerase chain reaction-amplified DNA. *Proceedings of the National Academy of Sciences of the USA*, **85**, 9436–9440.

62. QIAGEN. (2002) *QIAquick Spin Handbook (available online)*, http://www1.qiagen.com/literature/handbooks/PDF/DNACleanupAndConcentration/QQ_Spin/1021422_HBQQSpin_072002WW.pdf.

63. Giordano, B.C., Ferrance, J., Swedberg, S., Huhmer, A.F.R. and Landers, J.P. (2001) Polymerase chain reaction in polymeric microchips: DNA amplification in less than 240 seconds. *Analytical Biochemistry*, **291**, 124-132.

64. Lagally, E.T., Medintz, I. and Mathies, R.A. (2001) Single-molecule DNA amplification and analysis in an integrated microfluidic device. *Analytical Chemistry*, **73**, 565-570.

65. Northrup, M.A., Benett, B., Hadley, D., Landre, P., Lehew, S., Richards, J. and Stratton, P. (1998) A miniature analytical instrument for nucleic acids based on micromachined silicon reaction chambers. *Analytical Chemistry*, **70**, 918-922.

66. Belgrader, P., Smith, J.K., Weedn, V.W. and Northrup, M.A. (1998) Rapid PCR for identity testing using a battery-powered miniature thermal cycler. *Journal of Forensic Sciences*, **43**, 315-319.

67. Benett, W.J., Belgrader, M., Richards, J.B., Stratton, P., Hadley, D.R., Bodtker, B.H., Nasarabadi, S.L., Milanovich, F.P., Mariella, R.P.J. and Koopman, R.P. (2000), *Proceedings of SPIE-The International Society for Optical Engineering (Biochemical and Biomolecular Sensing)*, Boston, MA, Vol. 4200.

68. Bustin, S.A., Benes, V., Nolan, T. and Pfaffl, M.W. (2005) Quantitative real-time RT-PCR - a perspective. *Journal of Molecular Endocrinology*, **34**, 597-601.

69. Gunson, R.N., Collins, T.C. and Carman, W.F. (2006) Practical experience of high throughput real time PCR in the routine diagnostic virology setting. *Journal of Clinical Virology*, **35**, 355-367.

70. Mackay, I. (2004) Real-time PCR in the microbiology laboratory. *Clinical Microbiology and Infection*, **10**, 190-212.

71. Tan, W., Wang, K. and Drake, T.J. (2004) Molecular beacons. *Current Opinion in Chemical Biology*, **8**, 547-553.

72. Arya, M., Shergill, I.S., Williamson, M., Gommersall, L., Arya, N. and Patel, H.R. (2005) Basic principles of real-time quantitative PCR. *Expert Review of Molecular Diagnostics*, **5**, 209-219.

73. Gachon, C., Mingam, A. and Charrier, B. (2004) Real-time PCR: what relevance to plant studies? *Journal of Experimental Botany*, **55**, 1445-1454.

74. Sanger, F., Nicklen, S. and Coulson, A.R. (1977) DNA sequencing with chain-terminating inhibitors. *Proceedings of the National Academy of Sciences of the United States of America*, **74**, 5463-5467.

75. Metzker M.L., L., J., and Gibbs, R.A. . (1996) Electrophoretically uniform fluorescent dyes for automated DNA sequencing. . *Science* **271** 1420-1422.

76. Russell, P. (2002) *iGenetics*. Benjamin Cummings, San Francisco.

77. Ju, J.Y., Ruan, C.C., Fuller, C.W., Glazer, A.N. and Mathies, R.A. (1995) Fluorescence energy transfer dye-labeled primers for DNA sequencing and analysis. *Proceedings of the National Academy of Sciences of the United States of America*, **92**, 4347-4351.

78. Lee, L.G., Spurgeon, S.L., Heiner, C.R., Benson, S.C., Rosenblum, B.B., Menchen, S.M., Graham, R.J., Constantinescu, A., Upadhya, K.G. and Cassel,

J.M. (1997) New energy transfer dyes for DNA sequencing. *Nucleic Acids Research*, **25**, 2816-2822.

79. Metzker, M.L. (2005) Emerging technologies in DNA sequencing. *Genome Research*, **15**, 1767-1776.

APPENDIX A

AMPLIFICATION YIELD AFTER INDIVIDUAL CYCLES

Amplification formula: $Y=(1+x)^n$

Where,

Y = Copy yield, x = mean amplification efficiency, n = number of cycles

Considering 100% efficiency under ideal conditions and starting with single copy of template, we get: $Y = 2^n$

S. No.	Initial number of copies	Cycle (n)	Copy yield after n cycles (Y)
1	1	1	2
2	2	2	4
3	4	3	8
4	8	4	16
5	16	5	32
6	32	6	64
7	64	7	128
8	128	8	256
9	256	9	512
10	512	10	1024
11	1024	11	2048
12	2048	12	4096
13	4096	13	8192
14	8192	14	16384
15	16384	15	32768
16	32768	16	65536
17	65536	17	131072
18	131072	18	262144
19	262144	19	524288
20	524288	20	1048576
21	1048576	21	2097152
22	2097152	22	4194304
23	4194304	23	8388608

S. No.	Initial number of copies	Cycle (n)	Copy yield after n cycles (Y)
24	8388608	24	16777216
25	16777216	25	33554432
26	33554432	26	67108864
27	67108864	27	134217728
28	134217728	28	268435456
29	268435456	29	536870912
30	536870912	30	1073741824
31	1073741824	31	2147483648
32	2147483648	32	4294967296
33	4294967296	33	8589934592
34	8589934592	34	17179869184
35	17179869184	35	34359738368

APPENDIX B

PROPERTIES OF FEP

PROPERTIES	ASTM or Unit	FEP
General properties		
Chemical/Solvent Resistance	D543	Excellent
Water Absorption, 24h	%	<0.01
Deformation Under Load	D621/100°C	5.0
	D621/25°C	3.0
Refractive Index		1.338
Limiting Oxygen Index	>95	>95
Mechanical properties		
Specific Gravity	D792	2.15
Elongation %	D638	250~330
Tensile Strength (psi)	D638	2,800~5,000
Flexural Strength (psi)	D790	no break
Compressive Strength	D695	2,200
Tensile Elastic Modulus (Young's Modulus) (psi)	D638	50,000
(psi)	D790	78,000~92,000
Flexural Modulus 103MPa (103kgf/cm^2)	D790	0.5-0.6 (5.5-6.5)
Flex Life (MIT cycles)	D2176	5,000~80,000
Hardness Durometer Shore D	D636	D55
Coefficient of Friction	on steel	0.05
Abrasion Resistance 1000 revs.	Taber	14~20
Impact Strength IZOD 73°F/23°C, notched ft/lbs/in	D256	no break
Thermal properties		
Melting Point	°C (°F)	260 (500)
Upper Service Temperature(20,000h)	°C (°F)	200 (392)
Flame Rating**	UL 94	V-0
Thermal Conductivity	BTU/hr/ft^2/deg F in	1.4
	cal/sec/cm^2,°C/cm	6 x 10^{-4}

Linear Coefficient of Thermal Expansion 10-50 °C	D696	8.3~10.5
Heat of Fusion	BTU/LB	11
Heat of Combustion	BTU/LB	2200
Low Temperature Embrittlement	°C (°F)	-268 (-450)
Electrical Properties		
Dielectric Constant	D150/10^3Hz	2.1
	D150/10^6Hz	2.1
Dielectric Strength 10 mil film	D149	>2000
Volume Resistivity ohm-cm	D257	>10^{18}
Surface Resistivity ohm/sq.	D257	>10^{17}

VITA

Nitin Agrawal, son of Rama Shanker Agarwal and Meena Agarwal was born in 1976 in Bareilly (Uttar Pradesh), India and was brought up in Balco (Madhya Pradesh) where he attended Balco Township Higher Secondary School. After completing high school, he was admitted to the Department of Chemical Engineering, Regional Engineering College-Durgapur, West Bengal, India in 1995 and graduated with a Bachelor of Engineering degree in chemical engineering in May, 1999. Then he joined Larsen & Toubro Ltd. (L&T), Baroda, India as an executive engineer in August, 1999. After working for about two years, he resigned from his position at L&T to pursue graduate studies. In 2001, he was admitted to Wayne State University to study for a master's in chemical engineering from where he transferred to Texas A&M University, College Station, Texas in August 2002 to study for a Ph.D. in chemical engineering. He received the completion certificate in September 2006. After the completion of his doctoral program, he accepted a post-doctoral fellow position at the Center for Engineering in Medicine, Massachusetts General Hospital & Shriners Burns Institute, Harvard Medical School, Boston, MA.

Permanent address: 20 North City, Pocket B.

Nainital Road, Bareilly, U.P-243001

INDIA